

## ABSTRACT

EWING, BRYAN DARNELL. Performance of Post-Tensioned Clay Brick Masonry Walls with Openings. (Under the direction of Dr. Mervyn Kowalsky.)

This dissertation aims to advance the understanding of unbonded post-tensioned masonry wall systems. Previous research has shown that unbonded post-tensioned masonry walls can adequately resist in-plane loading but their possible use in regions of high seismic activity has not been widely accepted. The research described in this dissertation focuses primarily on clay brick masonry. The first study is on the in-plane cyclic behavior of unbonded post-tensioned masonry walls with openings. Openings can interrupt the standard path of the compression strut. The compression strut is how unbonded post-tensioned masonry walls distribute the lateral load to the foundation, and without it the wall can become unstable. The results show that the size and location of the opening has a major effect of the overall response of the wall. As the opening size increases the compression strut becomes more unstable.. Experimental studies involved the construction and testing of three walls. A parametric study was conducted to determine the effect of opening size and aspect ratio on the behavior of unbonded post-tensioned masonry walls with openings. Several tables are proposed for the initial design of these walls depending on the opening size and aspect ratio of the wall.

The latter part of the dissertation focuses on the Direct Displacement-Based Design (DDBD) of unbonded post-tensioned clay brick masonry walls. A unique problem of the use of clay brick masonry walls arose and was studied. Because clay brick masonry and the concrete foundation's Young moduli are different, the interaction between the two surfaces was analyzed. It is shown that the foundation locally confines the clay brick masonry, thereby

increasing its compressive strength. Without including this confinement, effect the lateral resisting strength is greatly underestimated. Previous methods are modified to predict the compressive strength of clay brick masonry at the wall/foundation interface. The method is verified against previous unbonded post-tensioned clay brick masonry walls and established methods of calculating the compressive strength of masonry prisms. Then using the proposed method of calculating the compressive strength of clay brick masonry at the interface, a design methodology is proposed for unbonded post-tensioned clay brick masonry walls.

Performance of Post-Tensioned Clay Brick Masonry Walls  
with Openings

by  
Bryan Ewing

A dissertation submitted to the Graduate Faculty of  
North Carolina State University  
in partial fulfillment of the  
requirements for the Degree of  
Doctor of Philosophy

Civil Engineering

Raleigh, North Carolina  
2008

APPROVED BY:

---

Dr. Mervyn Kowalsky (Chair)

---

Dr. Paul Zia (Member)

---

Dr. James Nau (Member)

---

Dr. Kara Peters (Member)

## BIOGRAPHY

Bryan Ewing was born in Chicago, IL in 1978. He received his Bachelor and Master of Civil Engineering degrees from North Carolina State University. Later he joined the Civil Engineering Ph.D. program at North Carolina State University where he focused on earthquake engineering and unbonded post-tensioned masonry walls. Bryan completed his Ph.D. degree in August 2008 and hopes to be a productive member of society. He intends on working in the private sector and returning to academia in his later years.

*Bryan D. Ewing  
Raleigh, North Carolina  
August 2008  
bryanewing@hotmail.com*

## ACKNOWLEDGEMENTS

The author would like to thank the following people and organizations:

- My parents, Charles and Barbara Ewing, for their support throughout this long process.
- The best big brother ever known Anthony Ewing, his wife Kem, and my nephew and niece Charles Thomas (CT) and Amaria.
- My advisor, Dr. Mervyn Kowalsky, for his patience and technical advice over the past years. Thanks for everything.
- The advisory committee members: Dr. James Nau, Dr. Kara Peters, and Dr. Paul Zia.
- The mechanical master Jerry Atkinson at the Constructed Facilities Laboratory for his expansive knowledge that he was willing to share with me. Thanks.
- Finally, I am grateful for the financial support from The Department of Civil, Construction, and Environmental Engineering at North Carolina State University, The North Carolina State Department of Transportation, Partnership for Advancing Technology in Housing (PATH) program, AmeriSteel, General Shale Masonry, and Pinnacle Masonry.

# TABLE OF CONTENTS

LIST OF TABLES.....	vii
LIST OF FIGURES.....	viii
1 INTRODUCTION.....	1
1.1 SIGNIFICANCE OF MASONRY CONSTRUCTION .....	1
1.2 STATEMENT OF PURPOSE.....	2
1.3 DISSERTATION ORGANIZATION .....	3
1.4 RESEARCH OBJECTIVE.....	4
1.5 RESEARCH METHODS .....	5
1.6 PRINCIPLES OF POST-TENSIONED WALLS .....	6
2 LITERATURE REVIEW.....	9
2.1 CURRENT MASONRY CODES.....	9
2.2 CONCLUSIONS OF PAST RESEARCH .....	9
2.3 EARLY STAGES OF CURRENT PROJECT AT NORTH CAROLINA STATE UNIVERSITY .....	10
2.3.1 <i>Clay Brick Masonry Prism Tests</i> .....	10
2.3.2 <i>Reinforced Masonry Flexural Walls</i> .....	11
2.3.3 <i>Post-tensioned Masonry Flexural Walls</i> .....	11
2.4 REFERENCES .....	12
3 CYCLIC BEHAVIOR OF UNBONDED POST-TENSIONED MASONRY WALLS WITH OPENINGS.....	16
3.1 ABSTRACT.....	17
3.2 INTRODUCTION.....	18
3.3 DESIGN METHODOLOGY.....	21
3.3.1 <i>Vertical Isolation</i> .....	21
3.3.2 <i>Horizontal Isolation</i> .....	22
3.4 PANEL APPROXIMATION.....	37
3.4.1 <i>Single Story Panel Approximation</i> .....	37
3.4.2 <i>Multi-story Panel Approximation</i> .....	39
3.5 CONCLUSION .....	40
3.6 REFERENCES .....	41

4	EFFECT OF VARYING CONFINEMENT STRESS ON THE AXIAL STRESS-STRAIN RELATIONSHIP OF CONCRETE AND MASONRY .....	43
4.1	ABSTRACT.....	44
4.2	INTRODUCTION.....	44
4.3	THEORETICAL MODEL.....	46
4.3.1	<i>Mechanics of Materials</i> .....	47
4.3.2	<i>Equivalent Uni-axial Strain</i> .....	49
4.4	STRESS-STRAIN RELATIONSHIP MODEL.....	50
4.4.1	<i>Poisson's Ratio</i> .....	52
4.4.2	<i>Masonry Failure Criteria</i> .....	52
4.4.3	<i>Masonry Wall Model Overview</i> .....	55
4.4.4	<i>Foundation Failure Criterion</i> .....	56
4.5	VERIFICATION OF THE MODEL.....	57
4.5.1	<i>Masonry Prism Compression Strength</i> .....	57
4.5.2	<i>Unbonded Post-tensioned Masonry Walls</i> .....	60
4.6	DESIGN APPLICATIONS OF THE MODEL .....	61
4.7	CONCLUSIONS .....	62
4.8	NOTATION .....	62
4.9	REFERENCES .....	63
5	DISPLACEMENT-BASED DESIGN OF UNBONDED POST-TENSIONED MASONRY WALLS .....	66
5.1	ABSTRACT.....	67
5.2	INTRODUCTION AND OBJECTIVES .....	67
5.3	DISPLACEMENT-BASED DESIGN APPROACH .....	69
5.4	DESIGN PROCEDURE FOR UNBONDED POST-TENSIONED MASONRY .....	73
5.4.1	<i>Building Specifics</i> .....	74
5.4.2	<i>Design Criteria</i> .....	74
5.4.3	<i>Obtaining Design Forces</i> .....	79
5.4.4	<i>Design Forces Checks</i> .....	80
5.4.5	<i>Evaluating Required Initial Pre-Stress</i> .....	81
5.4.6	<i>Initial Pre-Stress Checks</i> .....	82
5.4.7	<i>Time Dependent Effects</i> .....	82
5.5	EXPERIMENTAL VALIDATION .....	82
5.5.1	<i>Earthquake Record Selection</i> .....	83
5.5.2	<i>Testing Matrix</i> .....	84
5.5.3	<i>Results Comparison</i> .....	86

5.6	DESIGN EXAMPLE .....	87
5.7	CONCLUSIONS .....	89
5.8	REFERENCES .....	90
<b>6</b>	<b>SUMMARY AND CONCLUSIONS .....</b>	<b>94</b>
6.1	CONCLUSIONS .....	94
6.2	RECOMMENDATIONS .....	97
6.3	FUTURE WORK .....	98
<b>APPENDIX A: COMPRESSIVE BEHAVIOR OF CLAY BRICK MASONRY .....</b>		<b>100</b>
1.1	ABSTRACT .....	101
1.2	INTRODUCTION .....	102
1.3	RESEARCH OBJECTIVE AND METHODS .....	103
1.4	TEST RESULTS .....	106
1.4.1	<i>Single Wythe Prisms</i> .....	106
1.4.2	<i>Double Wythe Grouted Prisms - Unconfined</i> .....	106
1.4.3	<i>Double Wythe Grouted Prisms - Confined</i> .....	107
1.4.4	<i>Stress-strain relationships</i> .....	109
1.5	COMPARISON WITH KENT-PARK MODEL.....	110
1.6	LIMIT STATES OF CLAY BRICK MASONRY BASED ON EXPERIMENTAL RESULTS.....	112
1.7	EQUIVALENT STRESS BLOCK PARAMETERS .....	114
1.8	CONCLUSIONS AND RECOMMENDATIONS .....	115
1.9	ACKNOWLEDGEMENTS .....	117
1.10	REFERENCES .....	117
<b>APPENDIX B: ANSYS MODELING .....</b>		<b>119</b>
1.1	INTRODUCTION .....	120
1.2	ELEMENT TYPES .....	120
1.3	MATERIAL PROPERTIES .....	121
1.4	MODELING .....	123
<b>APPENDIX C: TESTING PICTURES .....</b>		<b>124</b>
1.1	OPENING PANEL 1 – CONTROL .....	125
1.2	OPENING PANEL 2 – CONFINEMENT PLATES .....	128
1.3	OPENING PANEL 3 – LONGITUDINAL REINFORCEMENT .....	129
1.4	SHAKE TABLE TESTS .....	130

# LIST OF TABLES

## LITERATURE REVIEW

TABLE 1: TESTING MATRIX .....	12
-------------------------------	----

## CYCLIC BEHAVIOR OF UNBONDED POST-TENSIONED MASONRY WALLS WITH OPENINGS

TABLE 1: WALL ASPECT RATIO OF 1 .....	38
TABLE 2: WALL ASPECT RATIO OF 2 .....	38
TABLE 3: WALL ASPECT RATIO OF 3 .....	39

## DISPLACEMENT-BASED DESIGN OF UNBONDED POST-TENSIONED MASONRY WALLS

TABLE 1: SEISMIC PERFORMANCE OBJECTIVES .....	68
TABLE 2: MASONRY STRAINS AT VARIOUS LIMIT STATES .....	75
TABLE 3: SUGGESTED $\theta_{STRUT}$ VALUES .....	78
TABLE 4: RETURN PERIOD FOR VARIOUS EARTHQUAKE INTENSITIES <sup>23</sup> .....	84
TABLE 5: PGA FOR SELECTED RECORDS .....	85
TABLE 6: POST-TENSIONING BAR FORCE MATRIX .....	85

## APPENDIX A: COMPRESSIVE BEHAVIOR OF CLAY BRICK MASONRY

TABLE 1: MATERIAL PROPERTIES .....	105
TABLE 2: DOUBLE WYTHE PRISM RESULTS .....	108
TABLE 3: HART ET AL. (1988) CONFINED CONCRETE MASONRY LIMIT STATES .....	113
TABLE 4: LIMIT STATES OF CLAY BRICK MASONRY .....	114
TABLE 5: EQUIVALENT STRESS BLOCK PARAMETERS .....	114

# LIST OF FIGURES

## INTRODUCTION

FIGURE 1: UNBONDED POST-TENSIONED MASONRY WALL .....	2
--	---

## CYCLIC BEHAVIOR OF UNBONDED POST-TENSIONED MASONRY WALLS WITH OPENINGS

FIGURE 1: ROCKING DEFORMATION IN UNBONDED POST-TENSIONED SYSTEMS .....	19
FIGURE 2: COMPRESSION STRUT OF UNBONDED POST-TENSIONED MASONRY WALL .....	20
FIGURE 3: EFFECT OF OPENINGS ON COMPRESSION STRUT .....	21
FIGURE 4: VERTICAL ISOLATION .....	22
FIGURE 5: HORIZONTAL ISOLATION .....	23
FIGURE 6: TEST SETUP .....	25
FIGURE 7: OBSERVED SLIDING .....	28
FIGURE 8: PIER SLIDING AND DAMAGE .....	28
FIGURE 9: STRUCTURAL RESPONSE OF WALL 1 .....	29
FIGURE 10: LOCATION OF CONFINEMENT PLATES IN WALL 2 .....	31
FIGURE 11: CONFINEMENT PLATE .....	31
FIGURE 12: INITIAL CRACK IN WALL 2.....	32
FIGURE 13: STRUCTURAL RESPONSE OF WALL 2.....	34
FIGURE 14: DESIGN OF WALL 3.....	35
FIGURE 15: STRUCTURAL RESPONSE OF WALL 3.....	36
FIGURE 16: EFFECT OF STORY LOADS ON SINGLE PANEL APPROXIMATION .....	40

## EFFECT OF VARYING CONFINEMENT STRESS ON THE AXIAL STRESS-STRAIN RELATIONSHIP OF CONCRETE AND MASONRY

FIGURE 1: UNBONDED POST-TENSIONED MASONRY WALL.....	46
FIGURE 2 MASONRY WALL AND FOUNDATION STRESS STATE BLOCKS .....	47
FIGURE 3 SAMPLE STRESS-STRAIN RELATIONSHIP .....	51
FIGURE 4 FLOWCHART OF STRESS-STRAIN RELATIONSHIP SOLVING PROCEDURE.....	56
FIGURE 5: MASONRY PRISM STRENGTH COMPARISON .....	59
FIGURE 6: STRESS-STRAIN RELATIONSHIPS.....	59
FIGURE 7 STRESS-STRAIN RELATIONSHIP COMPARISON.....	60
FIGURE 8 FORCE-DISPLACEMENT COMPARISONS .....	61
FIGURE 9: DEVELOPEMENT OF EQUIVALENT STRESS BLOCK.....	62

# DISPLACEMENT-BASED DESIGN OF UNBONDED POST-TENSIONED MASONRY WALLS

FIGURE 1: MDOF STRUCTURE DISPLACEMENT PROFILE.....	70
FIGURE 2: EQUIVALENT SDOF OSCILLATOR.....	70
FIGURE 3: EQUIVALENT VISCOUS DAMPING <sup>15</sup> .....	71
FIGURE 4: EFFECTIVE PERIOD.....	72
FIGURE 5: FORCE-DISPLACEMENT RESPONSE.....	72
FIGURE 6: DEVELOPMENT OF EQUIVALENT STRESS BLOCK.....	76
FIGURE 7: TENSILE LIMIT STATES.....	77
FIGURE 8: SUGGESTED $\theta_{STRUT}$ VALUES.....	78
FIGURE 9: ACCELERATION RECORDS FOR (A) LLOLLELO, (B) EL CENTRO, (C) NAHANNI EARTHQUAKES, AND (D) THEIR ACCELERATION RESPONSE SPECTRA.....	83
FIGURE 10: STRUCTURE RESPONSE TO EL CENTRO EARTHQUAKE.....	85
FIGURE 11: EXPERIMENTAL AND DESIGN RESULTS COMPARISON.....	86
FIGURE 12: DESIGN EXAMPLE.....	87
FIGURE 13: DESIGN EARTHQUAKE SPECTRA.....	88

## APPENDIX A: COMPRESSIVE BEHAVIOR OF CLAY BRICK MASONRY

FIGURE 1: PRISM CONFIGURATIONS.....	104
FIGURE 2: STRESS-STRAIN RELATIONSHIPS; (A) UNCONFINED; (B) ALTERNATE COURSE CONFINED; (C) EVERY COURSE CONFINED; (D) SOLID PLATE, EVERY COURSE CONFINED.....	108

## APPENDIX B: ANSYS MODELING

FIGURE 1: MASONRY STRESS-STRAIN RELATIONSHIP.....	121
FIGURE 2: CONCRETE FOUNDATION STRESS-STRAIN RELATIONSHIP.....	122
FIGURE 3: POST-TENSIONING STEEL BAR STRESS-STRAIN RELATIONSHIP.....	122
FIGURE 4: FINITE ELEMENT MODEL OF UNBONDED POST-TENSIONED MASONRY WALL.....	123

## APPENDIX C: TESTING PICTURES

FIGURE 1: CONSTRUCTION OF MASONRY WALL WITH OPENING.....	125
FIGURE 2: FORMATION OF BASE CRACK AND VERTICAL CRACK AT 0.35 DRIFT RATIO.....	125
FIGURE 3: BASE CRACK AT 0.75 DRIFT RATIO.....	126
FIGURE 4: EXCESSIVE CRACK WIDTH AT 1.25 DRIFT RATIO.....	126
FIGURE 5: VERTICAL CRACK AT 1.75 DRIFT RATIO.....	127
FIGURE 6: CRUSHING OF MASONRY AT 2.25 DRIFT RATIO.....	127
FIGURE 7: FINISHED WALL SETUP.....	128

FIGURE 8: CONTINUED VERTICAL CRACK GROWTH RESULTING ENTIRE SIDE OF WALL ROCKING AT 1.75 DRIFT RATIO ..... 128

FIGURE 9: OBSERVED SLIDING OF MASONRY WALL AT 1.75 DRIFT RATIO ..... 129

FIGURE 10: REDUCED CRACK WIDTH AT 0.75 DRIFT RATIO ..... 129

FIGURE 11: ROCKING MECHANISM AND LIMITED CRACK WIDTH AT 1.75 DRIFT RATIO ..... 130

FIGURE 12: SHAKE TABLE SETUP ..... 130

FIGURE 13: INSTRUMENTATION AND BOLT TIE-DOWNS ..... 131

FIGURE 14: MASONRY WALL "DAMAGE" AFTER 56 EARTHQUAKE RUNS ..... 131

# **1 INTRODUCTION**

## **1.1 SIGNIFICANCE OF MASONRY CONSTRUCTION**

Clay brick masonry is one of the most common construction materials used throughout the world. Brick structures date back thousands of years. However, due to the brittle nature of the failure mechanisms of clay brick, this material has typically been relegated to architectural or cosmetic applications. History has validated this observation. Earthquakes and other high-load and dynamic loading have caused significant damage and in some cases collapse.

Previous research provides evidence that clay brick may be used as a structural element. Clay brick walls are typically constructed from two wythes with a cavity between the them. The wythes are then longitudinally reinforced and grouted. Of course these reinforced walls exhibited better performance than unreinforced wall, but they still do not demonstrate good performance under seismic attack. The latest masonry wall configuration is to replace the longitudinal steel with post-tensioning steel as shown in Figure 1. Current on-going research has shown that walls with unbonded post-tensioning steel demonstrate the potential to be used as lateral load-resisting members. This research dissertation intends to further demonstrate that post-tensioned clay brick masonry can be used as structural elements in regions of high seismicity.

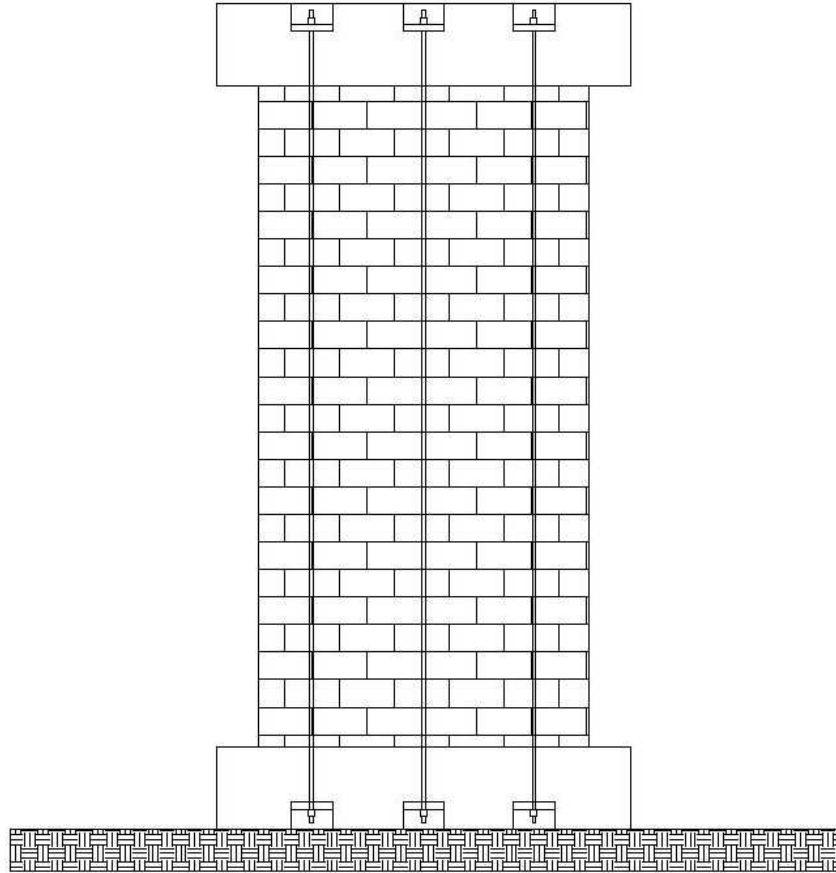


**Figure 1: Unbonded Post-tensioned Masonry Wall**

## **1.2 STATEMENT OF PURPOSE**

Post-tensioned clay brick masonry walls are a relatively new design concept. If these walls prove to be a reasonable alternative in seismic regions, then post-tensioned clay brick masonry walls will be one of the most promising construction methods.

Clay bricks have time-tested benefits including:

- 1) Clay bricks are aesthetically pleasing.
- 2) Masonry units are noncombustible. Wood can be treated with chemicals to make them fire resistant, but will ultimately burn and fuel the fire. Steel is noncombustible as well but will soften from the high heat caused by a fire. Masonry products have the highest fire protection ratings.

- 3) Clay brick masonry units are highly durable against wear and weathering. Wooden buildings require an additional investment of time and money to avoid moisture and insect damage.
- 4) The thermal performance of clay brick masonry walls is exceptional. Even though a vast majority of building materials absorbs heat, clay brick masonry walls, which can be upwards of 12 inches thick, can slow the migration of heat through the wall. This characteristic can reduce the size of air conditioning and heating equipment.

It is the purpose of this research program to develop more information about the performance of post-tensioned clay brick masonry walls and determine if they are suitable to be used as the structural system in regions of high seismicity.

### **1.3 DISSERTATION ORGANIZATION**

The dissertation will be divided into seven sections. The first section will introduce the topic and discuss relevant past research on unbonded post-tensioned masonry. Three drafts of journal articles will follow. Each describes in detail the problems encountered and their solutions.

The first article, “Cyclic Behavior of Unbonded Post-tensioned Masonry Walls with Openings” describes the first three experiments. The tests consist of unbonded post-tensioned clay brick masonry walls with a standard sized window. The testing program initially began without any addition detailing around the openings and, as the testing progress, improvements were made to the design to achieve optimal performance.

The second journal article, “Effect of Varying Confinement Stress on the Axial Stress-strain Relationship” is a product of attempting to model the performance of unbonded post-

tensioned masonry in previous experiments in ANSYS. There has been extensive research on the effect of constant lateral pressure on concrete. There also has been research on the use of confinement plates to improve the axial strength of masonry. However, the results of past research do not apply to unbonded post-tensioned masonry. Previous results are based on confinement steel ratios, steel yielding stress, and the spacing of the steel or kept the lateral pressure constant. None of those are present here in the contact. Also there is a different deformation mechanism present. Unbonded post-tensioned walls will rock not bend. So it was necessary to go back to basic mechanics to develop a stress-strain relationship

The last journal article will cover the procedure for using performance based design with unbonded post-tensioned masonry. “Displacement-based Design of Unbonded Post-tensioned Masonry Walls” will incorporate my earlier findings on masonry limit states with the new model of stress-strain behavior in the contact region.

Finally, the conclusions and appendices are included. Appendix A is a published journal article entitled “Compressive Behavior of Clay Brick Masonry.” The method used to create the finite element analysis described in Appendix B. The last appendix, Appendix C, contains pictures of the full-scale tests.

## **1.4 RESEARCH OBJECTIVE**

The primary goals of the research are: (1) Develop an understanding of the behavior of post-tensioned clay brick masonry structures and (2) Develop analysis and design methods suitable for implementation by engineers that will facilitate the use of post-tensioned masonry in structural design.

In order to accomplish these goals certain unknowns must be discovered. Most importantly an understanding of the force-displacement relationship must be obtained. The

strain profile between the unbonded post-tensioned masonry wall and the foundation. This compression stress-strain relationship is important in creating a performance-based design methodology.

In addition to the strain profile along the wall's base, understanding the effect that openings have on the performance of post-tensioned clay brick masonry walls is extremely important. Whether it is a window or door; openings in masonry walls disrupt the compression strut of post-tensioning masonry wall. The compression strut and its disruption caused by openings will be discussed later in this document.

The final objective includes gathering data on the dynamic performance of post-tensioned clay brick masonry walls. This involves predicting the performance of a wall using the calculated force-displacement relationship and a displacement response spectra relating to particular earthquake.

## **1.5 RESEARCH METHODS**

A variety of research methods will be used to explore the behavior of post-tensioned clay brick masonry walls. Both experimental and analytical studies have been conducted and are detailed below:

- Cyclic and Dynamic Testing of Post-tensioned Clay Brick Masonry Walls

Four tests have been completed. Three have been completed with one of these tests will potentially be retested. Cyclic testing will be conducted on post-tensioning walls with openings while simple single panel walls will be dynamically loaded by the shake table. The testing matrix will be discussed later within this dissertation.

- Model and Predict Behavior of Post-tensioned Clay Brick Masonry Walls using Finite Element Program ANSYS

Modeling of the walls will consist of examining in detail the performance of all of the post-tensioned clay brick masonry walls tested at North Carolina State University. There have been five previously cyclically tested specimens of various configurations of single panel walls. Also this project calls for an additional three post-tensioned clay brick masonry walls with openings that will be modeled as well. Finally, the dynamic response of single panel walls will be modeled.

- Compare the Response of Post-tensioned and Traditionally Reinforced Clay Brick Masonry Walls using ANSYS

Finite element program ANSYS and observations from full scale tests were used to better understand the differences in performance between post-tensioned and reinforced masonry walls.

- Development, Application, and Verification of Performance-based Seismic Engineering Approach for Post-tensioned Masonry Buildings

The last method involved applying the performance-based seismic engineering (PBSE) approach to unbonded post-tensioned masonry walls. Finite element analysis was done to understand the compression strain distribution along the foundation/wall interface. This is necessary to predict the performance of these types of masonry walls. The PBSE approach was then applied to a building design problem.

## **1.6 PRINCIPLES OF POST-TENSIONED WALLS**

There are several key principles that must be understood to properly design post-tensioned clay brick masonry walls. Some are advantageous like the wall's rocking mechanism behavior and self-centering nature. Others, like sliding and wall stability, can be

potentially dangerous if the masonry wall is not designed properly. However, sliding of the masonry wall and the disruption of the compressive strut can be easily avoided.

The lateral displacement of post-tensioned clay brick masonry is by means of a rocking mechanism. This is particularly true of unbonded post-tensioned masonry walls. Although this mechanism is unusual, the rocking behavior is extremely beneficial in a number of ways. First, the damage is restrained only to the toe compression areas with little to no damage to the remainder of the wall. Secondly, because of the afore-mentioned damage pattern the post-tensioned clay brick masonry wall is able to withstand high levels of lateral displacements prior to failure. The rocking mechanism will occur if the following conditions are met:

- Adequate shear strength of the masonry
- Stable compression strut (will be discuss later in this section)
- Base crack formation

Self-centering behavior means that following a seismic or removal of a lateral load the wall returns to a zero displacement position. In other words the wall's motion ends where it began. Post-tensioned walls exhibit this behavior because the combination of the wall's weight and the post-tensioning force closes the base crack following a seismic attack or ending of applied lateral load. In a typical reinforced masonry wall there maybe plastic deformation of the longitudinal steel keeping the wall from returning to zero deformation. The post-tensioned clay brick masonry wall will return to zero deformation as long as the masonry and the post-tensioning steel remain elastic. However, even if the post-tensioning steel begins to behave inelastically, the wall will still exhibit low levels of residual deformation. Clay brick masonry walls will demonstrate self-centering behavior as long as

the plastic deformation strain of the post-tensioning steel is less than the initial post-tensioning strain. Self-centering behavior has several benefits including:

- Low amounts of residual deformation in return cycle of loading which is advantageous in seismic regions
- Increased life-cycle of structure since the masonry is only exposed to compression cycles
- Immediate usage of structure following a seismic event

Sliding is wall displacement in the horizontal direction with respect to the foundation. Although sliding is not detrimental to a post-tensioned wall's performance, it can be problematic to non-structural elements if they are not designed for this type of displacement. Sliding is typically associated with walls with low aspect ratios. Standard preventative methods include roughening the wall/foundation interface and increasing the post-tensioning force.

The compression strut transfers the laterally applied load to the foundation. In post-tensioned clay brick masonry walls the stability of the compression strut is essential. What affect the compression strut's stability are de-bonding of post-tensioning steel, shear cracking, and openings. The cyclic testing program used in this research project attempts to discover how the latter affects the performance of post-tensioned clay brick masonry walls.

## **2 LITERATURE REVIEW**

### **2.1 CURRENT MASONRY CODES**

The current masonry code, ACI 530.1-08/ASCE 6-08/TMS 602-08<sup>1</sup>, adequately predicts the ultimate strength of post-tensioned masonry walls. Prestressed masonry is also discussed in the Australian<sup>2</sup>, Canadian<sup>19</sup>, and New Zealand<sup>10, 11</sup> codes. However, in no way do they allow for a performance-based design. In order for performance-based design to be effective, the designer must know the strains, both in the masonry and post-tensioning tendons, and their corresponding displacements. The current codes do not predict either.

### **2.2 BRIEF SUMMARY OF PAST RESEARCH**

Priestley and Tao<sup>16</sup> were the first to observe the self-centering mechanism of unbonded post-tensioned structures. They used debonded prestressing in moment frames. Ricles et. al.<sup>17</sup> also investigated the performance of post-tensioned steel moment frames. The study of post-tensioning was extended to rocking bridge structures by Mander et al.<sup>12</sup> and Percassi<sup>14</sup>.

Page and Huizer<sup>13</sup> performed tests on three walls. Their goal was to compare the performance between reinforced and post-tensioned masonry walls by monotonically loading them in the in-plane direction. Ultimately their research proved that the post-tensioning increases the lateral load capacity and shear stiffness.

Peter Laursen and Jason Ingham<sup>5, 6, 7</sup> conducted an experiment on the in-plane performance of unbonded post-tensioned concrete masonry walls under cyclic loading. Their research involved eight walls of different dimensions, grouting, and post-tensioning force. They concluded that their walls showed “a nearly non-linear elastic behavior dominated by a

rocking response” and that energy dissipation was minimal. Also a sliding mechanism was present. The main conclusion for seismic design is that the walls remained self-centering after the post-tensioning tendons yielded. Laursen’s next series of test examined the effect of confinement plates, supplemental mild steel, and high-strength fiber reinforcement on the behavior of unbonded post-tensioned masonry walls. As expected the confinement plates and fiber reinforcement strengthening techniques improved the allowable lateral deformation while maintaining the damage to the heel and toe regions of the wall. The final stage of testing consisted of two two-thirds scale models of a 4 or 5 story building. The walls used high-strength wire tendons and confinement plates. These walls exhibited all of the advantages of unbonded post-tensioned masonry walls and validated its use in office and apartment buildings.

## **2.3 EARLY STAGES OF CURRENT PROJECT AT NORTH CAROLINA STATE UNIVERSITY**

### **2.3.1 Clay Brick Masonry Prism Tests**

The author<sup>4</sup> has previously conducted experiments on clay brick masonry prisms. The objective was to experimentally capture the stress-strain characteristics of unconfined and confined clay brick masonry and compare the response with that predicted with the “modified” Kent-Park stress-strain curve. Based on the experimental results, five limit states for clay brick masonry in compression were proposed, as well as an equivalent stress blocks for design.

Thin (3 mm) galvanized steel plates placed in the mortar joints during construction provided prism confinement. The variables considered included volumetric ratio of confining

steel (0, ~0.015, and ~0.03) and the presence of machined holes within the confinement plates to improve the bond between the masonry and steel plate.

It was shown that confinement plates are extremely effective in enhancing the ultimate compressive strength as well as increasing the deformation capacity of the clay brick masonry prisms. Use of confinement plates in the test increased the unconfined ultimate strength by 40%. The peak strength of the confined masonry prisms occurred simultaneously or immediately after yielding of the confinement plates. Experimentally obtained stress-strain curves agreed reasonably well with the “modified” Kent-Park model.

### **2.3.2 Reinforced Masonry Flexural Walls**

Durham<sup>3</sup> has shown that traditionally reinforced masonry flexural walls fail in shear. Various height ratios and reinforcing steel ratios have been studied and their experiments had limited success in producing a masonry wall that achieved a desirable level of inelasticity. That is until Priestley used confinement plates within the bed joints to improve the ductility of masonry. With the combined use of shear reinforcement, the confinement plates allowed the masonry wall to exhibit a true flexural response. In fact, Durham<sup>3</sup> discovered that placing confinement plates within every bed joint in the compression region can improve the displacement capacity 88%.

### **2.3.3 Post-tensioned Masonry Flexural Walls**

Rosenboom and Kowalsky<sup>18</sup> constructed five unbonded double wythe clay brick masonry walls. The walls measured 2440 mm tall, 1220 mm long, and 300 mm wide and were tested under a cyclic loading. 25 mm bars were used to post-tension the walls. The parameters of the study were grouting the masonry cavity, bonding the post-tensioning bars,

placing confinement plates in the lower masonry joints, and using additional mild steel. The testing matrix is shown in Table 1.

**Table 1: Testing Matrix**

<b><u>Test #</u></b>	<b><u>Grouted</u></b>	<b><u>Bonded</u></b>	<b><u>Confined</u></b>	<b><u>Mild Steel</u></b>
1	Yes	No	No	No
2	Yes	No	Yes	No
3	Yes	No	No	Yes
4	Yes	Yes	No	No
5	No	No	No	No

The conclusion of the research is that the unbonded, fully grouted, and confined masonry wall performed the best. While supplemental mild steel did improve the hysteretic damping of the structure, it also introduced tensile stresses and cracking into the masonry. Masonry walls without a grouted cavity did not allow a stable compression strut to develop and bonded tendons introduced significant structural damage.

## **2.4 REFERENCES**

1. American Concrete Institute (2002). "Building Code Requirements for Masonry Structures." ACI 530-02.
2. AS 3700 (2001). Masonry Structures, Standards Australia International, Sydney, NSW, Australia.

3. Durham, A. S. (2002). "Influence of Confinement Plates on the Seismic Performance of Reinforced Clay Brick Masonry Walls," MS Thesis, North Carolina State University, Raleigh, NC.
4. Ewing, B.D. and Kowalsky, M. J. (2004). "Compressive Behavior of Unconfined and Confined Clay Brick Masonry." *Journal of Structural Engineering*, Vol. 130, No. 4, pp. 650-661.
5. Laursen, P. T. and Ingham, J. M. (2004). "Structural Testing of Enhanced Post-tensioned Concrete Masonry Walls," *ACI Structural Journal*, Vol. 101, No. 6, pp. 852-862.
6. Laursen, P. T. and Ingham, J. M. (2004). "Structural Testing of Large-scale Post-tensioned Concrete Masonry Walls," *ASCE Journal of Structural Engineering*, Vol. 130, No. 10, pp. 1497-.
7. Laursen, P. T. and Ingham, J. M. (2001). "Structural Testing of Single-storey Post-tensioned Concrete Masonry Walls," *The Masonry Society Journal*, Vol. 19, No. 1, pp. 69-82.
8. Lissel, S. L., Sayed-Ahmed, E. Y., and Shrive, N. G. (1999). "Prestressed Masonry – The Last Ten Years," 8<sup>th</sup> North American Masonry Conference, Austin, TX, June 6-9, pp. 599-610.
9. Masonry Standards Joint Committee. (2002). "Building Code Requirements for Masonry Structures (ACI 530-02/ASCE 5-02/TMS 402-02)," American Concrete Institute; Structural Engineering Institute of the American Society of Civil Engineers; The Masonry Society.
10. NZS 4229 (1999). *Concrete Masonry Buildings Not Requiring Specific Engineering Design*, Standards New Zealand, Wellington, New Zealand.
11. NZS 4230 (2004). *Design of Reinforced Concrete Masonry Structures*, Standards New Zealand, Wellington, New Zealand.

12. Mander, J. B., Contreras, R., and Garcia, R. (1998). "Rocking Columns: An Effective Means of Seismically Isolating a Bridge," Technical Report MCEER-98-0001, Proc. Of US-Italy Workshop on Seismic Protective Systems for Bridges, Columbia University, New York, pp. 335-348
13. Page, A. W. and Huizer, A. (1988). "Racking Tests on Reinforced and Prestressed Hollow Clay Masonry Walls," 8<sup>th</sup> International Brick/Block Masonry Conference, Dublin, Ireland, September 19-21, pp. 538-547.
14. Percassi, S. J. (2000). "Rocking Column Structures with Supplemental Damping Devices," MS Thesis, University of New York at Buffalo, Buffalo, NY.
15. Priestley, M. J. N., Sritharan, S., Conley, J. R., and Pampanin, S. (1999). "Preliminary Results and Conclusions from the PRESSS Five-Story Precast Concrete Test Building," PCI Journal, Vol. 44, No. 6, pp. 42-67.
16. Priestley, M. J. N. and Tao, J. R. (1993). "Seismic Response of Precast Prestressed Concrete Frames with Partially Debonded Tendons," PCI Journal, Vol. 38, No. 1, pp. 58-69.
17. Ricles, J. M., Sause, R., Garlock, M. N., and Zhao, C. (2001). "Post-tensioned Seismic-resistant Connections for Steel Frames," ASCE Journal of Structural Engineering, Vol. 127, No. 2, pp. 113-121.
18. Rosenboom, O. A. and Kowalsky, M. J. (2004). "Reversed In-plane Cyclic Behavior of Post-tensioned Clay Brick Masonry Walls," ASCE Journal of Structural Engineering, Vol. 130, No. 5, pp. 787-798.
19. S304.1-04 (2004). Design of Masonry Structures, Canadian Standards Association, Missisauga, Ontario, Canada.
20. Schultz, A. E. and Scolforo, M. J. (1991). "An Overview of Prestressed Masonry," The Masonry Society Journal, Vol. 10, No. 1, pp. 6-20.

21. Shrive, N. G. (1988). "Post-tensioned Masonry – Status & Prospects," The Canadian Society for Civil Engineering – Annual Conference, Calgary, Canada, May 25 – 27, pp. 679-696.

JOURNAL ARTICLE NUMBER ONE

**3 CYCLIC BEHAVIOR OF UNBONDED POST-TENSIONED  
MASONRY WALLS WITH OPENINGS**

BRYAN EWING

MERVYN KOWALSKY

# CYCLIC BEHAVIOR OF UNBONDED POST-TENSIONED CLAY MASONRY WALLS WITH OPENINGS

Bryan Ewing and Mervyn J. Kowalsky

*Department of Civil, Construction and Environmental Engineering, North Carolina State University,  
Campus-Box 7908, Raleigh, NC-27695, USA*

Keywords: Analysis, Brick masonry, Openings, Post tensioning,

## **3.1 ABSTRACT**

Presented in this paper are the results of a study on the response of unbonded post-tensioned clay brick masonry walls with openings and the detailing necessary for the wall to perform in the intended manner. The research revolves around a typical unbonded-clay brick masonry wall with a standard window opening. The objective was to assess the cyclic performance of the wall and determine how its performance could be improved. In all, three separate unbonded post-tensioned walls were constructed. The detailing options included the use of confinement plates in the toe and heel regions of the wall and placement of supplemental mild steel.

Thin galvanized steel plates placed within the mortar joints provided the source for masonry confinement. As compressive forces cause lateral expansion in the clay brick masonry, the steel plates restricted the expansion and introduced a confining stress on the masonry. This confining stress allows the masonry to achieve greater compressive strain capacity and higher strength. Supplemental mild steel was used to control shear cracking therefore allowing the wall to avoid undesirable premature shear failure.

It is shown that unbonded post-tensioned masonry walls with openings can exhibit dependable performance under seismic conditions. With proper detailing of the opening, the use of confinement plates and placement of supplemental mild steel, unbonded post-tensioned masonry walls with openings remain self-corrective after a seismic event.

### **3.2 INTRODUCTION**

The concept of unbonded post-tensioning for seismic resistance was first proposed by Priestley<sup>10</sup> and was subsequently extended to the construction of masonry walls.<sup>4, 6, 11</sup>

Traditionally clay brick masonry walls are constructed from two wythes built around reinforcing bars extending from the foundation with the center cavity filled with grout. The wall deforms by flexure where tensile stresses in the reinforcing bars distribute cracks along the height of the masonry wall. By contrast, unbonded post-tensioned clay brick masonry walls are built around conduits that prevent the grout from bonding to the post-tensioning bars. The post-tensioning bars, located within the conduits, are anchored in the foundation and stressed from the top of the wall. An unbonded post-tensioned clay brick masonry wall deforms by rocking along the wall/foundation interface as shown in Fig. 1 where damage is restricted to the heel and toe regions of the wall. After a seismic event, the restoring force of the post-tensioning steel brings the wall back to its original undeformed configuration.

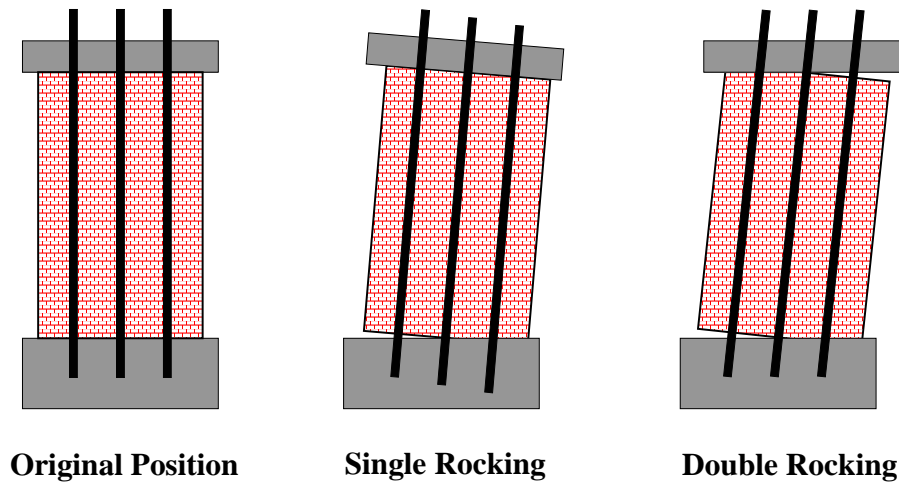


**Figure 1: Rocking Deformation in Unbonded Post-tensioned Systems**

Unbonded post-tensioned masonry walls have two main benefits over traditionally reinforced masonry walls: (1) They deform by rocking instead of flexure, and (2) They are self corrective. By rocking, the damage in the wall is localized to the toe and heel regions of the wall. Thus shear and flexural cracks observed in traditional walls are not present and as a result, walls can remain undamaged under large lateral deformations. Following a severe lateral loading, such as earthquake or hurricane strength wind loading, unbonded post-tensioned masonry walls do not have any residual deformations when designed properly.

The objective of this paper is to determine how to maintain these advantages when openings are introduced into the wall, as is often the case. Unbonded post-tensioned clay brick masonry transfers lateral loads to the foundation by means of a compression strut. Openings affect the path of the compression strut, and based on the strut and the wall geometry, regions of tension can develop. These tensile regions cause cracks in the masonry and as a consequence residual deformations, thus impacting the benefits of the self-corrective nature of the system.

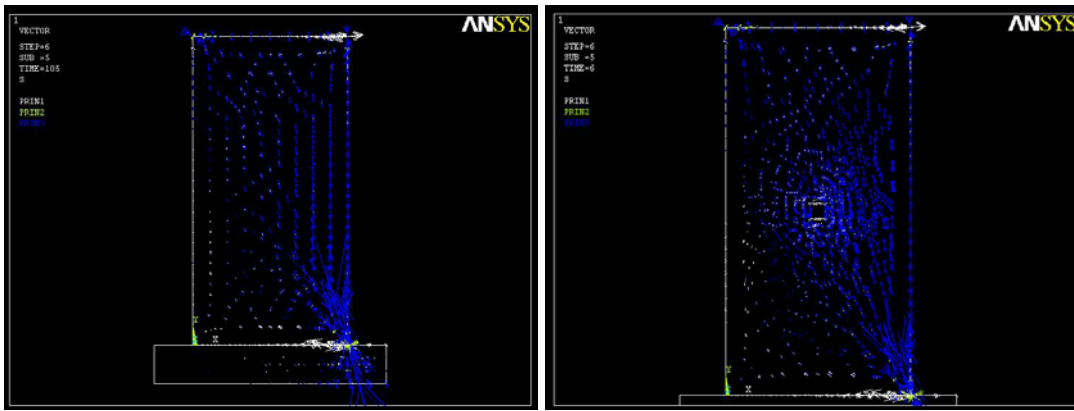
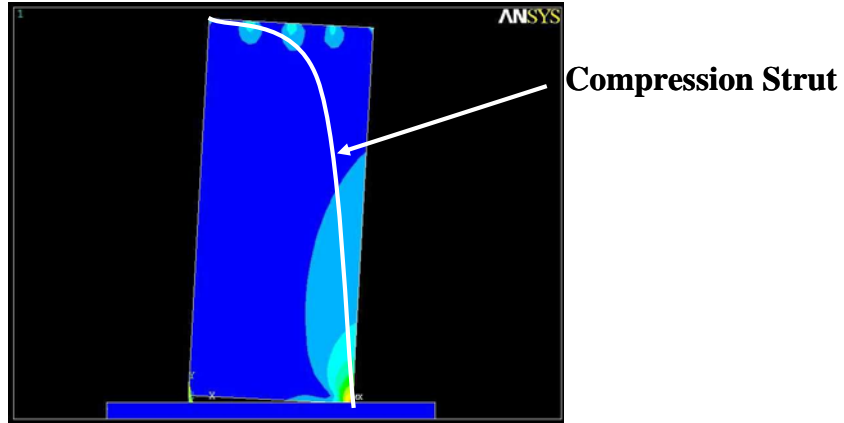


**Figure 2: Compression Strut of Unbonded Post-tensioned Masonry Wall**

Fig 2 shows the path of the compression strut of a typical unbonded post-tensioned panel. The introduction of a small hole in the figure on the right shows that this hole has little effect on the behavior. By contrast, the diagrams in Fig. 3 show how either a narrow vertical or horizontal hole adversely affects the wall's performance. The white arrows indicate areas of tension. The remainder of this paper will present different methods to ensure that damage is restricted to the toe and heel regions of the wall while retaining its self-corrective characteristics.



Figure 3: Effect of Openings on Compression Strut

### 3.3 DESIGN METHODOLOGY

There are three ways to maintain the integrity of unbonded post-tensioned masonry walls when openings are introduced. These include (1) vertical isolation, (2) horizontal isolation, and (3) single panel approximation. The isolation technique aims to divide a single unbonded post-tensioned masonry wall with openings into multiple sections that do not contain an opening. This is done with the use of cold joints and is detailed in the next two sections. Door openings should always be designed by using either of the isolation methods. The single panel approximation is based on the observation described earlier where a small hole in the wall has little effect on the wall performance. At low levels of lateral deformation, unbonded post-tensioned masonry walls with openings and a similarly sized wall without an opening globally behave the same. The critical opening dimensions that preclude the use of the single panel approximation will be discussed later in this paper.

#### 3.3.1 Vertical Isolation

Vertical isolation, as shown in Fig. 4, uses vertical cold joints to separate the wall into two rocking piers and a central opening. The opening is supported by the foundation and is

constructed with minimal reinforcement. Some reinforcement is needed for control of shrinkage, out-of-plane loading, and resistance to the inertial mass of this section upon earthquake forces. The two rocking piers are designed in the usual manner<sup>3</sup> for a cantilever pier. It is recommended to restrict the lateral deformation such that pounding between adjacent wall elements is minimized.

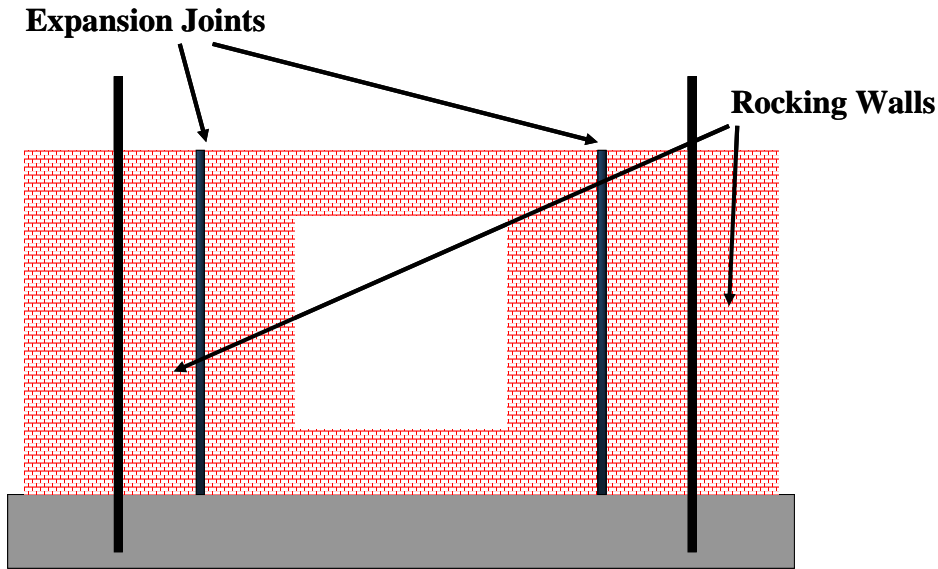


**Figure 4: Vertical Isolation**

### **3.3.2 Horizontal Isolation**

Fig. 5 contains an example of horizontal isolation where cold joints are placed at the top and bottom of the opening. These joints result in the formation of two rocking piers on either side of the opening. The bottom panel and top panel must be built to withstand the loads applied by the rocking piers. The bottom panel may be built traditionally while the top panel must be cast with the floor above it or the roof structure. The two piers deform by double rocking. This results in anti-symmetrical base crack profiles along the top and bottom of the piers which can be seen in Fig. 1. This anti-symmetry has interesting results. If the post-tensioning bars are placed symmetrically in the section and outside of the compression

zone, each bar will elongate by the same amount since the walls follow a double rocking mechanism. As a result, all of the bars will have identical bar forces and will yield simultaneously. Another characteristic of horizontal isolation and the anti-symmetric base profiles is that the resultant post-tensioning force has a longer moment arm than a wall undergoing a singularly rocking deformation. So at the same lateral displacement, double rocking wall requires a larger lateral force. Unbonded post-tensioned clay brick masonry walls with openings built using horizontal isolation are more robust than those that are vertically isolated. However, it is critical to properly detail the pier top and bottom, which is the focus of the experimental portion of the research.

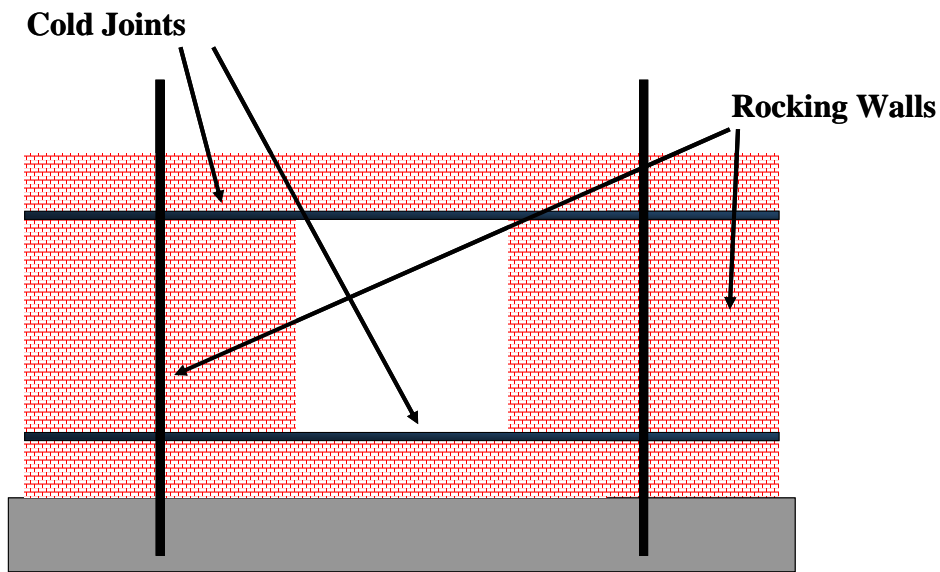


**Figure 5: Horizontal Isolation**

### **3.3.2.1 Wall Design**

The walls were designed to fit on a reusable concrete base that measured 2400 mm x 450 mm x 1200 mm. The lateral loading applied by an actuator was at a typical floor-to-ceiling height of 2440 mm. The wall, constructed of two clay brick wythes, measured 2285

mm x 2665mm and had a width of 300 mm. The bottom nine courses were constructed and then two identical piers measuring a height of 1520 mm were constructed such that an opening of 900 mm x 1520 mm was centered in the wall. Then four PVC pipes were placed, two in each pier, spaced 300 mm apart and centered within the pier. The PVC pipes allow the post-tensioning bars to be unbonded when the grout is poured within the wall's cavity.

Next, the wall is grouted in two lifts. The first lift fills in the bottom nine courses while the second lift fills in the two piers. Grouting the wall in two lifts creates a cold joint at the base of the piers. The benefit of constructing the walls in this manner ensures that the lateral force applied to the wall does not create any cracks that can not be closed by the post-tensioning force after the lateral load is removed. If the cold joint was not present then there would be a positive connection between the pier and the bottom courses. This positive connection would create a vertical crack at the end of the pier down to the foundation. The post-tensioning force would be unable to close this crack after the lateral load is removed.

Then, a reusable concrete bond beam is placed on top of the masonry wall and connected to an actuator. The bond beam measures 2440 mm x 450 mm x 450 mm and contains four ducts that allow threaded rods to pass through the member. These threaded rods are bolted to the actuator so that the actuator can apply cyclic loading to the wall. Again, there is no positive connection between the bond beam and piers. Just as before, at the base of the piers, the top of the piers will deform by rocking resulting in a double rocking mechanism. Here the lateral load applied to the wall at the bond beam is distributed equally to the piers through friction. Then friction at the base of the pier continues to transfer the load to the bottom nine courses and finally into the footing.

Finally, the 16 mm post-tensioning bars, located within the PVC, are tensioned. The post-tensioning force is one third of the yield force of the bar. The post-tensioning bar force is ultimately the designer's choice; However, it is important to note that if too high a force is selected, the wall will be unable to sustain large deformations prior to yielding of the post-tensioning steel. For the first test a 60 KN force in each bar is chosen. The completed setup can be seen in Fig. 6.



**Figure 6: Test Setup**

### ***3.3.2.2 Test Setup and Testing Methods***

Once the walls were constructed on the footing, the whole assembly was lifted and placed on a series of 150mm square high-density particle board sections at the four corners of the footing. A single post-tensioning bar was placed trough the footing, particle board, and strong floor. The post-tensioning bar was then stressed to prevent any rocking/over-turning of the wall and footing assembly. Hydrastone cement was poured under and around the footing

to ensure proper bond between the footing and the laboratory floor while providing a smooth contact surface between the footing and the strong floor. A steel beam and column guidance frame was constructed around the specimen to minimize any accidental out-of-plane deformation. Finally the hydraulic actuator was connected to the specimen with four threaded steel rods.

The instrumentation consisted of linear potentiometers, string potentiometers, and load cells. Linear potentiometers were used to measure the uplift at the toe and heel of each pier. They were also placed on the sides of the wall to capture the change in deformation along the length of the wall. The string potentiometer was located at the height of the actuator to measure displacement and the load cells captured the force in each post-tensioning bar in the wall. Finally, the actuator's load cell was able to measure the force applied to the wall. All of the instruments were connected to a data acquisition system that took measurements once a second which provided at least 120 data points per cycle of loading.

The initial post-tensioning force was one-third of the theoretical bar yield force. In previous testing<sup>11</sup> yielding of the post-tensioning bars was a critical parameter in the design of unbonded post-tensioned masonry walls. In these tests, the bar force was lowered from the 75% of yield used in the earlier tests.

During testing, the displacements were gradually increased in accordance to ACI ITG/T1.1-99 "Acceptance Criteria for Moment Frames Based on Structural Testing<sup>1</sup>." Since the displacement of the wall when the post-tensioning bars yield is hard to predict, the displacements were recorded as drift ratios - a percentage of the wall's height. At each drift ratio the wall was cycled three times. The loading history prescribed by ACI ITG/T1.1-99

accurately balances the softening of repeated cycles with the ultimate strength and displacement capacity of the wall.

### ***3.3.2.3 Wall Number 1: Unconfined***

The first wall was used as a control. There is no additional detailing within the wall to improve its performance. The wall is expected to rock until the post-tensioning bars yield, eventually resulting in a complete loss of stiffness near zero displacement. Also the two piers should be self-centering with a base crack at the cold joint at the base of the window opening.

#### ***3.3.2.3.1 Observations***

While approaching the first step in the loading history (drift ratio 0.25%), the base crack develops at the base of the window as expected. Also, as the piers are “double rocking” a second base crack opened at the top at interface between the masonry wall and the bond beam. This mechanism will have a significant effect on the design of unbonded post-tensioning walls that follow this “double rocking” pattern.

At the next drift ratio of 0.35% a vertical crack begins to develop. This vertical crack is the result of impending compression failure. On the third cycle at this drift ratio the crack extends from the toe region of the pier to the footing. Since the crack extends all the way to the footing, higher drift ratios open the crack further and at a drift ratio of 1% the wall begins to slide. Fig. 7 shows the relationship between lateral displacement and sliding, measured mechanically. Fig. 8 is a picture of the observed sliding.

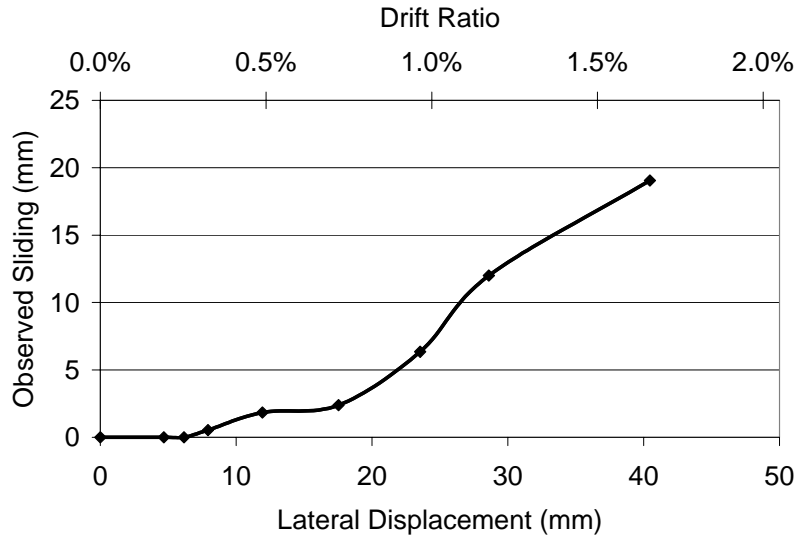


**Figure 7: Observed Sliding**



**Figure 8: Pier Sliding and Damage**

A combination of sliding and rocking is the mode of deformation for the remainder of the test. At a drift ratio of 1.75% the vertical crack grows to 7mm in width and the toe

regions of the piers begins to fail in compression. The wall becomes unstable because of the excessive sliding at a drift ratio of 2.25%.

### 3.3.2.3.2 Test Results

The response of this wall is undesirable. Upon inspection of the force-deformation hysteresis in Figure 9 and pictures of the test specimen in Figure 8 it is clear that the wall does not fully exhibit the benefits of unbonded post-tension construction. The problems are numerous.

- 1) There is a large amount of sliding, as much as 19mm.
- 2) Wide vertical cracks that cannot be closed by the post-tensioning force in the bars exist.
- 3) The wall is not self-centering as residual deformation exists.

Thus, a significant improvement in the detailing of the opening is necessary.

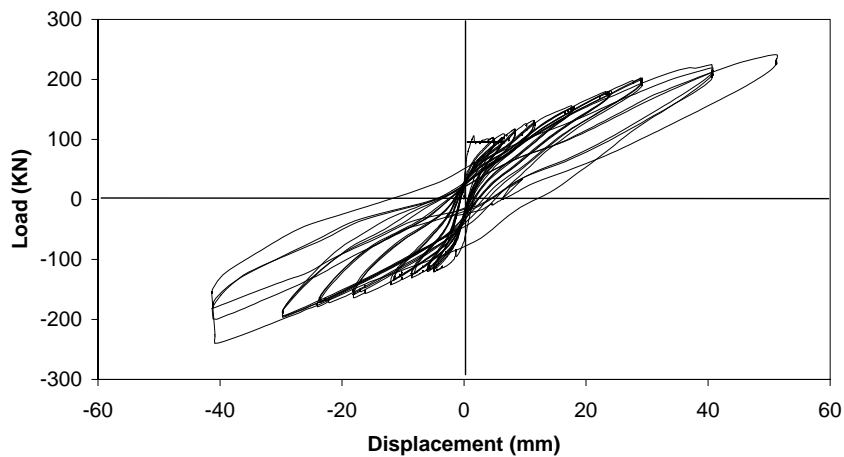


Figure 9: Structural Response of Wall 1

### 3.3.2.3.3 Recommendations for Next Test

Unbonded post-tensioned walls with a window opening displayed a deformation mechanism that was not seen in past tests. The combination of sliding and rocking caused the

wall to become prematurely unstable. The initial vertical crack allowed the wall to begin sliding. The sliding led to a large crack width that the post-tensioning could not close. Sliding also impacted the wall's capability to self-center. These are some of the major benefits for using unbonded post-tensioned masonry as a structural system which must be restored in order to utilize the proposed system.

In order to address these issues, the use of confinement plates was explored for the second test. The use of confinement plates in masonry was first proposed by Priestley and Bridgeman (1974). Using confinement plates in the toe regions of the wall will increase the compressive strength of the masonry, which in turn should delay the onset of the vertical crack and presumably improve the overall appearance of the wall. Also, previous tests<sup>2</sup> on masonry prisms shows that the bond between the masonry and the confinement plates is strong enough to yield and even fracture the steel that comprises the confinement plates. This strong bond should reduce the vertical crack growth after it forms.

#### ***3.3.2.4 Wall Number 2: Confinement Plates***

As mentioned above, the second test includes confinement plates in the bed joints of the masonry in the toe regions of the wall piers. The presence of the confinement plates should improve the performance of the wall by reducing the effect the initial vertical crack has on the deformation capacity of the wall. A picture of the wall that shows the location of the confinement plates is shown in Fig. 10 while the plate itself is shown in Fig. 11.

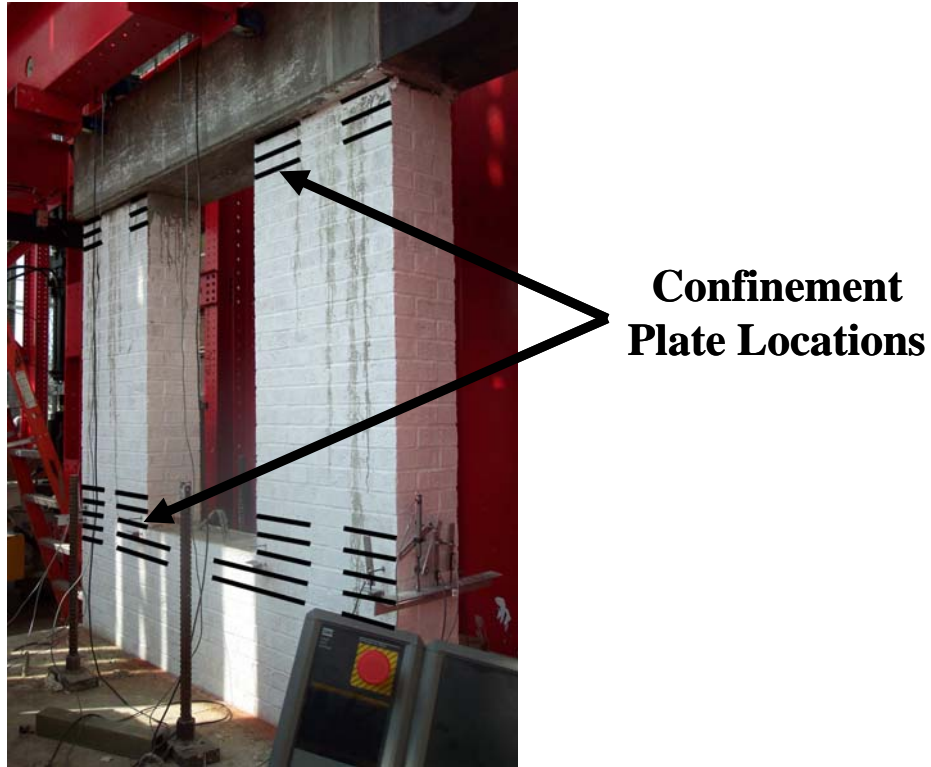


**Figure 10: Location of Confinement Plates in Wall 2**

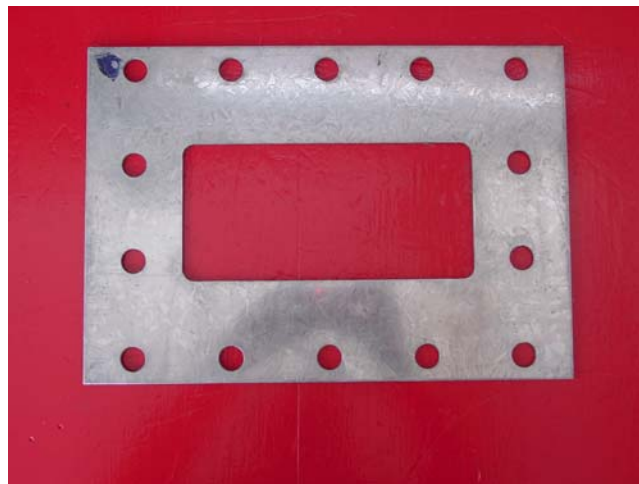


**Figure 11: Confinement Plate**

#### **3.3.2.4.1 Observations**

Similar to the unconfined test, the base crack immediately opens at the base of the window opening. The first important observation occurred at a drift ratio of 0.35%. At this

drift ratio, a singular shear crack develops in both piers. The shear crack begins 75mm from the corners at the bottom of the window opening and extends to the footing as shown in Fig. 12. This will prove to be problematic. As observed in the previous test, as the crack grows from the base of the pier to the footing, the deformation mechanism changes from rocking to sliding. On the positive side, the confinement plates increased the compression strength of the masonry and thus delays the formation of the vertical crack.



**Figure 12: Initial Crack in Wall 2**

At a drift ratio of 1.0%, sliding becomes the dominant form of deformation. In fact, the base crack begins to decrease in size. At the previous drift ratio of 0.75%, the base crack was 7mm wide at its largest point. Now the same base crack measures 2.5mm. The shear crack width went from being immeasurable with a ruler to just over 8mm.

As testing continues, the wall is no longer self-centering at a drift ratio of 1.25%. This is a result of the combination of the sliding and rocking deformation mechanism. At the peak displacement the shear is large in comparison to the base crack. Upon load reversal the wall rocks back and the in-plane force gradually reduces. At zero in-plane force the shear crack remains open as there is no force in the system to close the crack. Therefore the entire pier has rigidly displaced the width of the shear crack. The beneficial ability of unbonded post-tensioned masonry to self-center is now no longer present in this wall. Finally at a drift ratio of 1.75% the in-plane load begins to decrease and the test is halted because the 20mm shear crack makes the wall unstable.

#### ***3.3.2.4.2 Test Results***

The force displacement history is shown in Figure 13. The effect that sliding has on the behavior of the wall is obvious. As displacement increases the wall loses its self-centering characteristic. On the last loading cycle the relationship between the shear crack width and residual displacement is clear. As mentioned above at a displacement of 40mm (drift ratio 1.75%) the shear crack measures 20mm in width. As the wall unloads a residual displacement of approximately 20mm is observed.

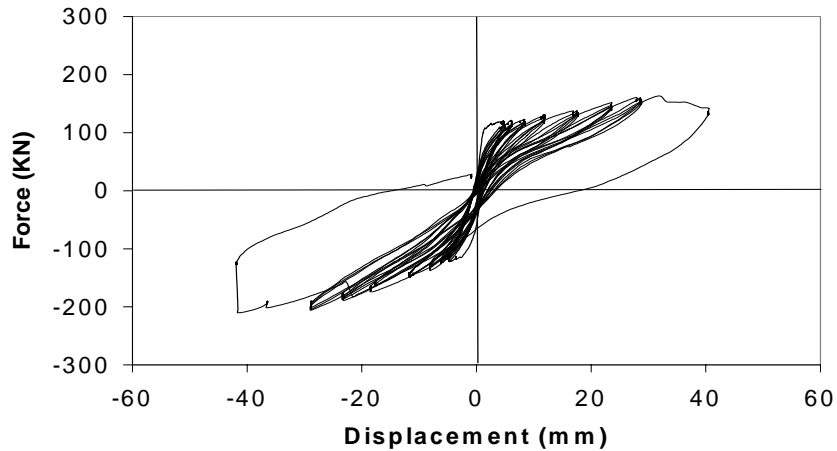


**Figure 13: Structural Response of Wall 2**

### ***3.3.2.4.3 Recommendations for Next Test***

Just like the previous test, a crack that extends from the base of the rocking pier to the footing is the cause of premature failure. Steel, in the form of confinement plates, was used to increase the axial strength of the masonry and thus prevent the compressive vertical crack from occurring. It is therefore logical to use steel again to prevent the shear crack from opening. The proposed solution was to place horizontal mild steel in the wall below the window to minimize shear cracking.

### ***3.3.2.5 Wall Number 3: Horizontal Steel***

The third version of the wall used four 25mm horizontal steel reinforcing bars in the grouted cavity below the window. Two of the bars were placed one joint below the opening and the other two were placed one joint above the footing. For design, the horizontal steel should be selected in accordance to the recommendations made by Kowalsky<sup>5</sup> for the serviceability limit state. This corresponds to a steel limit strain of 0.015. Any strain beyond this point would require repair, thusly interrupting the use of the structure. However, to simplify design and avoid requiring the complete stress-strain relationship of the reinforcing

steel being used, their stress should be limited to ninety percent of yield. Therefore, based on the base shear,  $V_b$ , the required amount of steel to be at each location, just below the opening and above the foundation, is found by equation 1.

$$A_s = \frac{V_b}{0.9\sigma_y} \quad (\text{Eq. 1})$$

In addition to the reinforcing bars, confinement plates were again placed in the bed joints of the piers. The combined use of reinforcing bars and confinement plates should result in improved performance of the unbonded post-tensioned masonry wall with openings. The design of this specimen is shown in Fig. 14.

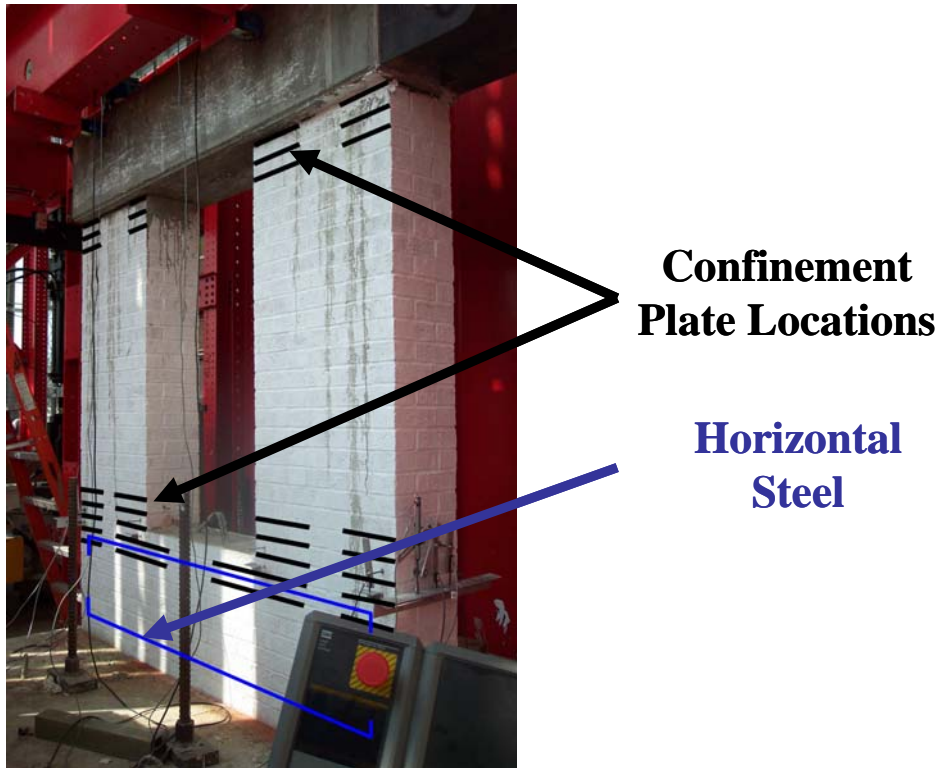


Figure 14: Design of Wall 3

### 3.3.2.5.1 Observations

Once again, the base crack develops at the base of the window opening, and just as the previous test, a diagonal shear crack begins to develop at the drift ratio of 0.25%. However

the shear crack does not widen, and the form of deformation is rocking for the entire test. Testing is stopped at the drift ratio of 1.75% due to load cell capacity limitations. At this point the base crack measured 12mm in width. The shear crack measured 1.5mm just below the window opening and the horizontal steel never allowed the shear crack to get wider than 1mm below its placement at the bed joint below the window. For the first time in the series of testing crushing of the mortar joint and spalling of the masonry was observed at the base of the pier.

### 3.3.2.5.2 Test Results

Figure 15 shows the force-displacement curve for the test with confinement plates and horizontal steel. The wall remains self-centering throughout the experiment. This test configuration proves to be the best as the piers rock in the intended manner. The horizontal steel prevents hairline shear and vertical cracks from widening. Without the presence of these cracks, sliding has been minimized. When comparing the force-displacement curve in Figure 15 with those of previous configurations, it is clear that there is minimal residual deformation as the curves pass close to the origin throughout the wall response.

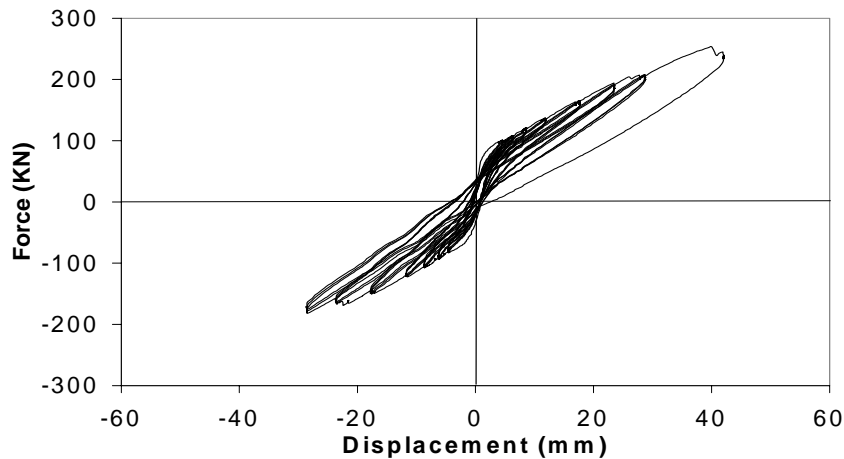


Figure 15: Structural Response of Wall 3

### **3.4 PANEL APPROXIMATION**

As discussed earlier, an alternative approach for design is to idealize a wall with an opening as a single panel. The concept of a ‘single panel approximation’ suggests that unbonded clay brick masonry walls with openings behave similarly to those without openings until the compressive strut is destabilized. As discussed previously, figures 2 and 3 show the effect of opening size on the compressive strut. At one extreme it is clear that a ‘pinhole’ size opening in a wall have little effect on its force-displacement curve. However, there is an opening size where the behavior will change from single to dual panel rocking, thus requiring the detailing previously described in this paper. Discussed in the following section is a finite element-based parametric study to investigate the impact of opening size on wall performance.

#### **3.4.1 Single Story Panel Approximation**

A parametric study in ANSYS is used to find this divergent point in the force-displacement curves of single story structures. The parameters of the study were (1) aspect ratio of the unbonded post-tensioned masonry wall, (2) axial load ratio, and (3) the horizontal and vertical size of the opening. With each increase in the aspect ratio an additional opening was added. For example a wall with an aspect ratio of two consisting of two identically sized openings located one on top of the other. The results of the parametric study are shown in Tables 1-3. Each aspect ratio has its own allowable drift table. The table is divided into a nine sections based on the horizontal and vertical opening aspect ratio. Within each of these nine sections there are five different axial load ratios. For example, a wall that measures 1200mm long by 2400mm tall that contains 600 mm square openings with an axial load ratio of 5% can achieve a drift ratio of 0.75% before its force-displacement curve begins to diverge

from the response of an identical wall without an opening. Openings in the wall have a greater effect as the aspect ratio is increased. Furthermore, the vertical dimension of the opening has a greater effect on response than the horizontal dimension of the opening.

**Table 1: Wall aspect ratio of 1**

		<b>X OPENING ASPECT RATIO</b>					
		0.25		0.5		0.75	
<b>Y OPENING ASPECT RATIO</b>	0.25	axial 1%	drift 2.00%	axial 1%	drift 2.00%	axial 1%	drift 2.00%
		5%	2.00%	5%	2.00%	5%	2.00%
		10%	2.00%	10%	2.00%	10%	2.00%
		15%	2.00%	15%	2.00%	15%	1.75%
	20%	2.00%	20%	2.00%	20%	1.75%	
	0.5	axial 1%	drift 2%	axial 1%	drift 2.00%	axial 1%	drift 2.00%
		5%	2.00%	5%	2.00%	5%	2.00%
		10%	2.00%	10%	2.00%	10%	2.00%
		15%	2.00%	15%	1.75%	15%	1.75%
	20%	2.00%	20%	1.75%	20%	1.75%	
	0.75	axial 1%	drift 2.00%	axial 1%	drift 2.00%	axial 1%	drift 2.00%
		5%	2.00%	5%	2.00%	5%	2.00%
10%		2.00%	10%	2.00%	10%	2.00%	
15%		2.00%	15%	1.75%	15%	1.75%	
20%	2.00%	20%	1.75%	20%	1.50%		

**Table 2: Wall aspect ratio of 2**

		<b>X OPENING ASPECT RATIO</b>					
		0.25		0.5		0.75	
<b>Y OPENING ASPECT RATIO</b>	0.25	axial 1%	drift 2.00%	axial 1%	drift 1.25%	axial 1%	drift 1.00%
		5%	2.00%	5%	1.25%	5%	0.75%
		10%	1.75%	10%	1.00%	10%	0.50%
		15%	1.75%	15%	0.75%	15%	0.35%
	20%	1.50%	20%	0.75%	20%	0.35%	
	0.5	axial 1%	drift 1.00%	axial 1%	drift 1.25%	axial 1%	drift 1.00%
		5%	0.75%	5%	0.75%	5%	0.75%
		10%	0.75%	10%	0.50%	10%	0.50%
		15%	0.50%	15%	0.50%	15%	0.35%
	20%	0.50%	20%	0.35%	20%	0.35%	
	0.75	axial 1%	drift 1.00%	axial 1%	drift 0.75%	axial 1%	drift 0.75%
		5%	0.50%	5%	0.50%	5%	0.50%
10%		0.50%	10%	0.50%	10%	0.35%	
15%		0.35%	15%	0.35%	15%	0.25%	
20%	0.25%	20%	0.25%	20%	0.20%		

**Table 3: Wall aspect ratio of 3**

		X OPENING ASPECT RATIO					
		0.25		0.5		0.75	
Y OPENING ASPECT RATIO	0.25	axial 1%	drift 1.75%	axial 1%	drift 1.25%	axial 1%	drift 0.75%
		5%	1.50%	5%	1.25%	5%	0.75%
		10%	1.50%	10%	0.75%	10%	0.35%
		15%	1.25%	15%	0.75%	15%	0.35%
		20%	1.25%	20%	0.50%	20%	0.25%
	0.5	axial 1%	drift 1.00%	axial 1%	drift 1.25%	axial 1%	drift 0.75%
		5%	0.75%	5%	0.75%	5%	0.75%
		10%	0.75%	10%	0.50%	10%	0.35%
		15%	0.50%	15%	0.35%	15%	0.25%
		20%	0.50%	20%	0.35%	20%	0.20%
	0.75	axial 1%	drift 0.75%	axial 1%	drift 0.75%	axial 1%	drift 0.25%
		5%	0.35%	5%	0.50%	5%	0.25%
10%		0.25%	10%	-	10%	-	
15%		-	15%	-	15%	-	
20%		-	20%	-	20%	-	

### 3.4.2 Multi-story Panel Approximation

While the tables previously discussed were developed assuming that the entire axial load of the building is applied at the roof level, multi-storey buildings will have axial loads applied to the wall at each storey. Therefore, use of the tables to design multi-storey buildings introduces a minor error in the design. However, it is important to note that the lever arms applied to each axial load in a multistorey building are greater than the single lever arm utilized when the entire load is placed at the roof level. As a consequence, the real multi-storey building will be somewhat stiffer than the structure utilized to generate Tables 1 through 3 resulting in a conservative design. The following equation is used to calculate the axial load ratio required to use the tables:

$$Axial\ Ratio = \frac{\sum N + R}{A_{section}} \quad (Eq. 2)$$

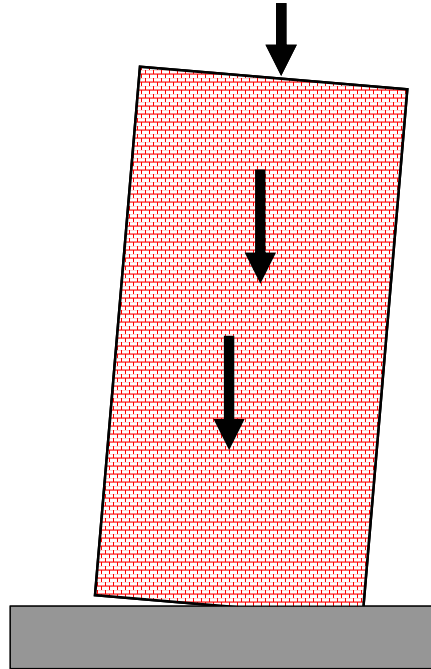


**Figure 16: Effect of Story Loads on Single Panel Approximation**

From here the same method is used as described above. Consider the following example: For a wall with an aspect ratio of two; an axial load ratio, as found by equation 2, of 5%; and X and Y opening aspect ratios of 50%; the resulting allowable drift is 0.75%.

### **3.5 CONCLUSION**

After examining the results of the full-scale testing and a parametric study using ANSYS the following conclusions can be reached:

- 1) It is possible to design unbonded post-tensioned clay brick masonry walls with openings to maintain all of the benefits of walls without openings.
- 2) Designs using horizontal isolation must be detailed properly. The bottom and top panels requires confinement plates and supplemental horizontal mild steel to prevent excessive cracks from developing.

- 3) Unbonded post-tensioned clay brick masonry walls with openings approximately behave like their counterparts without openings until the compressive strut is disrupted by excessive displacement.

### 3.6 REFERENCES

1. American Concrete Institute. (1999). "Acceptance Criteria for Moment Frames Based on Structural Testing," *ACI Provisional Standard*.
2. Ewing, B.D. and Kowalsky, M. J. (2004). "Compressive Behavior of Unconfined and Confined Clay Brick Masonry." *Journal of Structural Engineering*, Vol. 130, No. 4, pp. 650-661.
3. Ewing, B.D. and Kowalsky, M.J. (2008). "Displacement-based Design of Unbonded Post-tensioned Masonry Walls." *To be submitted*.
4. Holden, T., Restrepo, J., and Mander, J. (2003). "Seismic Performance of Precast Reinforced and Prestressed Concrete Walls," *Journal of Structural Engineering*, Vol. 129, No. 3, pp 286-296.
5. Kowalsky, M.J. (2000). "Deformation Limit States and Implications on Design of Circular RC Bridge Columns." *ASCE Journal of Structural Engineering*, Vol. 126, No. 8, pp. 869-878.
6. Laursen, P. T. and Ingham, J. M. (2004). "Structural Testing of Large-Scale Post-Tensioned Concrete Masonry Walls," *Journal of Structural Engineering*, Vol. 130, No. 10, pp 1497-1505.
7. Masonry Standards Joint Committee. (2002), "Building Code Requirements for Masonry Structures (ACI 530-02/ASCE 5-02/TMS 402-02)," American Concrete Institute; Structural Engineering Institute of the American Society of Civil Engineers; The Masonry Society.

8. Paulay, T. and Priestley, M.J.N. (1992). *Seismic Design of Reinforced Concrete and Masonry Buildings*, A Wiley-Interscience Publication, New York, 1992.
9. Priestley, M.J.N. and Bridgeman, D.O. (1974). "Seismic Resistance of Brick Masonry Walls." *Bulletin of the New Zealand National Society for Earthquake Engineering*, Vol. 7, No. 4, pp 167-187.
10. Priestley, M.J.N., and Tao, J.R. (1993). "Seismic Response of Precast Prestressed Concrete Frames with Partially Debonded Tendons." *PCI Journal*, Vol. 38, No. 1, pp 58-69.
11. Rosenboom, O. A. and Kowalsky, M. J. (2004). "Reversed In-Plane Cyclic Behavior of Post-Tensioned Clay Brick Masonry Walls," *Journal of Structural Engineering*, Vol 130, No. 5, pp. 787-798.

JOURNAL ARTICLE NUMBER TWO

**4 EFFECT OF VARYING CONFINEMENT STRESS ON THE AXIAL  
STRESS-STRAIN RELATIONSHIP OF CONCRETE AND  
MASONRY**

BRYAN EWING

MERVYN KOWALSKY

# EFFECT OF VARYING CONFINEMENT STRESS ON THE AXIAL STRESS-STRAIN RELATIONSHIP OF CONCRETE AND MASONRY

Bryan Ewing

*Department of Civil, Construction and Environmental Engineering, North Carolina State University,  
Campus-Box 7908, Raleigh, NC-27695, USA*

Keywords: Analysis, Brick masonry, Stress strain relations

## 4.1 ABSTRACT

A problem arose when attempting to predict the behavior of a rocking unbonded post-tensioned masonry wall on a footing. Importing a stress-strain curve captured experimentally from uni-axial loading into a finite element program did not accurately predict the complete force-displacement envelope of the masonry wall. After further analysis it was determined that differences in the Young's modulus between the masonry wall and the footing causes a local varying confining stress. Previous solutions could not be adapted to this situation as they depend on variables not present in this case such as steel confinement ratio and yielding stress, or utilization of a constant confining stress throughout the axial loading path. A method for predicting the effect of varying confinement stress on the axial stress-strain relationship was developed for the interaction between a rocking unbonded post-tensioned masonry wall and its foundation. This method is described in this paper.

## 4.2 INTRODUCTION

Understanding the behavior of concrete subjected to confining stress is essential to solving a wide range of engineering problems. Researchers have studied this problem and developed constitutive models to describe the behavior of concrete. Although these models

adequately predict the behavior of concrete under confining stresses, many of the parameters are not present in masonry wall rocking mechanism problems. Parameters such as steel confinement ratio and yield stress are not applicable to problems where a structure rocks upon its foundation. Furthermore, in many of these constitutive models the confining stress is kept constant throughout the loading path. The existing models are not able to predict the behavior of rocking structures which is the motivation behind the research described in this paper.

The specific engineering problem that this paper will examine is the behavior of an unbonded post-tensioned clay brick masonry wall. Although masonry consists of various components (clay brick or concrete block, mortar, and grout) it is considered to be monolithic and behave in a similar manner as concrete for design and analysis purposes. Figure 1 shows the key components of an unbonded post-tensioned clay brick masonry wall and its rocking deflected shape. The area of interest is the interface between the base of the wall and the foundation. At this interface the wall and the foundation experience the same axial stress but have different Young's modulus and possibly different Poisson's ratio; thusly they will have different lateral expansions. The masonry wall has a lower modulus than the foundation and it will expand more laterally. However, due to displacement compatibility at the interface between the masonry wall and the foundation, caused by the frictional forces between the two, prevents the wall from laterally expanding as it would otherwise. The masonry wall's inability to expand results in a compressive stress that confines the masonry. Furthermore as the axial load increases, the confinement stress increases as well. In order to design or analyze an unbonded post-tensioned masonry wall the effect of varying confinement stress on the uni-axial stress strain relationship must be determined.

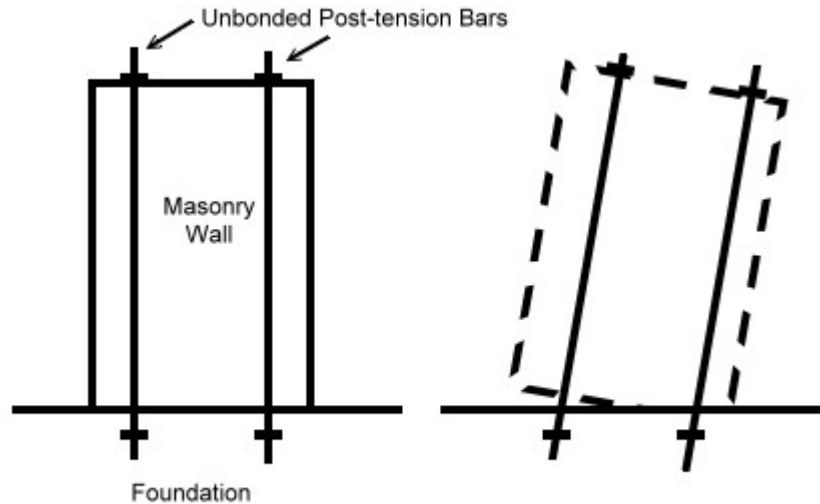


**Figure 1: Unbonded Post-tensioned Masonry Wall**

### **4.3 THEORETICAL MODEL**

The model is derived from basic material mechanics as shown in Figure 2. Two elements are shown. The top element from the wall and the bottom element from the foundation initially have the same cross-sectional area and are subjected to the same axial stress. However, the wall element has a lower modulus and laterally expands more than the foundation element. This is not possible as both elements' displacements must remain compatible, assuming adequate frictional bond has developed. Applying compatibility in lateral displacements causes a compressive stress in the wall and a tensile stress in the foundation. Tensile stresses are carried by the combination of concrete and steel reinforcement in the foundation until cracking of the concrete. Once the concrete cracks, the steel reinforcement is forced to solely carry the tensile stress. By using fundamental mechanics of materials and the stress-strain relationship<sup>3,12</sup>, developing a stress-strain relationship for masonry and concrete that has gradually increasing confinement stresses is possible.

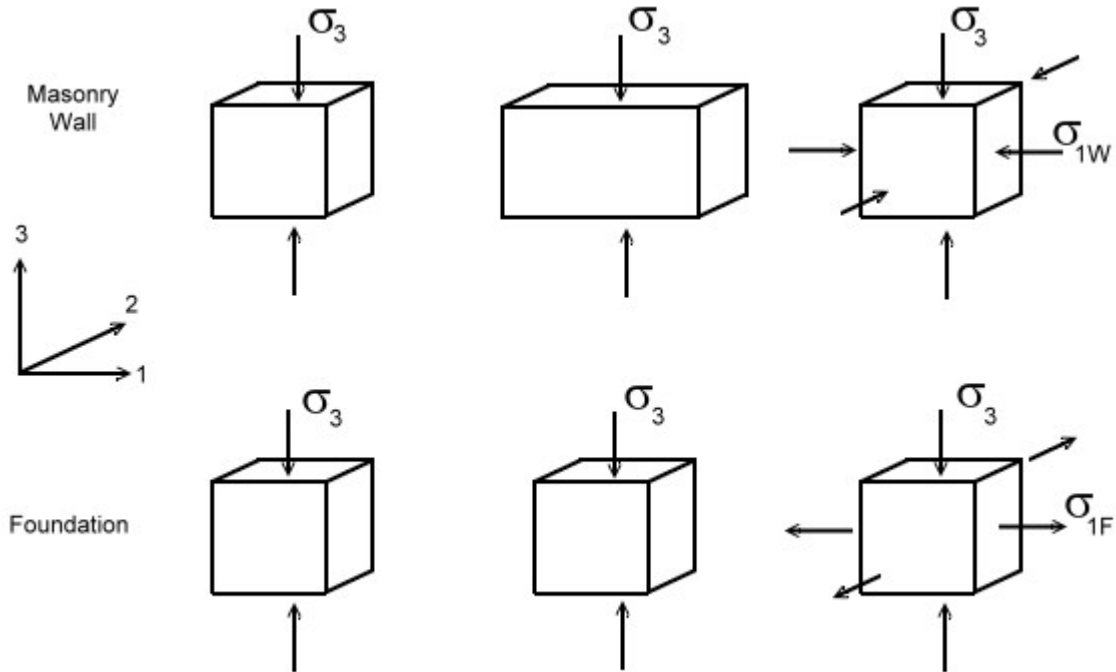


Figure 2 Masonry Wall and Foundation Stress State Blocks

#### 4.3.1 Mechanics of Materials

The first step in solving the problem is understanding the mechanics involved. From examining Figure 2 several compatibility relationships are observed. The basic principle is that as an incremental axial stress is applied to the wall and foundation that the lateral displacements within the masonry wall and foundation are the same. The compatibility equations<sup>5</sup> are as follows:

Wall:

$$\Delta \varepsilon_{1w} = (1 - \nu_{1w}) \frac{\Delta \sigma_{1w}}{E_{1w}} - \nu_{3w} \frac{\Delta \sigma_3}{E_{3w}} \quad (\text{Eq. 1})$$

Foundation:

$$\Delta \varepsilon_{1w} = (1 - \nu_{1f}) \frac{\Delta \sigma_{1f}}{E_{1f}} - \nu_{3f} \frac{\Delta \sigma_3}{E_{3f}} \quad (\text{Eq. 2})$$

Foundational Steel:

$$\Delta \varepsilon_s = \Delta \varepsilon_{1w} \quad (\text{Eq. 3})$$

In addition to compatibility, the forces must be in equilibrium. Equation 4 shows the summation of the lateral forces.

$$\Delta F_w + \Delta F_f + \Delta F_s = 0 \quad (\text{Eq. 4})$$

where,

$$\Delta F_w = A_{\text{section}} \Delta \sigma_{1w} \quad (\text{Eq. 5})$$

$$\Delta F_f = A_{\text{section}} \Delta \sigma_{1f} \quad (\text{Eq. 6})$$

$$\Delta F_s = \rho_s A_{\text{section}} E_s \Delta \varepsilon_s \quad (\text{Eq. 7})$$

The reinforcing steel ratio,  $\rho_s$ , is equal to the ratio of the area of steel to the sectional area of the foundation element and is assumed to remain constant throughout the foundation's deformation.

Substituting equations 5-7 into equation 4 and then simplifying the result concludes in the equilibrium equation that governs the elements behavior as shown in equation 8.

$$\Delta \sigma_{1w} + \Delta \sigma_{1f} + \rho_s E_s \Delta \varepsilon_s = 0 \quad (\text{Eq. 8})$$

Finally the vertical strains are calculated by equations 9 and 10.

$$\Delta \varepsilon_{3w} = \frac{\Delta \sigma_3}{E_{3w}} - 2\nu_{3w} \frac{\Delta \sigma_{1w}}{E_{1w}} \quad (\text{Eq. 9})$$

$$\Delta \varepsilon_{3f} = \frac{\Delta \sigma_3}{E_{3f}} - 2\nu_{3f} \frac{\Delta \sigma_{1f}}{E_{1f}} \quad (\text{Eq. 10})$$

### 4.3.2 Equivalent Uni-axial Strain

Elwi<sup>3</sup> defines the incremental equivalent uni-axial strain,  $d\varepsilon_{iu}$ , as “the increment of strain in direction  $i$  that the material would exhibit if subjected to a (uni-axial) stress increment  $d\sigma_i$  with other stress increments equal to zero.” The term is fictitious but allows one to use a uni-axial stress-strain relationship to develop a bi- or tri-axial relationship. Incremental equivalent uni-axial strain has the form

$$d\varepsilon_{iu} = \frac{d\sigma_i}{E_i} \quad (\text{Eq. 11})$$

Elwi<sup>3</sup> explains the derivation of the incremental equivalent uni-axial strain in great detail. To briefly summarize, the relationship between the incremental stresses and strains is

$$\{d\sigma\} = [C]\{d\varepsilon\} \quad (\text{Eq. 12})$$

where the symmetrical constitutive matrix  $[C]$  is written as

$$[C] = \frac{1}{\phi} \begin{bmatrix} E_1(1 - \mu_{32}^2) & \sqrt{E_1 E_2}(\mu_{13}\mu_{32} + \mu_{12}) & \sqrt{E_1 E_3}(\mu_{12}\mu_{32} + \mu_{13}) & 0 \\ & E_2(1 - \mu_{13}^2) & \sqrt{E_2 E_3}(\mu_{12}\mu_{13} + \mu_{32}) & 0 \\ & & E_1(1 - \mu_{12}^2) & 0 \\ & & & G_{12}\phi \end{bmatrix} \quad (\text{Eq. 13})$$

and

$$\mu_{12}^2 = \nu_{12}\nu_{21} \quad (\text{Eq. 14a})$$

$$\mu_{23}^2 = \nu_{23}\nu_{32} \quad (\text{Eq. 14b})$$

$$\mu_{13}^2 = \nu_{13}\nu_{31} \quad (\text{Eq. 14c})$$

$$\phi = 1 - \mu_{12}^2 - \mu_{23}^2 - \mu_{13}^2 - 2\mu_{12}\mu_{23}\mu_{13} \quad (\text{Eq. 14d})$$

$$G_{12} = \frac{1}{4\phi} \left[ E_1 + E_2 - 2\mu_{12}\sqrt{E_1 E_2} - \left( \sqrt{E_1}\mu_{23} + \sqrt{E_2}\mu_{31} \right)^2 \right] \quad (\text{Eq. 14e})$$

Elwi<sup>3</sup> further writes equation 12 as

$$\begin{Bmatrix} d\sigma_1 \\ d\sigma_2 \\ d\sigma_3 \\ d\tau_{12} \end{Bmatrix} = \begin{bmatrix} E_1 B_{11} & E_1 B_{12} & E_1 B_{13} & 0 \\ E_2 B_{21} & E_2 B_{22} & E_2 B_{23} & 0 \\ E_3 B_{31} & E_3 B_{32} & E_3 B_{33} & 0 \\ 0 & 0 & 0 & G_{12} \end{bmatrix} \begin{Bmatrix} d\varepsilon_1 \\ d\varepsilon_2 \\ d\varepsilon_3 \\ d\gamma_{12} \end{Bmatrix} \quad (\text{Eq. 15})$$

The coefficients  $B_{ij}$  can be found by comparing equation 15 with the terms in equation 13. And the incremental equivalent uni-axial strain is derived by substituting equation 15 into equation 11. The solution for finding the incremental equivalent uni-axial strain is

$$d\varepsilon_{iu} = B_{i1}d\varepsilon_1 + B_{i2}d\varepsilon_2 + B_{i3}d\varepsilon_3; i = 1,3 \quad (\text{Eq. 16})$$

#### 4.4 STRESS-STRAIN RELATIONSHIP MODEL

The uni-axial stress-strain relationship that will be utilized in this paper is the one initially developed by Saenz<sup>13</sup>. Elwi<sup>3</sup> incorporates the concept of equivalent uni-axial strain and writes the Saenz's equation as

$$\sigma_i = \frac{E_o \varepsilon_{iu}}{1 + (R + R_E - 2) \frac{\varepsilon_{iu}}{\varepsilon_{ic}} - (2R - 1) \left( \frac{\varepsilon_{iu}}{\varepsilon_{ic}} \right)^2 + R \left( \frac{\varepsilon_{iu}}{\varepsilon_{ic}} \right)^3} \quad (\text{Eq. 17})$$

where

$$R_E = \frac{E_o}{E_{\text{sec}}} \quad (\text{Eq. 18a})$$

$$E_{\text{sec}} = \frac{\sigma_{ic}}{\varepsilon_{ic}} \quad (\text{Eq. 18b})$$

$$R_\sigma = \frac{\sigma_{ic}}{\sigma_{if}} \quad (\text{Eq. 18c})$$

$$R_\varepsilon = \frac{\varepsilon_{if}}{\varepsilon_{ic}} \quad (\text{Eq. 18d})$$

$$R = R_E \frac{R_\sigma - 1}{(R_\epsilon - 1)^2} - \frac{1}{R_\epsilon} \quad (\text{Eq. 18e})$$

The relationships between  $\sigma_{ic}$  and  $\epsilon_{ic}$  and between  $\sigma_{if}$  and  $\epsilon_{if}$  are shown in Figure 3.

Elwi<sup>3</sup> suggested using certain values for  $\sigma_{if}$  and  $\epsilon_{if}$ . The suggestions were:

$$\sigma_{if} = \frac{\sigma_{ic}}{4} \quad (\text{Eq. 19})$$

$$\epsilon_{if} = 4\epsilon_{ic} \quad (\text{Eq. 20})$$

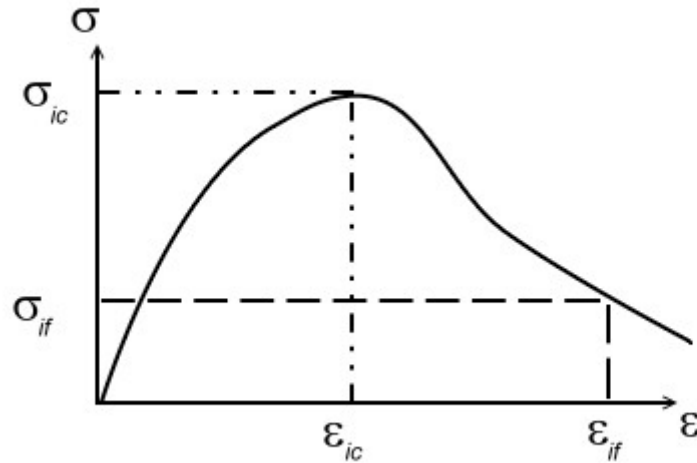


**Figure 3 Sample Stress-strain Relationship**

During the development of the stress-strain relationship of masonry and concrete subjected to a varying confinement stress it is necessary to find the instantaneous modulus. This can be found by taking the derivative of equation 17 with respect to the equivalent uniaxial strain. The resulting modulus is

$$E_i = E_o \frac{1 + (2R - 1) \left( \frac{\epsilon_{iu}}{\epsilon_{ic}} \right)^2 - 2R \left( \frac{\epsilon_{iu}}{\epsilon_{ic}} \right)^3}{\left[ 1 + (R + R_E - 2) \left( \frac{\epsilon_{iu}}{\epsilon_{ic}} \right) - (2R - 1) \left( \frac{\epsilon_{iu}}{\epsilon_{ic}} \right)^2 + R \left( \frac{\epsilon_{iu}}{\epsilon_{ic}} \right)^3 \right]^2} \quad (\text{Eq. 21})$$

#### 4.4.1 Poisson's Ratio

The Poisson's ratio changes along the curve of the stress-strain relationship. The increasing confinement stresses are directly related to the lateral expansion of the masonry wall and the foundation. The amount of the lateral deformation is a function of the Poisson's ratio and therefore it is important to accurately predict how Poisson's ratio changes along the path of the stress-strain curve. Ottosen<sup>9</sup> proposed the following equations:

$$\nu = \nu_o, \text{ when } \beta \leq \beta_a \quad (\text{Eq. 22a})$$

$$\nu = \nu_f - (\nu_f - \nu_o) \sqrt{1 - \left( \frac{\beta - \beta_a}{1 - \beta_a} \right)^2}, \text{ when } \beta > \beta_a \quad (\text{Eq. 22b})$$

Ottosen<sup>9</sup> also proposed values for the initial Poisson's ratio  $\nu_o = 0.2$ , final Poisson's ratio,  $\nu_f = 0.36$ , and  $\beta_a = 0.8$ . The nonlinearity index,  $\beta$ , that was proposed by Ottosen<sup>9</sup> was later updated by Tiecheng<sup>15</sup>. Tiecheng<sup>15</sup> uses the following equation which is a function of the initial,  $J_2$ , and peak,  $J_{2f}$ , stress states:

$$\beta = \frac{\sqrt{J_2}}{\sqrt{J_{2f}}} \quad (\text{Eq. 23a})$$

$$J_2 = \frac{(\sigma_1 - \sigma_2)^2 + (\sigma_1 - \sigma_3)^2 + (\sigma_2 - \sigma_3)^2}{6} \quad (\text{Eq. 23b})$$

#### 4.4.2 Masonry Failure Criteria

Two additional unknowns in equations 17 and 21 are the peak stress,  $\sigma_{ic}$ , and peak strain,  $\varepsilon_{ic}$ . Substantial research<sup>1, 2, 5, 6, 8, 9, and 11</sup> has enabled the accurate prediction of the axial peak stress for concrete subjected to various levels of confining stresses. Ahmad<sup>1</sup> has developed equations to find the peak axial strain. With these two final pieces, an engineer can

use equations 17 and 21 to develop a stress-strain relationship for masonry and concrete under a varying confinement stress.

#### 4.4.2.1 Peak Stress

Sfer<sup>14</sup> performed a comparison of concrete cylinder test compressive strengths with values predicted by expressions developed by Richart<sup>12</sup>, Newman<sup>8</sup>, and Etse<sup>4</sup>. Richart<sup>12</sup> developed an expression that is widely accepted as an acceptable equation to predict the compressive strength of concrete under a confining stress. Newman<sup>8</sup> also proposed a relationship to describe the behavior. The Richart<sup>12</sup> and Newman<sup>8</sup> equations are shown in equations 24 and 25, respectively.

$$f_c + 4.1\sigma_L - \sigma_3 = 0 \quad (\text{Eq. 24})$$

$$\sqrt{A\left(\frac{\sigma_L}{f_c}\right)^2 + B\left(\frac{\sigma_L}{f_c}\right) + 1} - \left(\frac{\sigma_3}{f_c}\right) = 0 \quad (\text{Eq. 25})$$

where A and B are coefficients.

Ultimately, Sfer<sup>14</sup> shows that the extended Leon<sup>7</sup> model proposed by Etse<sup>4</sup> accurately predicts the compressive strength over a wider range of confining stresses than those of Richart<sup>12</sup> and Newman<sup>8</sup>. For this reason the Etse<sup>4</sup> model is the one the author will use and is described in the following equations.

$$\frac{3\rho^2}{2f_c^2} + \frac{m}{f_c} \left( -P + \frac{\rho}{\sqrt{6}} \right) = 0 \quad (\text{Eq. 26})$$

where

$$m = \frac{f_c^2 - f_t^2}{f_c f_t} \quad (\text{Eq. 27a})$$

$$P = \frac{\sigma_1 + \sigma_2 + \sigma_3}{3} \quad (\text{Eq. 27b})$$

$$\rho = \sqrt{\frac{1}{3}[(\sigma_1 - \sigma_2)^2 + (\sigma_1 - \sigma_3)^2 + (\sigma_2 - \sigma_3)^2]} \quad (\text{Eq. 27c})$$

#### 4.4.2.2 Peak Strain

The last remaining unknown in equation 17 is the peak equivalent strain,  $\varepsilon_{ic}$ . The peak equivalent strain, as shown in figure 3, is the strain that corresponds to the maximum equivalent stress. Ahmad<sup>1</sup> performed regression analysis and determined the equivalent peak strain is governed by two equations. The third equation is simply a law of solid mechanics and it provides a way to solve for the third peak strain, one for each dimension. The equations are as follows:

$$\frac{\gamma_{oct}}{(\gamma_{oct})_o} = -4.8629 + 12.756 \frac{\tau_{oct}}{P} \quad (\text{Eq. 28})$$

$$\frac{\varepsilon_{oct}}{\varepsilon_o} = 0.197877 \frac{P}{\sigma_o} e^{0.9475} \quad (\text{Eq. 29})$$

$$\frac{2\sigma_2 - \sigma_1 - \sigma_3}{2\sigma_1 - \sigma_2 - \sigma_3} = \frac{2\varepsilon_2 - \varepsilon_1 - \varepsilon_3}{2\varepsilon_1 - \varepsilon_2 - \varepsilon_3} \quad (\text{Eq. 30})$$

where

$$\gamma_{oct} = \frac{2}{3} \sqrt{(\varepsilon_1 - \varepsilon_2)^2 + (\varepsilon_2 - \varepsilon_3)^2 + (\varepsilon_3 - \varepsilon_1)^2} \quad (\text{Eq. 31a})$$

$$\varepsilon_{oct} = \frac{1}{3} (\varepsilon_1 + \varepsilon_2 + \varepsilon_3) \quad (\text{Eq. 31b})$$

$$(\gamma_{oct})_o = 0.001839 f_c^{0.1287} \quad (\text{in MPa}) \quad (\text{Eq. 31c})$$

$$\tau_{oct} = \frac{1}{3} \sqrt{(\sigma_1 - \sigma_2)^2 + (\sigma_2 - \sigma_3)^2 + (\sigma_3 - \sigma_1)^2} \quad (\text{Eq. 31d})$$

### 4.4.3 Masonry Wall Model Overview

The model is now complete. The model works on the premise that as an incremental axial stress,  $\Delta\sigma_3$ , is applied the wall and foundation will laterally expand. However, since the wall and foundation have different moduli they would normally expand different amounts. However, these lateral expansions must be compatible. This compatibility requirement induces a compressive confining stress in the wall and a lateral tensile stress in the foundation. The lateral expressions, equations 1 and 2, are set equal to each other resulting in two unknowns. The resulting equation is shown in equation 32.

$$\Delta\sigma_{1f} = E_{1f} \frac{(1-\nu_{1w}) \frac{\Delta\sigma_{1w}}{E_{1w}} - \nu_{3w} \frac{\Delta\sigma_3}{E_{3w}} + \nu_{3f} \frac{\Delta\sigma_3}{E_{3f}}}{(1-\nu_{1f})} \quad (\text{Eq. 32})$$

For an applied incremental axial stress,  $\Delta\sigma_3$ , the lateral stresses in the wall and foundation,  $\Delta\sigma_{1w}$  and  $\Delta\sigma_{1f}$ , can be found by simultaneously solving equations 4 and 32. Once these values are found the stress-strain relationship's tangent modulus can be found from equation 21. Then the process is repeated until the complete stress-strain relationship is solved. The incremental axial stress step is controlled by monitoring the change in modulus from one step to the next. Too large of an incremental axial stress will predict a larger stress-strain envelope while too small of a step will unnecessarily increase the calculation cost of the problem. Limiting the change in wall modulus,  $E_3$ , to ten percent seems to be a good balance. Figure 4 contains the flowchart describing the entire process.

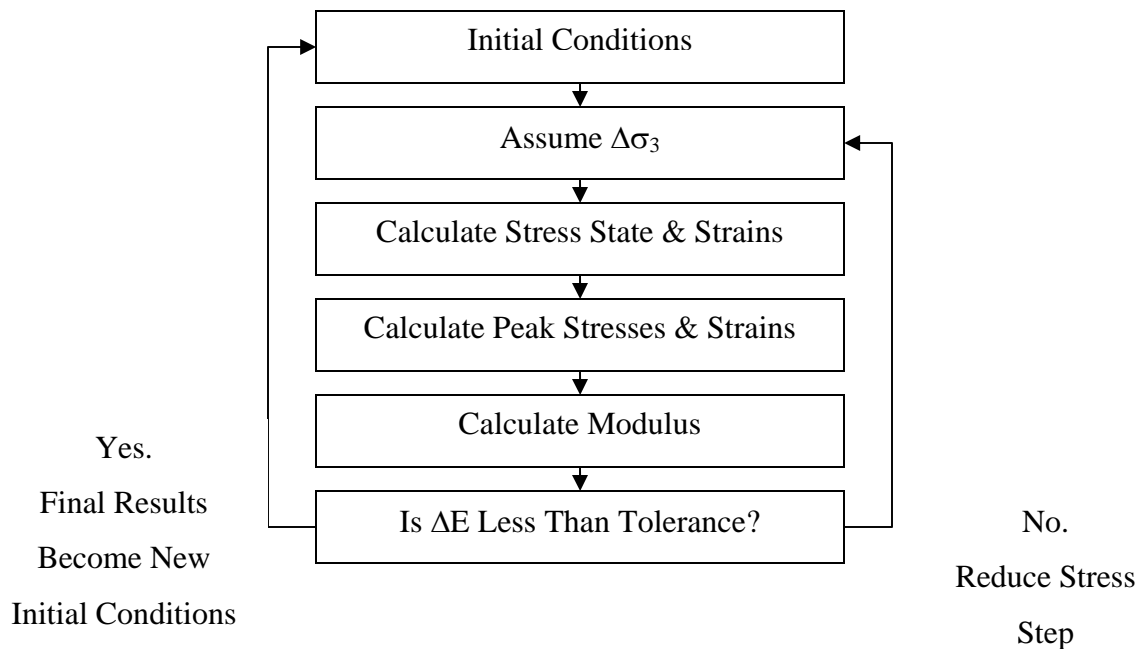


**Figure 4 Flowchart of Stress-strain Relationship Solving Procedure**

#### 4.4.4 Foundation Failure Criterion

In addition to calculating the stress state of the masonry it is necessary to verify the failure criterion of the foundation. Hilsdorf<sup>6</sup> proposed the failure envelope in Eq. 33. After each iteration of the masonry model, failure criterion of the foundation should be checked.

$$\frac{f_t}{f_{tf}} + \frac{f_c}{f_{cf}} = 1 \quad (\text{Eq. 33})$$

Where  $f_{tf}$  and  $f_{cf}$  are the biaxial tensile and uni-axial compressive strengths of the foundation, respectively. The current lateral tensile stress,  $f_t$ , was evaluated from Eq. 6 during each iteration. Where the axial compressive stress,  $f_c$ , is simply  $\sigma_3$ .

## 4.5 VERIFICATION OF THE MODEL

In order to determine the validity of the model it is compared against other established, more empirical models. These models simply predict the overall all compressive strength of masonry prisms. In addition to previous models, experimental results and finite element analysis will be used as verification. The proposed model will initially be compared with a simpler structure than unbonded post-tensioned masonry. The first validation will be against the behavior of masonry prism compression testing.

### 4.5.1 Masonry Prism Compression Strength

Pauley<sup>10</sup> states that the compressive strength of a single wythe masonry prism can be found by using equations 34 and 35. The single wythe prism strength,  $f'_p$ , is a function of the uni-axial compressive,  $f'_{cb}$ , and the biaxial tensile,  $f'_{tb}$ , strengths of the clay brick masonry unit as well as the compressive mortar strength,  $f'_j$ . The relationship is as follows:

$$f'_p = \frac{f'_{cb}(f'_{tb} + \alpha f'_j)}{1.5(f'_{tb} + \alpha f'_{cb})} \quad (\text{Eq. 34})$$

Where  $\alpha$  is a function of the mortar joint height,  $j$ , and the clay brick height,  $h$ .

$$\alpha = \frac{j}{4.1h} \quad (\text{Eq. 35})$$

In the case of a double wythe masonry prism, Pauley<sup>10</sup> indicates its strength can be found by Eq. 36.

$$f'_m = x f'_p + (1 - x) f'_g \quad (\text{Eq. 36})$$

Where  $x$  is the ratio single wythe prism area to the gross area of the total prism and  $f'_g$  is the strength of the grout.

In addition to the previous empirical relationship, researchers<sup>5,11,12</sup> have used the modified Kent-Park curve to predict the stress-strain relationship for double wythe masonry prisms. The details of the modified Kent-Park curve are described in equations 37-40.

Rising curve:

$$\varepsilon_c \leq 0.002 \quad (\text{Eq. 37})$$

$$f_m = 1.067 f'_m \left[ \left( \frac{2\varepsilon_c}{0.00267} \right) - \left( \frac{\varepsilon_c}{0.00267} \right)^2 \right] \quad (\text{Eq. 38})$$

And the descending curve is defined as:

$$f_m = f'_m [1 - Z_m (\varepsilon_c - 0.00267)] \quad (\text{Eq. 39})$$

Where

$$Z_m = \frac{0.5}{\left( \frac{3 + 0.29 f'_m}{145 f'_m - 1000} \right) - 0.00267 K} \quad (\text{Eq. 40})$$

Figure 5 shows the comparison of the strengths predicted by the Hilsdorf model and the model proposed in this paper with the average of the actual results from tests conducted by Ewing<sup>4</sup>. The stress-strain relationships of the modified Kent-Park curve using the actual average compressive strength of the masonry prism is plotted against an actual test and the proposed model in Fig. 6. The proposed model provides better agreement in terms of strength with the actual clay brick masonry prism tests and its stress-strain relationship is adequate enough to be used for design purposes. To validate the proposed model further, it is compared against the behavior of an unbonded post-tensioned masonry clay brick wall.

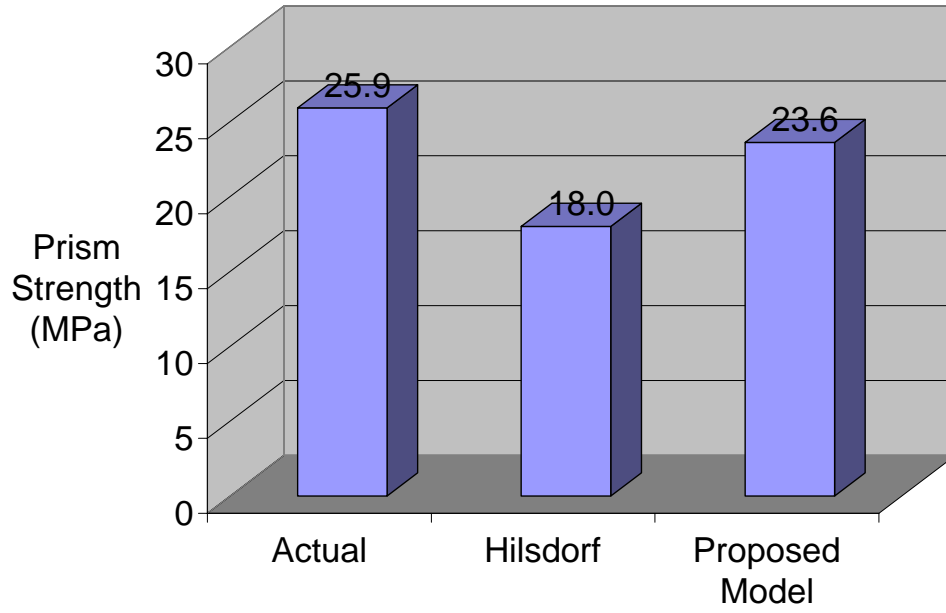


Figure 5: Masonry Prism Strength Comparison

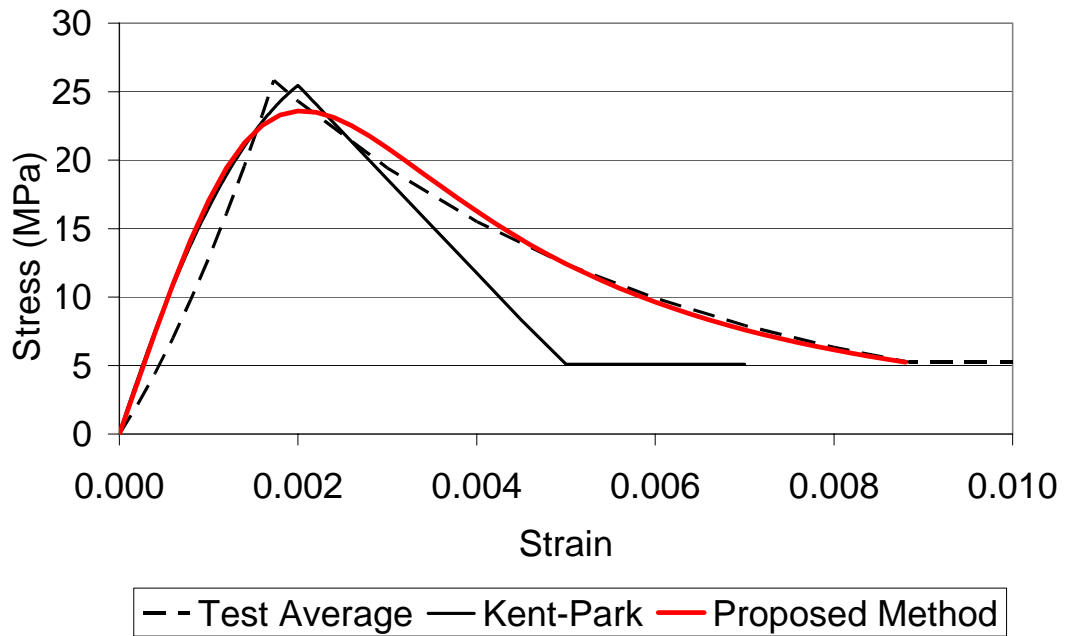


Figure 6: Stress-Strain Relationships

#### 4.5.2 Unbonded Post-tensioned Masonry Walls

A comparison of the uni-axial and tri-axial compression stress-strain relationships are shown in Figure 7. Including the compressive confinement stress on the wall has a significant effect on the ultimate strength and strain capacity of the masonry. The ultimate strength increases from 25.9 MPa to 31.3 MPa. That is about a 21% increase in strength. Figure 8 shows the force-displacement curves from unbonded post-tensioned masonry wall from those tested by Rosenboom<sup>14</sup> in comparison with those predicted using ANSYS, a finite element program, using the uni-axial and tri-axial stress-strain relationships. Figure 8 provides evidence that the theoretical model used in this paper accurately predicts the response of the masonry wall.

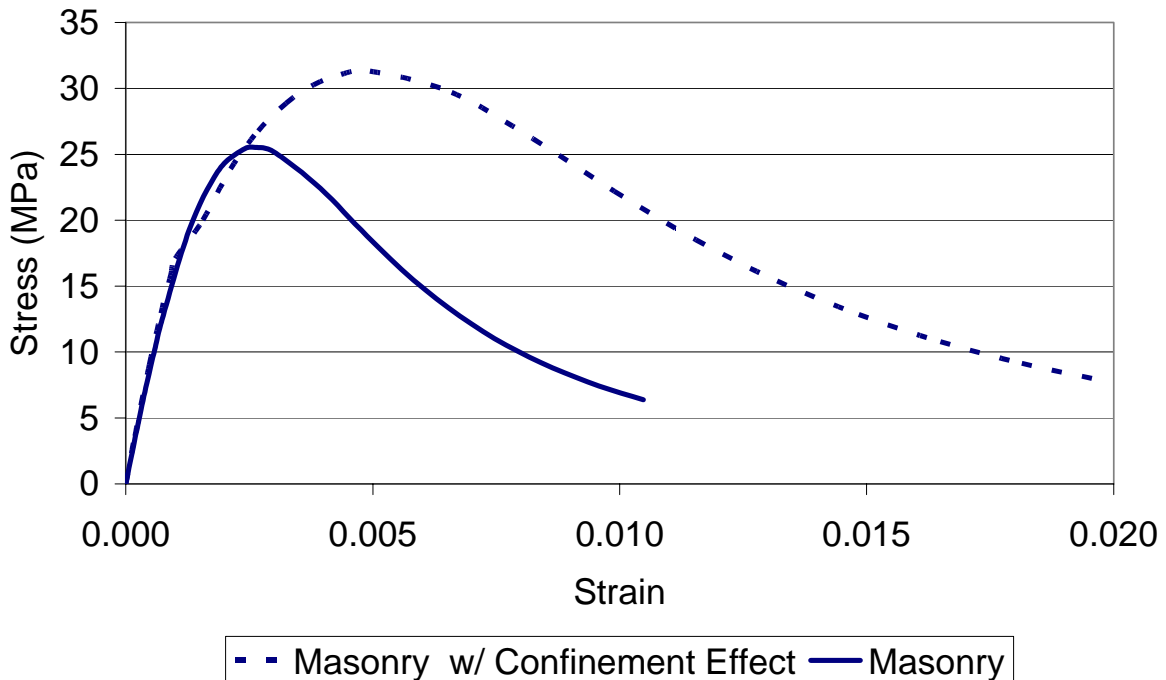


Figure 7 Stress-strain Relationship Comparison

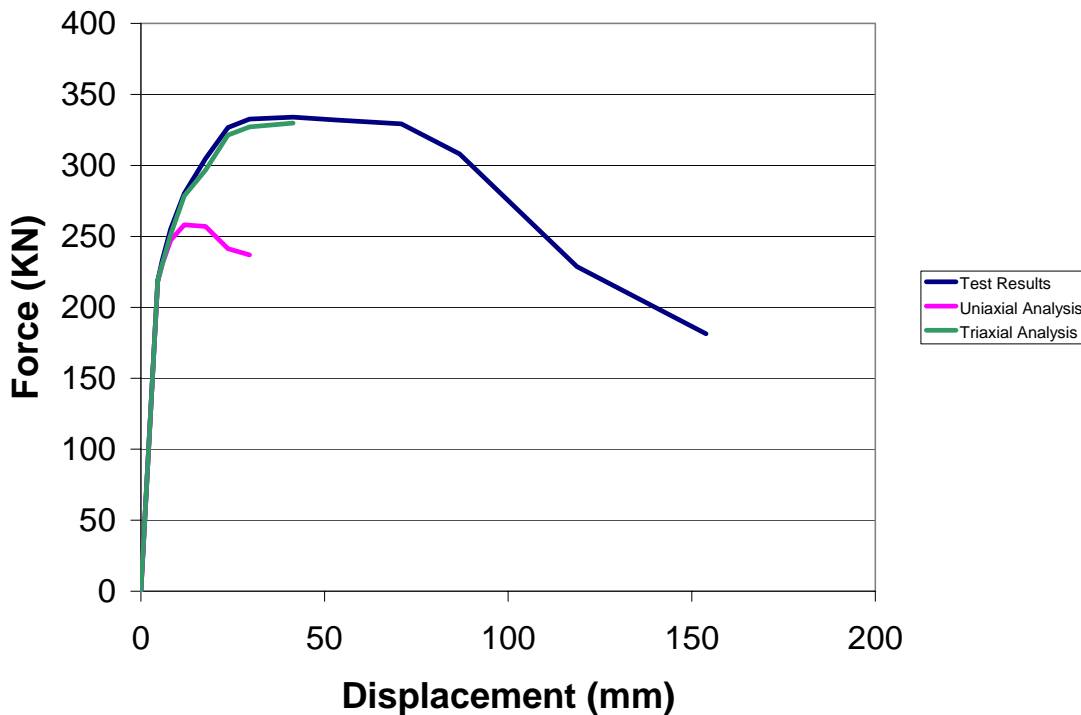
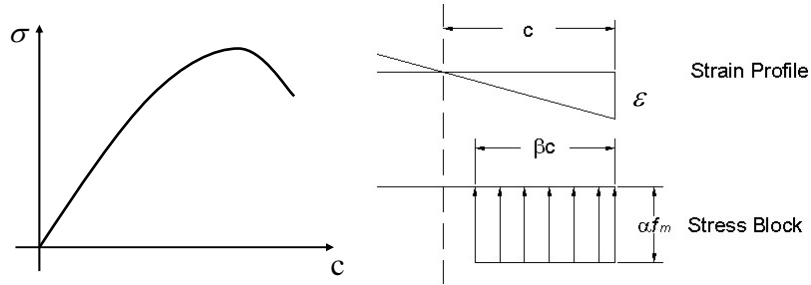


Figure 8 Force-Displacement Comparisons

#### 4.6 DESIGN APPLICATIONS OF THE MODEL

An accurate stress-strain relationship is critical to the engineer and the safety of his design. An improper stress-strain relationship results in several problems including (1) under or over-estimation of structure strength, (2) erroneous member sizing, and (3) unnecessary and expensive detailing of the unbonded post-tensioned clay brick masonry wall. As shown in section 4.5.2 the differences in predicted and actual behavior can be significant. Figures 7 and 8 show percent error in the 20-25% range. For the engineer, knowing the correct equivalent stress block parameter is important. The equivalent stress block allows the engineer to easily and quickly calculate the compressive strength of the masonry at the wall/foundation interface. A graphical representation of this process is shown in Fig. 9. The equivalent stress block is specified by two parameters,  $\alpha$  and  $\beta$ , such that (1) the average

stress,  $\alpha f'_c$ , extends  $\beta c$  from the extreme compression fiber and (2) the equivalent stress block has the same area and centroidal height as the original stress-strain relationship<sup>8</sup>.



**Figure 9: Development of Equivalent Stress Block**

## 4.7 CONCLUSIONS

The model proposed to model the confinement effect of the foundation on the behavior of masonry for its use in the design of unbonded post-tensioned walls is accurate. It predicts that the true compressive strength of the masonry wall at the wall/foundation interface can be over 20% stronger than the compressive strength obtained from laboratory testing of clay brick masonry prisms. The model is validated by comparing the predicted behavior against other established models for clay brick masonry and experimental tests conducted by Rosenboom<sup>14</sup> and Ewing<sup>5</sup>. The proposed model allows an engineer to define the correct  $\alpha$  and  $\beta$  parameters for design. For the case shown in figure 8, the lateral compressive strength can be as far as 25%. This would have resulted in the over-engineering and extra material construction cost.

## 4.8 NOTATION

$\Delta \varepsilon_{1w}$  = incremental lateral strain in wall

$\Delta \varepsilon_{1f}$  = incremental lateral strain in foundation

$\Delta\varepsilon_s$  = incremental strain in reinforcing steel within the foundation

$\Delta\sigma_{1w}$  = incremental lateral stress in wall

$\Delta\sigma_{1f}$  = incremental lateral stress in foundation

$\Delta\sigma_3$  = incremental axial stress

$E_{1w}$  = instantaneous lateral modulus of the wall

$E_{1f}$  = instantaneous lateral modulus of the foundation

$E_{3w}$  = instantaneous axial modulus of the wall

$E_{3f}$  = instantaneous axial modulus of the foundation

$E_o$  = initial axial modulus

$f_c$  = unconfined axial compressive strength

$f_t$  = unconfined axial tensile strength

$\sigma_L$  = lateral confining stress

$\nu_{1w}$  = instantaneous lateral Poisson's ratio in wall

$\nu_{1f}$  = instantaneous lateral Poisson's ratio in foundation

$\nu_{3w}$  = instantaneous axial Poisson's ratio in wall

$\nu_{3f}$  = instantaneous axial Poisson's ratio in foundation

## 4.9 REFERENCES

1. Ahmad, S. and Shah, S. (1982) "Complete Tri-axial Stress-strain Curves for Concrete." *ASCE Journal of the Engineering Structural Division*, Vol. 108, No. 4, pp 728-741.

2. Darwin, D. and Pecknold, D.A. (1977) "Nonlinear Biaxial Law for Concrete." *ASCE Journal of the Engineering Mechanics Division*, Vol. 103, No. 2, pp 229-241.
3. Elwi, A. and Murray, D. (1979) "A 3D Hypoelastic Concrete Constitutive Relationship." *ASCE Journal of the Engineering Mechanics Division*, Vol. 105, No. 4, pp 623-641.
4. Este, G. and Willam, K. (1994) "Fracture Energy Formulation for Inelastic Behavior of Plain Concrete." *ASCE Journal of the Engineering Mechanics Division*, Vol. 120, No. 9, pp 1983-2011.
5. Ewing, B. D. and Kowalsky, M. J. (2003). "Compressive Behavior of Unconfined and Confined Clay Brick Masonry." *Journal of Structural Engineering*, Vol. 130, No. 4, pp. 650-661.
6. Gere, J.M. and Timoshenko, S.P. (1997). *Mechanics of Materials*, PWS Publishing Company, Boston.
7. Hilsdorf, H.K. (1969). "An Investigation into the Failure Mechanism of Brick Masonry Under Axial Compression in Designing." *Engineering and Constructing with Masonry Products*, F.B. Johnson, Ed., Gulf Publishing, Houston, May, pp. 34-41.
8. Leon, A. (1935) "Über die Scherfestigkeit des Betons." *Beton und Eiser*, Berlin, Germany, Vol. 34, No. 8, (In German).
9. Newman, J.B. (1979) "Concrete Under Complex Stresses." *Development in Concrete Technology-1*, F.D. Lydon, Ed., Applied Science, London.
10. Ottosen, N.S. (1979) "Constitutive Model for Short-time Loading of Concrete." *ASCE Journal of the Engineering Mechanics Division*, Vol. 105, No. 1, pp 127-141.
11. Paulay, T. and Priestley, M.J.N. (1992). *Seismic Design of Reinforced Concrete and Masonry Buildings*, A Wiley-Interscience Publication, New York, 1992.

12. Priestley, M.J.N., and Elder, D.M. "Stress-Strain Curves for Unconfined and Confined Concrete Masonry." *ACI Journal*, Vol. 80, No. 3, pp 192-201.
13. Richart, F.E., Brandtzaeg, A., and Brown, R.L. (1928) "A Study of the Failure of Concrete Under Combined Compressive Stresses." *Engineering Experiment Bulletin No. 185*, Univ. of Illinois, Urbana, IL.
14. Rosenboom, O.A. and Kowalsky, M.J. (2004). "Reversed In-Plane Cyclic Behavior of Post-Tensioned Clay Brick Masonry Walls." *ASCE Journal of Structural Engineering*, Vol. 130, No. 5, pp. 787-798.
15. Saenz, I.P. (1964) discussion of "Equation for the Stress-strain Curve of Concrete." By P. Desayi and S. Krishnan, *ACI Journal, Proceedings*, Vol. 61, No. 9, pp. 1229-1235.
16. Sfer, D., Carol, I., Gettu, R., and Etse, G. (2002) "Study of the Behavior of Concrete under Tri-axial Compression." *ASCE Journal of the Engineering Mechanics Division*, No. 2, pp 156-163.
17. Tiecheng, W., Mingqi, L., and Lai, W. (2003) "Stress-strain Relation for Concrete Under Tri-axial Loading." *16<sup>th</sup> ASCE Engineering Mechanics Conference*, July 16-18, 2003, University of Washington, Seattle.

JOURNAL ARTICLE NUMBER THREE

**5 DISPLACEMENT-BASED DESIGN OF UNBONDED POST-TENSIONED MASONRY WALLS**

BRYAN EWING

MERVYN KOWALSKY

# DISPLACEMENT-BASED DESIGN OF UNBONDED POST-TENSIONED CLAY MASONRY WALLS

Bryan D. Ewing and Mervyn J. Kowalsky

*Department of Civil, Construction and Environmental Engineering, North Carolina State University,  
Campus-Box 7908, Raleigh, NC-27695, USA*

Keywords: Masonry Construction, Seismic Design, Post-tensioning

## 5.1 ABSTRACT

A method for designing unbonded post-tensioned clay brick masonry walls is proposed in this paper. Experimental studies and analysis have provided a means of designing unbonded post-tensioned clay brick masonry walls to perform well under seismic demands. The proposed approach is performance-based, thus allowing for specification of performance at discrete levels of seismic intensity. The performance criterion includes the wall displacement, masonry compression strain, and the tensile strain in the post-tensioning steel. A series of shake table tests provide experimental verification and an example at the end of the paper demonstrates the design process.

## 5.2 INTRODUCTION AND OBJECTIVES

In the case of modern performance-based seismic design (PBSD), the objective of the engineer is to design a structure whereby it will achieve pre-defined levels of performance under pre-defined levels of seismic hazard. The term ‘performance’ can be considered to be synonymous with ‘damage’. Consider Table 1, which was first conceptually proposed by the Structural Engineers Association of California (SEAOC) document, Vision 2000, and then quantified by SEAOC in their 1999 document on PBSD<sup>23</sup>. Along the top of the table, several

damage levels are represented as SP1 through SP4. Vertically, earthquake levels are expressed as EQ1 through EQ4 and defined on the basis of return period. The combination of a limit state (SP1 through SP4) and an earthquake level (EQ1 through EQ4) constitutes a performance level. A series of performance levels constitutes a performance objective. In the example shown in Table 1, performance objective 1 implies that a structure will achieve damage level 1 under earthquake level 1, damage level 2 under earthquake level 2, damage level 3 under earthquake level 3, and damage level 4 under earthquake level 4.

**Table 1: Seismic performance objectives**

Limit States EQ Intensity	SP1	SP2	SP3	SP4
EQ1: 25 Year	①			
EQ2: 72 Year	②			
EQ3: 1650 Year	③			
EQ4: 2475 Year				

In order to design a structure to achieve pre-defined performance objectives as shown in Table 1, several items are required. First, an accurate estimation of seismic hazard for various return periods is essential. Second, the damage levels for which a structure is to be designed must be defined. Lastly, a design procedure capable of arriving at a suitable design that will meet the target performance objective must be established.

Within the context of PBSB, the goals of this paper are to: (1) Define performance limit states for unbonded post-tensioned clay masonry, and (2) Describe how the existing displacement-based design approach can be used for the performance-based design of these systems. In order to accomplish these goals, this paper summarizes (1) the concept of

displacement-based design, (2) explains why it is a useful design method for PBSD, (3) describes the unbonded post-tensioned clay masonry structural system, (4) proposes performance limit states for unbonded post-tensioned clay masonry structural systems, (5) discusses how displacement-based design may be applied to this structural system, (6) provides experimental data through shake table testing to investigate the accuracy of the proposed method, and (7) provides a design example.

### **5.3 DISPLACEMENT-BASED DESIGN APPROACH**

The Displacement-based design approach described in this paper was first proposed by Priestley (1993) and is based on a substitute linear structure with an equivalent damping and secant stiffness as first proposed by Gulkan<sup>5</sup>. Over the next 15 years, research extended the procedure to the design of bridge and building systems<sup>10, 11, 15</sup>. Although unbonded post-tensioned masonry walls are not discussed in the text by Priestley et al. (2007), it describes the method in detail so only the basic concepts are summarized here.

The Displacement-based design approach is a response spectrum-based design method whereby the structure is modeled as an equivalent SDOF system having properties of equivalent stiffness and equivalent damping. The basic steps of the procedure are as follows:

- 1) **Obtain target displacement,  $\Delta_T$ .** The target displacement is based on either drift or strain criteria for each of the limit states under consideration. The target drift and displacement profile for an unbonded post-tensioned clay brick masonry wall is shown in Fig. 1.

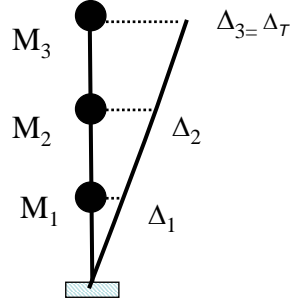


**Figure 1: MDOF Structure Displacement Profile**

- 2) **Reduce MDOF structure to an equivalent SDOF oscillator.** Find the values  $\Delta_{sys}$  and  $M_{sys}$  for the SDOF oscillator by equating the work done by the MDOF and SDOF structures in Fig. 2.

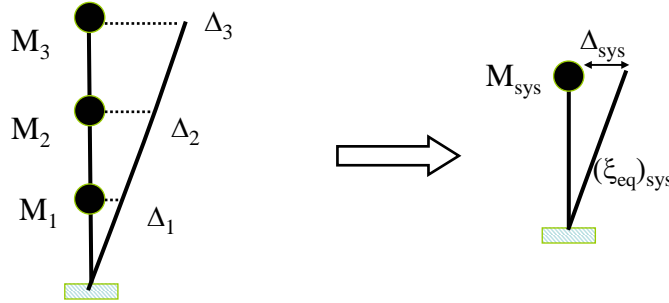


**Figure 2: Equivalent SDOF Oscillator**

$$\Delta_{sys} = \frac{\sum (M_i \Delta_i^2)}{\sum (M_i \Delta_i)} \quad (\text{Eq. 1})$$

$$M_{sys} = \sum \left( M_i \frac{\Delta_i}{\Delta_{sys}} \right) \quad (\text{Eq. 2})$$

- 3) **Calculate Yield Displacement.**  $\Delta_y$
- 4) **Calculate Displacement Ductility.** The displacement ductility,  $\mu_d$ , is defined as the target displacement divided by the yield displacement.

$$\mu_d = \frac{\Delta_T}{\Delta_y} \quad (\text{Eq. 3})$$

5) **Calculate Equivalent viscous damping,  $\xi_{eff}$**  . Relationships between equivalent viscous damping and ductility have been previously established as shown in Fig. 3. For unbonded post-tensioned construction, Eq. 4 is recommended by Priestley<sup>15</sup>. Dwairi<sup>3</sup> and Preistley<sup>14</sup> are sources for additional investigations on the equivalent viscous damping of unbonded post-tensioned structures.

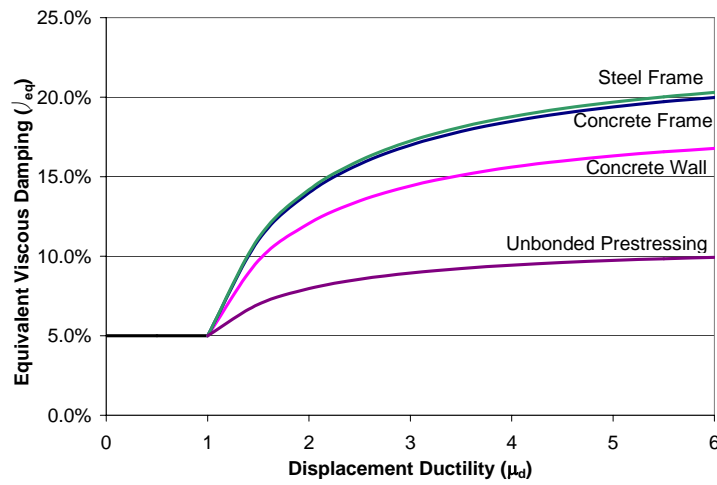


**Figure 3: Equivalent Viscous Damping<sup>15</sup>**

$$\xi_{eff} = \begin{cases} 0.05 & \text{for } 0 \leq \mu_d < 1 \\ 0.05 + .186 \left( \frac{\mu_d - 1}{\pi \mu_d} \right) & \text{for } \mu_d \geq 1 \end{cases} \quad (\text{Eq. 4})$$

6) **Find Effective Period,  $T_{eff}$ , and Effective Stiffness,  $K_{eff}$**  . Utilizing the design response spectra, the target displacement, and the equivalent viscous damping, the effective period is obtained as shown in Fig. 4. The effective stiffness is then obtained with Eq. 5.

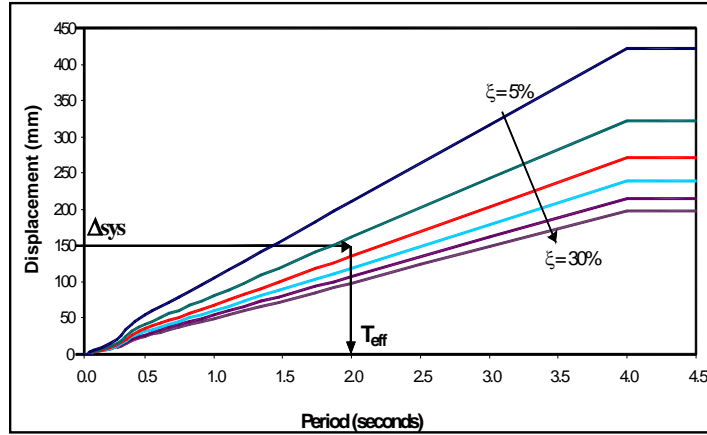


Figure 4: Effective Period

$$K_{eff} = 4\pi^2 \frac{M_{sys}}{T_{eff}^2} \quad (\text{Eq. 5})$$

- 7) **Calculate the design base shear,  $V_b$ .** This is found by multiplying the effective stiffness from step 6 by the design system displacement from step 2. The design base shear force is obtained as shown in Fig. 5. If the response spectra is idealized by a corner point period,  $T_c$  and corner point displacement,  $\Delta_c$ , the base shear can be calculate directly from Eq. 6.

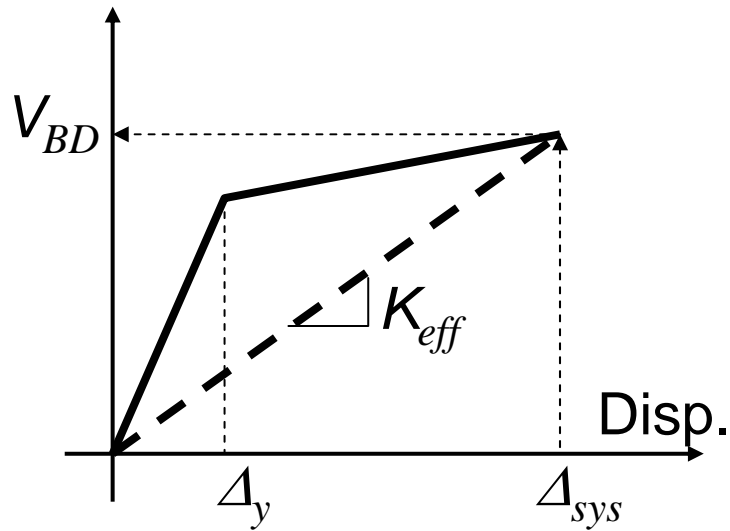


Figure 5: Force-Displacement Response

$$V_b = \frac{4\pi^2 M_{sys} \Delta_c^2}{\Delta_{sys} T_c^2} \frac{7}{2 + \zeta_{eff}} \quad (\text{Eq. 6})$$

- 8) **Design the structure** by distributing the design base shear to each story and utilizing the procedure described later for unbonded post-tensioned masonry.

## 5.4 DESIGN PROCEDURE FOR UNBONDED POST-TENSIONED MASONRY

Priestley<sup>19</sup> initially proposed the use of unbonded post-tensioned structures to resist seismic forces in 1993. Steel moment frames<sup>2, 21</sup> and concrete buildings<sup>19</sup> incorporating unbonded post-tensioning have been researched in later years. Recently, unbonded post-tensioning has been applied to masonry walls<sup>8, 11, 12, and 22</sup>. Before getting into the specifics of the design procedure for masonry, it is necessary to describe the unbonded post-tensioned masonry system.

The system consists of a wall constructed with a central cavity that houses ducting for post-tensioning steel. The ducting prevents the tendons from bonding with the grout that is subsequently placed. Once the grout has cured, the tendons are stressed. The end result is a lateral force-resisting system that, if designed properly, develops a singular horizontal crack at the wall/foundation interface while rocking under the influence of seismic forces where the post-tensioned steel provides a restoring force to the system. As a result, there is no residual deformation once after a seismic event. Furthermore, due to the rocking response of the system, structural damage is restricted to the heel and toe regions of the wall since flexural tension is not developed in the masonry. A key variable in the design is the level of initial

post-tensioning strain in the tendons such that the performance limit states are achieved at their chosen earthquake intensity level.

#### **5.4.1 Building Specifics**

The specifics of the building, mainly the geometry, are needed to perform the Displacement-based design approach. The building geometry includes the number of stories and their respective weights, wall height, and wall width. In addition to the building geometry, design criteria selections are made. The design criteria selections are comprised of defining the masonry limit states (MLS) and steel tensile limit states (TLS) for each specific earthquake intensity level.

#### **5.4.2 Design Criteria**

##### **5.4.2.1 Masonry Limit States**

Research conducted by Ewing<sup>4</sup> and Hart<sup>6</sup> on the compressive behavior of clay brick and concrete block masonry, respectively, provides suggestions for masonry limit states.

Possible MLS are as follows:

- 1) Initiation of splitting cracks
- 2) Excessive cracking/spalling
- 3) Yielding of confinement plates, if present
- 4) Maximum dependable compression strain
- 5) Ultimate compression strain

It is important to realize that MLS #5 does not equate to wall and/or system failure but to the degradation from crushing of the masonry at the extreme compression fiber. This is undesirable since the degradation effectively shortens the length of the wall and reduces the

moment arm of the post-tensioning steel, therefore reducing the lateral force the wall can withstand. The suggested strain limits by Ewing<sup>4</sup> for clay brick masonry with varying levels of confinement are summarized in Table 2. Masonry confinement is provided by galvanized steel plates placed in the mortar joints at each course or every other course, which was originally proposed by Priestley and Bridgeman (1974).

**Table 2: Masonry strains at various limit states**

<b>Limit States</b>	<b>Unconfined</b>	<b>Alternate Course</b>	<b>Every Course</b>
1. Initiation of splitting cracks	0.0012	-	-
2. Excessive cracks/spalling	0.0016	-	-
3. Yielding of confinement plates	-	0.0021	0.0023
4. Dependable compression strain	0.0039	0.0168	0.0387
5. Ultimate compression strain	0.0049	0.0245	0.0595

#### **5.4.2.2 Equivalent Stress Block for Masonry Limit States**

The equivalent stress block is specified by two parameters,  $\alpha$  and  $\beta$ , such that (1) the average stress,  $\alpha f'_m$ , extends  $\beta c$  from the extreme compression fiber and (2) the equivalent stress block has the same area and centroidal height as the original stress-strain relationship<sup>17</sup>. Equivalent rectangular stress blocks are defined for the clay brick masonry limit states described in the above section 5.4.2.1. The purpose for multiple definitions is to accommodate the displacement-based design methodology which may require that structures be evaluated at a different masonry limit states. A sectional analysis utilizing proper foundation steel, foundation concrete, and masonry stress-strain constitutive relationships should be employed first to ascertain the correct stress-strain relationship of the masonry.

Then equivalent stress block parameters can be calculated. A graphical representation of this process is shown in Fig. 6.

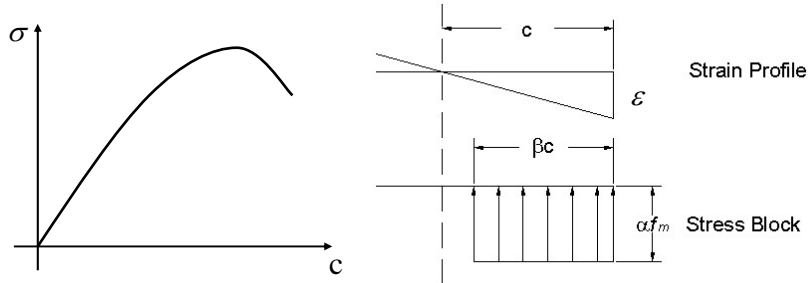


**Figure 6: Development of Equivalent Stress Block**

#### 5.4.2.3 Tensile Limit States

Tensile limit states are more arbitrary in nature and can therefore be defined at the engineer's discretion. Including the well-defined TLS yielding and rupture of the post-tensioning material, possible TLS are:

- 1) Limit to linearly Elastic Behavior ELIMINATE
- 2) Yielding of PT Tendon/Bar KEEP
- 3) Lost of Initial Pre-Stress KEEP
- 4) Onset of plastic Response of PT Tendon/Bar ELIMINATE
- 5) Rupture of PT Tendon/Bar KEEP

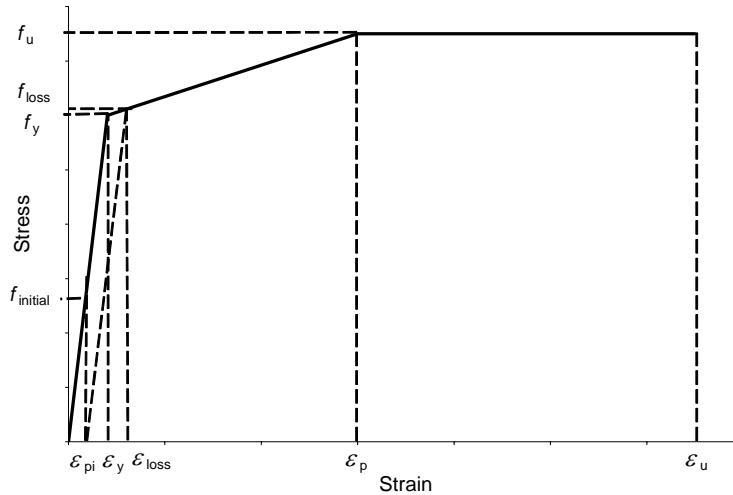


**Figure 7: Tensile Limit States**

Fig. 7 shows the locations of the TLS on the stress-strain relationship of a typical post-tensioning bar. One of the most critical of the TLS is the loss of initial pre-stress. If a specific performance level requires that the post-tensioning tendons remain elastic, then steps three through five can be skipped since the response is elastic. To determine the effective period and stiffness in step Six, a viscous damping of 5% may be assumed. For all other TLS the DBD approach must be completed in its entirety.

#### **5.4.2.4 Compressive Strut**

The diagonal compressive strut formed under the influence of lateral forces must be stable in order for the wall to perform adequately. Presently, an algebraic expression that describes the exact path of the compressive force from the location of the equivalent lateral base shear force to the toe of the wall is not known. The path of the compressive strut varies depending on the aspect ratio of the wall and the  $C_m$  to  $V_b$  ratio. However, analysis of experimental tests conducted by Rosenboom<sup>22</sup> and ANSYS finite element parametric studies show that for a wall with an aspect ratio of two the angle between the foundation and the compression strut,  $\theta_{strut}$ , is approximately 78 degrees, on average. Table 3 shows the

relationship between  $\theta_{strut}$  and wall aspect ratio, based on analysis.  $\theta_{strut}$  is shown in Fig. 8. The purpose of this variable, as will be shown in the next section, is to remove one of the unknowns in the equations of equilibrium, Eqs. 8 and 11. With the introduction of this variable only two unknowns remain, the contact length  $c$  and resultant tensile force  $T$ . The two design equations can be solved since only two unknown variables remain.

**Table 3: Suggested  $\theta_{strut}$  values**

Aspect Ratio	$\theta_{strut}$
1	75°
2	78°
3	82°
4+	85°

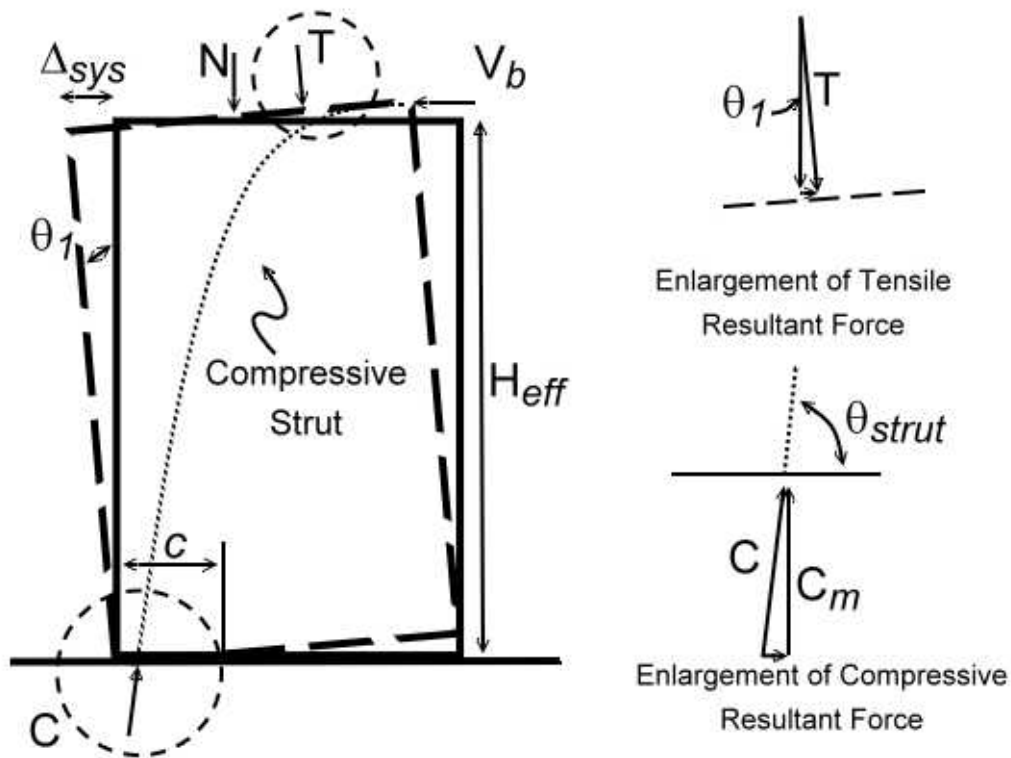


**Figure 8: Free Body Diagram of Unbonded Post-tensioned Masonry Wall**

### 5.4.3 Obtaining Design Forces

Fig. 8 represents the free body diagram of the deflected shape of an unbonded post-tensioned wall under the influence of a lateral load. The design forces, compressive force  $C$ , and resultant tensile force  $T$ , can be obtained from horizontal (Eq. 7) and vertical (Eq. 10) force equilibrium. The story weight and frictional force is represented by  $N$  and  $F_f$  respectively.

$$\sum F_x = 0 \quad (\text{Eq. 7})$$

$$\frac{C_m}{\tan \theta_{strut}} + T \sin \theta_1 - V_b = 0 \quad (\text{Eq. 8})$$

Solving for the resultant tension force,  $T$ , creates an expression as a function of the base shear demand and the compressive strength.

$$T = \frac{V_b}{\sin \theta_1} - \frac{C_m}{\tan \theta_{strut} \sin \theta_1} \quad (\text{Eq. 9})$$

Summing the forces in the vertical direction results in Eq. 11.

$$\sum F_y = 0 \quad (\text{Eq. 10})$$

$$C_m - \sum N - T \cos \theta_1 = 0 \quad (\text{Eq. 11})$$

Substituting Eq. 9 into Eq. 11 results in:

$$C_m \left( 1 + \frac{1}{\tan \theta_{strut} \tan \theta_1} \right) - \sum N - \frac{V_b}{\tan \theta_1} = 0 \quad (\text{Eq. 12})$$

Where:

$$\sin \theta_1 = \frac{\Delta_{target}}{H_{wall}} = \frac{\Delta_{sys}}{H_{eff}} \quad (\text{Eq. 13})$$

$$C_m = \alpha f_m \beta c b_w \quad (\text{Eq. 14})$$

Eq. 12 is a function of one unknown,  $c$ , the length of the wall in contact with the foundation. The design forces, compressive strut force, base shear demand, and resultant tensile force, can be determined once  $c$  is known by using the above equations.

#### 5.4.4 Design Forces Checks

Once the design forces are obtained, three major structural integrity checks must be made: (1) Protection against slippage, (2) maximum inter-story drift limits, and (3) minimum resultant tensile force. For unbonded post-tensioned masonry walls sliding could become a significant problem if the wall is poorly designed. Sliding of post-tensioned walls is caused by the combination of large base shear demands and the smooth interface between the post-tension wall and foundation. Post-tensioned wall sliding results in residual deformation, which can undermine one of the primary benefits of using post-tension walls as the lateral force resisting system – the origin centered self-corrective nature of post-tensioned walls. While some tend to equate the performance of sliding with base-isolation, sliding is an undesirable behavior for unbonded post-tensioned walls. When a system of unbonded walls is allowed to slide, then some walls may slide more than others. Furthermore, some walls may not slide at all. This relative sliding will result in a subset of walls that have residual deformation between their top and base. To prevent sliding the frictional force at the wall/foundation interface must be greater than the horizontal component of the compressive strut at the base of the wall as indicated in Eqs. 15 - 17.

$$\phi f_f > \frac{C_m}{\tan \theta_{strut}} \quad (\text{Eq. 15})$$

$$\phi \mu C_m > \frac{C_m}{\tan \theta_{strut}} \quad (\text{Eq. 16})$$

$$\mu > \frac{1}{\phi \tan \theta_{strut}} \quad (\text{Eq. 17})$$

$\mu = 0.8$  for most cases and  $\phi = 0.5 - 0.8$  based on the engineers discretion.

The second structural integrity check, the inter-story drift limit, is defined in Eq. 18.

$$\frac{\Delta_{top}}{H_w} \leq DRIFT\ LIMIT \quad (\text{Eq. 18})$$

A minimum resultant force check is the third structural integrity check. This requirement is based on the MSJC code (2008).

$$T \geq 0.025 f'_m b_w c \quad (\text{Eq. 19})$$

#### 5.4.5 Evaluating Required Initial Pre-Stress

Now that the design forces have been calculated and checked against the design criteria, the initial pre-stress forces need to be determined. Eq. 20 sets the resultant tensile force equal to the sum of the tension forces in the post-tensioning bars.

$$T = \sum (f_{ti} A_{pti}) \quad (\text{Eq. 20})$$

Assuming that the same size post-tensioning bar is used, Eq. 20 becomes:

$$T = A_{pti} \sum f_{ti} \quad (\text{Eq. 21})$$

Where:

$$f_{ti} = E_s \left[ \frac{(x_i - c) \Delta_{sys}}{H_{eff} L_{unbonded}} + \varepsilon_{pi} \right] \quad (\text{Eq. 22})$$

Substituting Eq. 21 into Eq. 22 and solving for  $\sum \varepsilon_{pi}$  results in Eq. 25

$$T = A_{pti} \sum \left[ E_s \left( \frac{(x_i - c) \Delta_{sys}}{H_{eff} L_{unbonded}} + \varepsilon_{pi} \right) \right] \quad (\text{Eq. 23})$$

$$\frac{T}{E_s A_{pti}} = \frac{\Delta_{sys}}{H_{eff} L_{unbonded}} \sum (x_i - c) + \sum \varepsilon_{pi} \quad (\text{Eq. 24})$$

$$\sum \varepsilon_{pi} = \frac{T}{E_s A_{pti}} - \frac{\Delta_{sys}}{H_{eff} L_{unbonded}} \sum (x_i - c) \quad (\text{Eq. 25})$$

And finally the initial pre-stress force for each tendon can be found by

$$\varepsilon_{pi} = \frac{\sum \varepsilon_{pi}}{N_{bars}} \quad (\text{Eq. 26})$$

$$T_{initial} = E_s A_{pti} \varepsilon_{pi} \quad (\text{Eq. 27})$$

#### 5.4.6 Initial Pre-Stress Checks

The tensile limit state for each tendon must be met for the initial pre-stress tensile strain found from Eq. 28.

$$\left[ \frac{(x_i - c) \Delta_{sys}}{H_{eff} L_{unbonded}} + \varepsilon_{pi} \right] \leq TENSILE \ LIMIT \quad (\text{Eq. 28})$$

#### 5.4.7 Time Dependent Effects

Time dependent effects consider post-tensioning losses related to clay brick masonry shrinkage, stress relaxation, anchorage losses, and any other potential sources of losses. The MSJC<sup>12</sup> estimates post-tensioning losses at 25%.

$$T_{ps \ force} = \frac{T_{initial}}{(1 - \%_{losses})} = \frac{T_{initial}}{0.75} \quad (\text{Eq. 29})$$

### 5.5 EXPERIMENTAL VALIDATION

Full-scale seismic experimental testing was conducted to verify the behavior of post-tensioned clay brick masonry walls and validate the proposed design methodology. A

1220mm long by 2440 mm high double with clay brick wall of 300mm thickness was constructed. The wall and a separately constructed concrete foundation were designed to easily install and remove the post-tensioning bars. The variables in the test program included post-tensioning bar force and location. .

### 5.5.1 Earthquake Record Selection

In selecting the earthquake records for testing, the displacement and velocity capacity of the shake table were controlling factors. The shake table has a maximum stroke of 250mm and a peak velocity of 800mm/sec. Any earthquake record selected must fit within these parameters. It was also desired to utilize records with velocity pulses as well as records with long duration of strong ground motion. Ultimately the records selected were the Llolelo, El Centro, and Nahanni earthquakes as shown in Fig. 9.

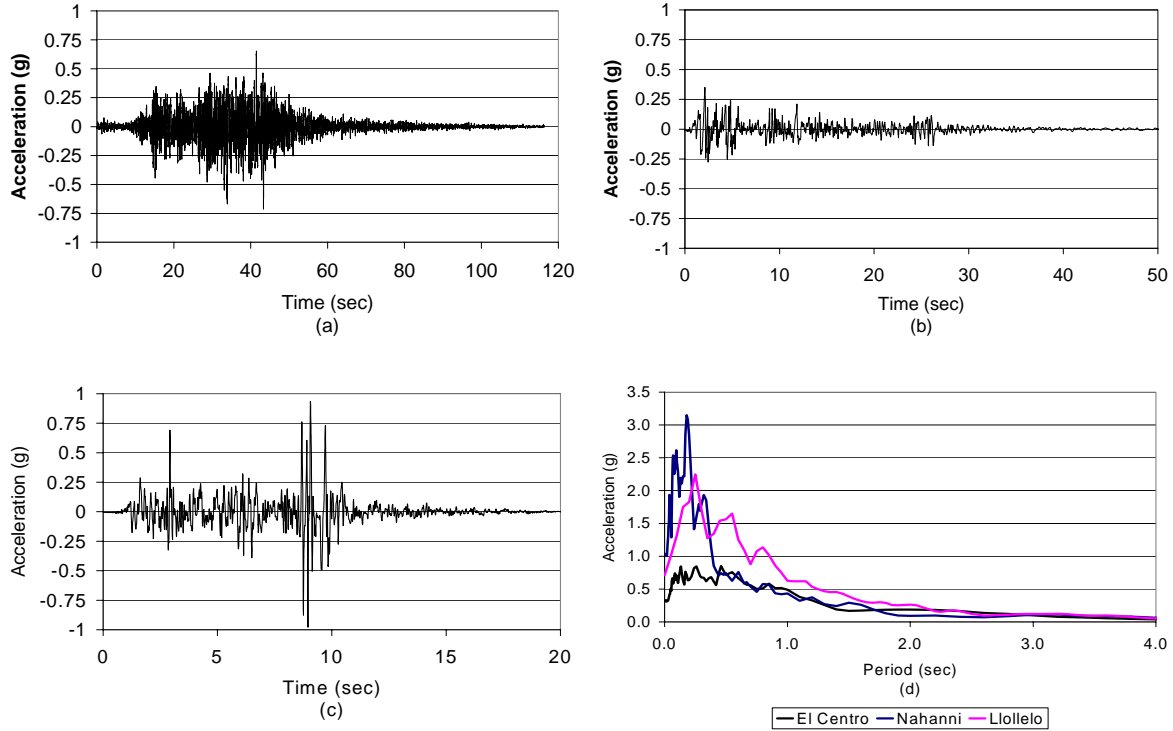


**Figure 9: Acceleration Records for (a) Llolelo, (b) El Centro, (c) Nahanni Earthquakes, and (d) their Acceleration Response Spectra**

### 5.5.2 Testing Matrix

The procedure for conducting the tests was to gradually increase the intensities of the earthquakes until failure of the clay brick masonry wall, or the maximum capacity of the shake table is achieved. In order to do this the selected earthquake records were scaled to four or five earthquake intensities for a southern California location according to the SEAOC guidelines<sup>23</sup> for return period of an earthquake. Table 4 shows the guidelines for the earthquake intensities as a function of the return period.

**Table 4: Return period for various earthquake intensities<sup>23</sup>**

<b>EQ</b>	<b>Description</b>	<b>Return Period (years)</b>
EQ I	Frequent	25
EQ II	Occasional	72
EQ III	Rare	250 – 800
EQ IV	Maximum Considered	800 - 2500

Table 5 displays the testing matrix where the peak ground acceleration for each earthquake is listed at the varying intensities. If the peak ground acceleration exceeded the definition of EQ IV, then the full-scale earthquake is listed as EQ V. Each of the scaled records was run at the post-tensioning levels described in Table 6, resulting in a total of 56 runs. The response of the structure to the full-scaled El Centro earthquake is shown in Fig. 10.

**Table 5: PGA for selected records**

EQ Record EQ Intensity	Llollelo	El Centro	Nahanni
EQ1	0.115 g	0.127 g	0.158 g
EQ2	0.173 g	0.190 g	0.237 g
EQ3	0.260 g	0.348 g	0.356 g
EQ4	0.477 g	0.522 g	0.653 g
EQ5	0.712 g	-	0.978 g

**Table 6: Post-tensioning bar force matrix**

Number of PT Bars	PT Bar Force
3	90 KN
3	45 KN
2	45 KN
1	27 KN

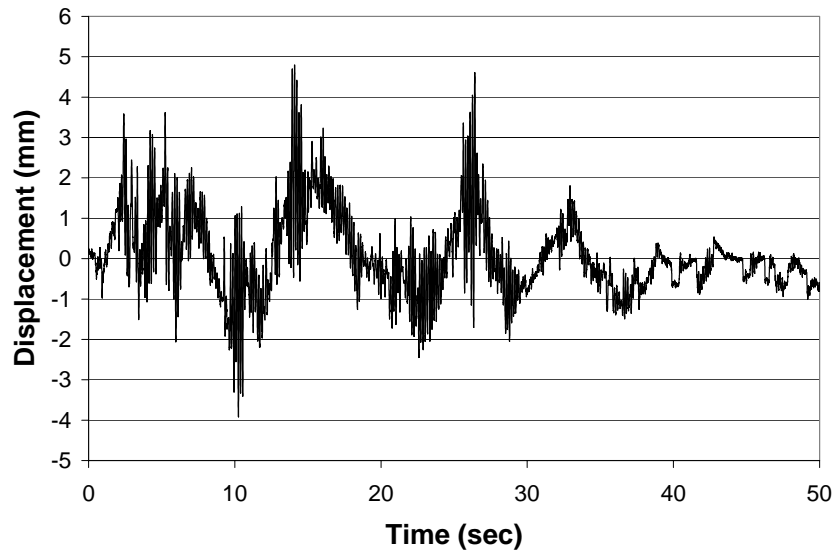


**Figure 10: Structure Response to El Centro Earthquake**

### 5.5.3 Results Comparison

A comparison between the exact results from the experimental tests and the design methodology are shown in Fig. 11 for the single post-tensioning bar configuration subjected to all 14 earthquake records. The other tests are not shown because they resulted in levels of deformation well below the elastic limit. The fact that spread of the data points are less than ten percent difference and that the overwhelming majority of the data points are above one means that the design method suggested is a reasonably accurate way to predict the response of the clay brick post-tensioned masonry wall.

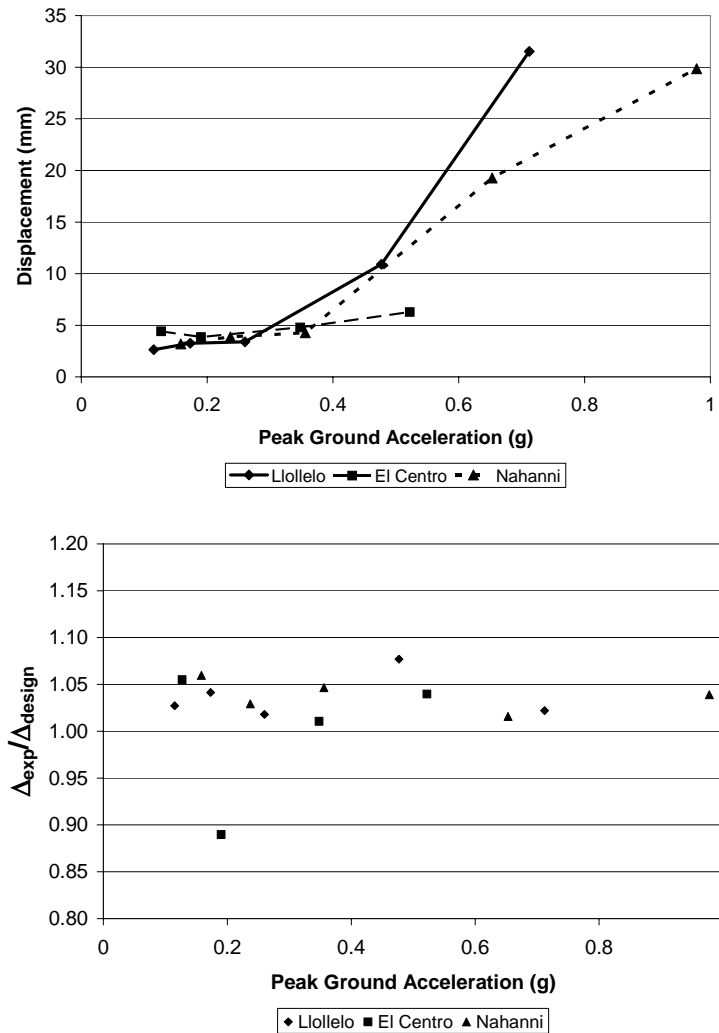


Figure 11: Experimental and Design Results Comparison

## 5.6 DESIGN EXAMPLE

To demonstrate the proposed methodology a design example of a unbonded clay brick masonry wall in a two story structure located in the Seattle, WA area under a EQ III seismic event and is detailed in Fig. 12. The masonry wall measures 3.6 meters long by 7.2 meters high and 300mm thick with an unbonded post-tensioning length of 7.3 meters. The floor load and roof loads are 360 KN and 140 KN respectively. Since the wall has an aspect ratio of two it is designed to have a strut angle of 78 degrees as suggested in Table 3. The masonry has a strength of 37.5 MPa and stress block parameters of  $\alpha = 0.8913$  and  $\beta = 0.8064$ . A graphical representation of the profile for the stress and strain along the contact region of the wall and its stress block is shown in Fig. 6. The acceleration and displacement spectra for EQ III for Seattle, WA from DEQAS-R are shown in Fig. 13. The displacement that corresponds to a period of four seconds is 635mm. Finally, the target drift is one percent or 72mm.

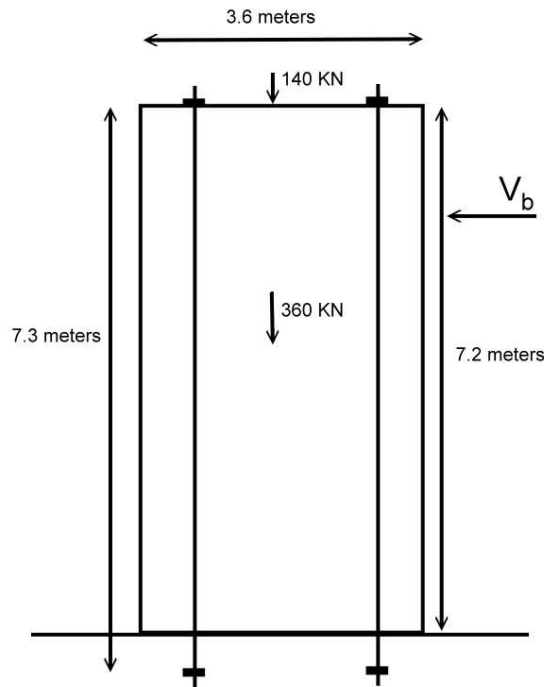
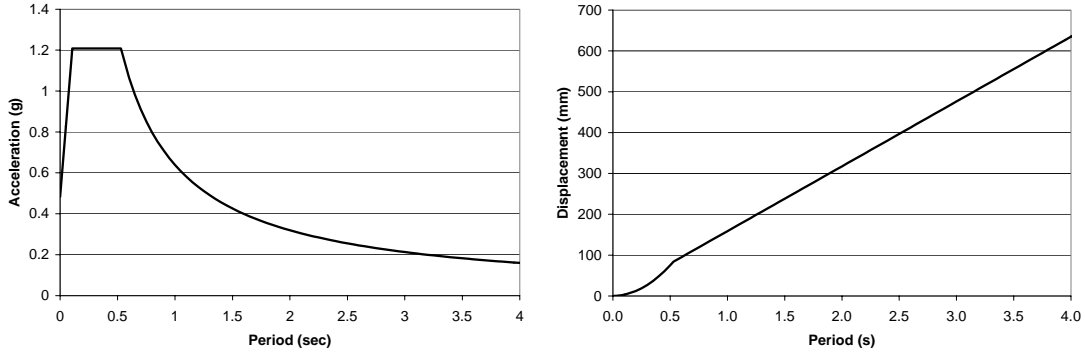


Figure 12: Design Example



**Figure 13: Design Earthquake Spectra**

Since the target displacement is specified, the next step is finding the  $\Delta_{sys}$  and  $M_{sys}$  as defined in Eqs. 1 and 2.

$$\Delta_{sys} = \frac{140 * 72^2 + 360 * 36^2}{140 * 72 + 360 * 36} = 51.75mm$$

$$M_{sys} = 140 \frac{72}{51.75} + 360 \frac{36}{51.75} = 445.2KN / g$$

The next step is to calculate the design base shear,  $V_b$ , by substituting the above values into Eq. 3. The resultant base shear is 872.2 KN. Eq. 9 is solved and results in a wall length of contact,  $c$ , of 512mm. Next the resultant tension force,  $T$ , is found by using Eq. 6.

$$T = \frac{V_b}{\sin \theta_1} - \frac{C_m}{\tan \theta_{strut} \sin \theta_1} = 3442KN$$

Now that the design forces are known, the force design checks of section 5.4.4 are done. The prevention of sliding is verified by Eq. 19. Using a  $\phi$  of 0.8, Eq. 19 results in:

$$\mu = 0.8 > \frac{1}{0.5 \tan 78^\circ} = 0.425$$

Therefore, sliding is not an issue. The drift limit was the source of the target displacement so there is no need to check its validity. The last check is of the minimum resultant force. The design meets this requirement specified in Eq. 19 as seen here:

$$T = 3442 \text{ KN} \geq 0.025(37500)(0.3)(0.51206) = 144.0 \text{ KN}$$

The final step is to calculate the initial post-tensioning strain,  $\varepsilon_{pi}$ , which will have a resultant tension force of 344.2KN. There are numerous solutions to this part of the problem. One solution is to use four 46mm diameter post-tensioning bars ( $E = 200 \text{ GPa}$  and  $f_y = 620 \text{ MPa}$ ) with an area of  $1690 \text{ mm}^2$  symmetrically located within the wall spaced at 200mm. Therefore the bars are located at 1.5m, 1.7m, 1.9m, and 2.1m. Then solving Eq. 25 results in:

$$\sum \varepsilon_{pi} = \frac{T}{E_s A_{pti}} - \frac{\Delta_{sys}}{H_{eff} L_{unbonded}} \sum (x_i - c) = 0.00312$$

The initial post-tensioning strain is found by Eq. 26.

$$\varepsilon_{pi} = \frac{\sum \varepsilon_{pi}}{N_{bars}} = \frac{0.0312}{4} = 0.00078$$

The peak tensile force in the tendon furthest from the wall toe is checked using Eq. 28.

$$\left[ \frac{(x_i - c)\Delta_{sys}}{H_{eff} L_{unbonded}} + \varepsilon_{pi} \right] = 0.00296 \leq TENSILE \ LIMIT = 0.00310$$

Lastly the post-tensioning jacking force is calculated using Eq. 29.

$$T_{ps \ force} = \frac{T_{initial}}{0.75} = \frac{200 \times 10^6 (0.00169)(0.00078)}{0.75} = 352 \text{ KN}$$

## 5.7 CONCLUSIONS

The objective of this paper is to outline a displacement-based design procedure for unbonded post-tensioned clay brick masonry walls. The following conclusions may be drawn:

(1) Unbonded post-tensioned clay brick masonry walls have the same advantages under dynamic loading that were observed during cyclic testing. The walls are self-centering

when properly designed. A rigid rocking mechanism was observed and damage was localized to the toe and heel regions of the wall.

(2) Walls with a low initial post-tensioning strain are effective in resisting seismic loading.

(3) The displacement-based design method proposed in this paper is capable of designing unbonded post-tensioned clay brick masonry walls. The results were shown to be very accurate for a broad range of post-tensioning force and earthquake intensities through the use of shake table testing.

## 5.8 REFERENCES

1. Alshebani, Milad M. and Sinha, S. N. (2000) "Stress-Strain Characteristics of Brick Masonry Under Cyclic Biaxial Compression." *Journal of Structural Engineering*, Vol. 126, No. 9, pp 1004-1007.
2. Christopoulos, C., Filiatrault, A., Uang, C.M., and Folz, B. (2002). "Post-Tensioned Energy Dissipating Connections for Moment-Resisting Steel Frames." *ASCE Journal of Structural Engineering*, Vol 128, No. 9, pp. 1111-1120.
3. Dwairi, H. M., Kowalsky, M.J., and Nau J.M. (2007). "Equivalent Damping in Support of Direct Displacement-Based Design." *Journal of Earthquake Engineering*, Vol. 11, No. 3, pp. 1-19.
4. Ewing, B. D. and Kowalsky, M. J. (2003). "Compressive Behavior of Unconfined and Confined Clay Brick Masonry." *Journal of Structural Engineering*, Vol. 130, No. 4, pp. 650-661.
5. Gulkan, P. and Sozen, M.A. (1974). "In elastic Responses of Reinforced Concrete Structures to Earthquake Motions." *ACI Journal, Proceedings*, Vol. 71, No. 12, pp. 604-610.

6. Hart, G., Noland, J., Kingsley, G., Englekirk, R., and Sajjad, N. A. (1988). "The Use of Confinement Steel to Increase the Ductility in Reinforced Concrete Masonry Shear Walls." *The Masonry Society Journal*, Vol. 7, No. 2, pp T19-T42.
7. Hilsdorf, H. K. (1969)., "An Investigation into the Failure Mechanism of Brick Masonry Under Axial Compression in Designing," *Engineering and Constructing with Masonry Products*, F. B. Johnson, Ed., Gulf Publishing, Houston, May 1969, pp. 34-41.
8. Holden, T., Restrepo, J. , and Mander, J. (2003). "Seismic Performance of Precast Reinforced and Prestressed Concrete Walls." *ASCE Journal of Structural Engineering*, Vol. 129, No. 3, pp 286-296.
9. Kent, D. C. and Park, R. (1971). "Flexural Members with Confined Concrete," *ASCE Journal*, Vol. 97, No. 7, pp. 186-195.
10. Kowalsky, M.J. (2002). "A Displacement-Based Approach for the Seismic Design of Continuous Concrete Bridges." *Journal of Earthquake Engineering and Structural Dynamics*, Vol. 31, No. 3, pp. 506-516.
11. Kowalsky, M.J. and Wight, G.D. (2006). "Direct Displacement-Based Design of Unbonded Post-Tensioned Concrete Masonry Walls." *8<sup>th</sup> U.S. National Conference on Earthquake Engineering*, San Francisco, CA, Apr. 18-22, 10 pp.
12. Laursen, P.T. and Ingham, J.M. (2004). "Structural Testing of Large-Scale Post-Tensioned Concrete Masonry Walls." *ASCE Journal of Structural Engineering*, Vol. 130, No. 10, pp. 1497-1505.
13. Masonry Standards Joint Committee. (2008), "Building Code Requirements for Masonry Structures (ACI 530-08/ASCE 5-08/TMS 402-08)," American Concrete Institute; Structural Engineering Institute of the American Society of Civil Engineers; The Masonry Society.
14. Paulay, T. and Priestley, M.J.N. (1992). *Seismic Design of Reinforced Concrete and Masonry Buildings*, A Wiley-Interscience Publication, New York, 1992.

15. Priestley, M. J. N. and Grant, D. N. (2005). "Viscous Damping in Seismic Design and Analysis." *Journal of Earthquake Engineering*, Vol. 9, Special Issue 2, pp. 229-255.
16. Priestley, M.J.N., Calvi, G.M., and Kowalsky, M.J.(2007). "Direct Displacement-Based Seismic Design of Structures." IUSS Press, Pavia Italy, ISBN 978-88-6198-000-6. 740 pages.
17. Priestley, M.J.N. and Bridgeman, D.O. (1974). "Seismic Resistance of Brick Masonry Walls." *Bulletin of the New Zealand National Society for Earthquake Engineering*, Vol. 7, No. 4, pp 167-187.
18. Priestley, M.J.N., and Elder, D.M. "Stress-Strain Curves for Unconfined and Confined Concrete Masonry." *ACI Journal*, Vol. 80, No. 3, pp 192-201.
19. Priestley, M.J.N., Sritharan, S., Conley, J.R., and Pampanin, S. (1999), "Preliminary Results and Conclusions from the PRESSS Five-Story Precast Concrete Test Building." *PCI Journal*, Vol. 44, No. 6, pp. 42-67.
20. Priestley, M.J.N., and Tao, J.R. (1993). "Seismic Response of Precast Prestressed Concrete Frames with Partially Debonded Tendons." *PCI Journal*, Vol. 38, No. 1, pp 58-69.
21. Ricles, J.M., Sause, R., Garlock, M.M., and Zhao, C. (2001). "Post-Tensioned Seismic-Resistant Connections for Steel Frames." *ASCE Journal of Structural Engineering*, Vol. 127, No. 2, pp 113-121.
22. Rosenboom, O.A. and Kowalsky, M.J. (2004). "Reversed In-Plane Cyclic Behavior of Post-Tensioned Clay Brick Masonry Walls." *ASCE Journal of Structural Engineering*, Vol. 130, No. 5, pp. 787-798.
23. SEAOC Blue Book, vision 2000. (1996). Structural Engineers Association of California (SEAOC). Sacramento, CA.

24. Yule, D.E., Kala, R.V, and Matheu, E.E. (2005). “Determination of Standard Response Spectra and Effective Peak Ground Accelerations for Seismic Design and Evaluation.” CHETN-VI-41, 16 pages.

## 6 SUMMARY AND CONCLUSIONS

### 6.1 CONCLUSIONS

The research breaks down into two main goals: (1) Determine the effect of openings on the behavior of unbonded post-tensioned clay brick masonry and (2) Develop a method to design these walls. To examine the effect of openings on unbonded post-tensioned clay brick masonry walls a total of three walls were constructed. After each test a new wall was constructed in an attempt to correct the deficiency in the previous test. Based on the assessment of the experimental tests the following was concluded:

- Detailing of the clay brick masonry is necessary to keep the benefits, primarily the self-centering behavior and damage localized to the heel and toe regions of the wall, of unbonded post-tensioned masonry walls.
- Excessive crack growth causes the wall to slide instead of rock. The sliding mechanism results in undesirable residual deformation and increased difficulty in structural repairs.
- While confinement plates increase the compressive strength of the masonry wall, it is not adequate to reduce excessive crack growth and maintain the wall's self-centering behavior.
- Horizontal steel is required to restrain the growth of cracks. If properly design, horizontal steel will ensure that the wall deforms by rocking, self-centering behavior is achieved, and damage is localized to the heel and toe regions of the wall where repairs are possible.

Following the full-scale tests, analytical studies were conducted to examine the behavior of unbonded post-tensioned clay brick masonry walls with openings of different

sizes and walls of varying aspect ratio. The conclusions of the parametric study are as follows:

- Structures can be sub-divided into unbonded post-tensioned masonry wall panels that maintain its self-centering behavior by means of horizontal or vertical isolation.
- Unbonded post-tensioned clay brick masonry walls with openings behave similar to otherwise identical walls without openings until the opening causes the compressive strut to destabilize. The author refers to this process as “single story approximation.”
- The single story approximation can be extended to walls of identical aspect ratio to multiple story walls.

Next, research shifted towards the application of Direct Displacement-Based Design to unbonded post-tensioned clay brick masonry walls. Upon inspection of finite element modeling of previously tested walls an unusual phenomenon was discovered. The finite element model was able to accurately predict the behavior of the masonry wall up to a point. The model was not able to predict the ultimate strength of the unbonded post-tensioned clay brick masonry wall. The source of the discrepancy was attributed to local confinement by the foundation on the masonry clay brick masonry wall. A study was conducted to determine the effect of the foundation on the stress-strain relationship of clay brick masonry. The conclusions of the study are as follows:

- The proposed methodology verified that the interface between the clay brick masonry wall and foundation plays an important part on the behavior of the wall.

- The actual local compressive strength of clay brick masonry is 21% higher, from 25.9 MPa to 31.3 MPa, than observed from prism testing.
- The proposed method for defining the stress strain behavior of the clay brick masonry is able to accurately predict the force-displacement response of unbonded post-tensioned clay brick masonry walls.
- By using the methodology discussed in this dissertation, correct equivalent stress block parameters can be found for use in determining the compressive strength of masonry for design purposes.

Lastly, the research concentrated on using Direct Displacement-Based Design principles with the knowledge of the behavior and limit states of clay brick masonry to prescribe a method to design and predict the damage in the wall at various earthquake intensities. A test specimen was constructed and tested on a shake table by varying the intensity of three real earthquakes and the initial post-tensioning strain. A grand total of 56 runs were conducted. Based on the results of the shake table testing the Performance-Based Design of unbonded post-tensioned clay brick masonry walls methodology was described and compared to the test results. The conclusions of this section of the dissertation are as follows:

- Unbonded post-tensioned clay brick masonry walls have the same advantages under dynamic loading that were observed during cyclic testing. The walls are self-centering when properly designed. A rigid rocking mechanism was observed and damage was localized to the toe and heel regions of the wall.
- Walls with a low initial post-tensioning strain are effective in resisting seismic loading. The final post-tensioning bar force of 27 KN was applied by hand with a long wrench without the assistance of a hydraulic pump.

- The displacement-based design method proposed in this paper is an excellent way to design unbonded post-tensioned clay brick masonry walls. The results were shown to be reasonably accurate for a broad range of post-tensioning force and earthquake intensities through the use of shake table testing.

## **6.2 RECOMMENDATIONS**

This dissertation has explored the behavior of unbonded post-tensioned clay brick masonry walls. Three large scale tests of walls with openings and over 56 earthquake shake table tests were conducted. In addition to these tests, parametric studies were done to predict the behavior of walls with different sized openings and aspect ratios.

Based on this research it is recommended that the designer uses horizontal and vertical isolation practices wherever possible to avoid having to design unbonded post-tensioned masonry walls with openings. If openings can not be avoided the proposed design tables in section 3.4.1 can serve as a basis for the initial design. It is important to recognize that these tables are based on a relatively small number of variations, but are expected to yield acceptable results. However, if these tables are applied to single set of parameters, there is a possibility of errors in estimating the drift ratio. Furthermore, if the unconfined masonry strength is adequate to resist the design base shear force, then the incorporation of confinement plates should be avoided and the stability of the unbonded post-tensioned masonry wall should rely only on the horizontal steel placed around the opening.

It is also recommended that Performance-Based Design should be based on the equivalent stress blocks derived from the stress-strain relationship calculated from the proposed methodology in section four.

### **6.3 FUTURE WORK**

Although the research showcased in this dissertation has advanced the knowledge of unbonded post-tensioned clay brick masonry walls, more still is needed. Future work should concentrate on the following:

- Structural testing of “L,” “T,” and “I” shaped walls. These configurations are typically found in buildings and design recommendations are necessary.
- Application of unbonded post-tensioned clay brick masonry walls to modular construction, low- to mid-rise residential and commercial structures, and light industrial buildings.
- Development of a simple procedure to predict the appropriate locations of confinement plates without the use of time-consuming and complicated finite element analysis.

# APPENDIX

A P P E N D I X A

# **1 COMPRESSIVE BEHAVIOR OF CLAY BRICK MASONRY**

B R Y A N E W I N G

M E R V Y N K O W A L S K Y

# COMPRESSIVE BEHAVIOR OF CLAY BRICK MASONRY

Bryan Ewing and Mervyn J. Kowalsky

*Department of Civil, Construction and Environmental Engineering, North Carolina State University,  
Campus-Box 7908, Raleigh, NC-27695, USA*

Keywords: Stress Strain Relations, Masonry Construction, Confinement Plates

## 1.1 ABSTRACT

Presented in this paper are the results of an investigation of the compressive behavior of grouted clay brick masonry prisms. The objective is to experimentally capture the stress-strain characteristics of unconfined and confined clay brick masonry and compare the response with that predicted with the “modified” Kent-Park stress-strain Curve. Based on the experimental results, five limit states for clay brick masonry in compression are proposed, as well as equivalent stress blocks for design. Thin galvanized steel plates placed in the mortar joints during construction provided prism confinement. The variables considered included volumetric ratio of confining steel (0, ~0.015, and ~0.03) and the presence of machined holes within the confinement plates to improve the bond between the masonry and steel plate. It is shown that confinement plates are extremely effective in enhancing the ultimate compressive strength as well as increasing the deformation capacity of the clay brick masonry prisms. Use of confinement plates increased the unconfined ultimate strength by 40%. Failure of the confined masonry prisms occurred simultaneously or immediately after yielding of the confinement plates. Experimentally obtained stress-strain curves agreed reasonably well with the “modified” Kent-Park model.

## 1.2 INTRODUCTION

Typically, confinement of cementitious materials is achieved through the use of ties, spirals, or circular hoops. Such configurations are difficult to achieve in masonry walls where the cross sections are typically very long in one dimension while relatively thin in the other. For masonry, one approach for confinement is to utilize thin galvanized steel plates placed in the mortar joints during construction. The confinement plates serve the same purpose as transverse reinforcement in a typical concrete member. As the masonry compression strain increases, the masonry dilates, and the tensile strain in the plates increases. In turn, the masonry is placed in a state of tri-axial compression, thus increasing the strength and ductility of the masonry.

The use of thin steel plates in mortar bed joints of masonry structures for confinement was first proposed by Priestley and Bridgeman in 1974 (Priestley, 1974). Through a series of racking tests on large scale clay brick masonry walls, it was noted that confinement plates placed within the mortar bed joints restricted the lateral expansion of the joint and the differential expansion between the clay brick unit and the joint. As a result, the plates inhibited vertical splitting cracks caused by tensile forces introduced into the clay brick unit by the differential expansion of the mortar joint and brick.

In 1983, Priestley and Elder conducted a series of tests on the influence of confinement on the compressive behavior of concrete block masonry (Priestley, 1983). Their research indicated that the use of confinement plates increased the strength and deformation capacity of concrete block masonry prisms. In addition, they modified a stress-strain model developed by Kent and Park (1971) and utilized it to accurately predict the response of confined concrete masonry. The modified Kent-Park model they developed takes into account

the volumetric ratio of confinement steel; yield strength and geometry of the confinement plates; and unconfined masonry strength. This model is used in this paper to examine the stress-strain characteristics of clay brick masonry.

In 1988, Hart et al. (Hart, 1988) reviewed various approaches for confinement of concrete masonry and proposed four performance limit states and associated stress and strain definitions as a function of confinement type. One of the confinement types considered in their research was the steel plates first proposed by Priestley and Bridgeman (1974) that are used in the research described in this paper.

To the knowledge of the authors, no research to date has been conducted on the compressive behavior of confined clay masonry. The aspect ratio of typical clay brick units makes the use of confinement attractive as they can be spaced much tighter than the 203mm spacing typical of concrete block units. As a result, it is expected that confinement plates will have a substantial effect on the compressive strength and strain capacity of clay brick masonry beyond that observed for concrete block masonry. Data regarding the influence of the plates on compression behavior is needed such that accurate analytical models for prediction of member response can be developed.

### **1.3 RESEARCH OBJECTIVE AND METHODS**

There are three goals in the experimental research described in this paper. Of interest is the effect of confinement on: (1) Ultimate strength, (2) Ultimate masonry compressive strain, and (3) Overall shape of the stress-strain relationship. In order to accomplish these goals, tests were carried out upon fifteen clay brick masonry prisms. The test results are then compared with existing analytical models for stress-strain response and recommendations

made as to appropriate performance limit states and equivalent rectangular stress blocks for design.

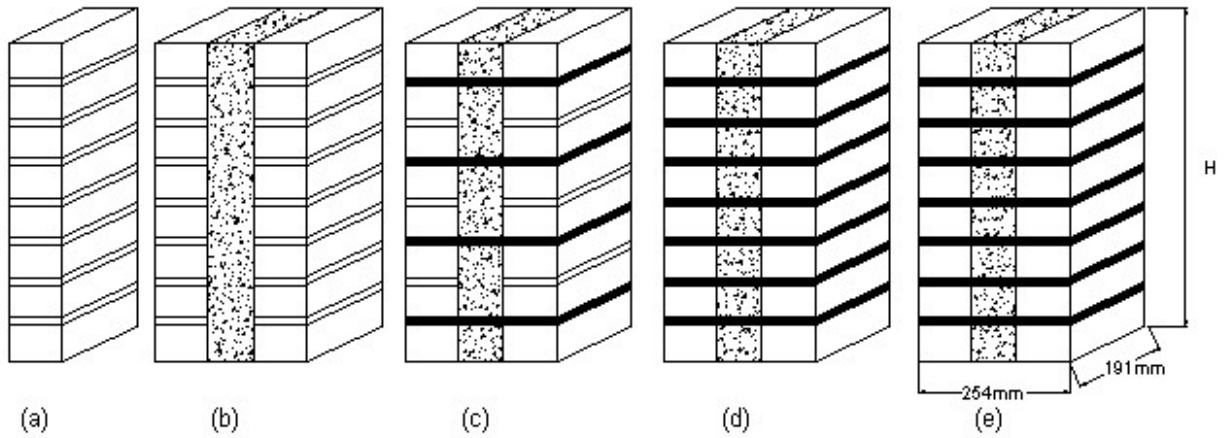


**Figure 1: Prism Configurations**

Current research underway at NCSU follows the work described in this paper and aims to assess the influence of the plates on reinforced and post-tensioned clay masonry walls.

The confinement plates used in this research are divided into two different types: (1) Standard Plates and, (2) Solid Plates. The standard plates have additional machined holes to improve its bond with the mortar. The solid plates do not have these additional holes.

The tests are divided into two categories consisting of three single wythe and twelve double wythe grouted clay brick masonry prisms. The single wythe prisms are constructed to evaluate their strength,  $f'_p$ , in comparison with the value predicted by Paulay and Priestley (1992).

**Table 1: Material properties**

Clay Brick	$f'_c$ (MPa)	34.0
	$f'_{tb}$ (MPa)*	1.72
Mortar**	$f'_j$ (MPa)	15.7
Grout**	$f'_g$ (MPa)	23.6
Galvanized Steel (confinement plates)	$f_y$ (MPa)	266

\* prescribed MSJC value

\*\* 30 - 35 day strength

1 Mpa = 145 psi

The double wythe prisms are constructed in such a way to represent the compressive zones of clay brick masonry walls subjected to in-plane loading. The double wythe prisms were separated into four different groups of three prisms each. The first three groups consist of prisms (1) Without confinement, (2) With alternate courses of confinement, and (3) With confinement every course. The confinement plates for these groups have holes for increased bond in addition to the central hole for grout. The fourth group was added to determine the effectiveness of the bonding holes and consisted of prisms with confinement in every course that were designed to have the same volumetric ratio as the standard plates. The motivation to investigate the effect of the bonding holes is cost related. The added drilled holes create a substantial additional manufacturing cost. Fig. 1a-e illustrates the four different double wythe configurations and the single wythe configuration, while Table 1 contains the component material properties. For more information about how the values were obtained refer to Ewing and Kowalsky (2003).

## 1.4 TEST RESULTS

### 1.4.1 Single Wythe Prisms

Three single wythe prisms were tested to determine the strength and compare experimental results with Eq. 1 as suggested by Paulay et al. (1992).

$$f'_p = \frac{f'_{cb} (f'_{tb} + \alpha f'_j)}{\mu_u (f'_{tb} + \alpha f'_{cb})} \quad (\text{Eq. 1})$$

where  $f'_{cb}$  is the uniaxial compressive strength of the masonry unit,  $f'_{tb}$  is the biaxial tensile strength of the masonry unit,  $\mu_u$  is the stress nonuniformity coefficient and is equal to 1.5 (Hilsdorf, 1969). The variable  $\alpha$  is given by Eq. 2.

$$\alpha = \frac{j}{4.1h} \quad (\text{Eq. 2})$$

where  $j$  is the mortar joint thickness and  $h$  is the height of the masonry unit. The uniaxial compressive strength,  $f'_{cb}$ , is altered to account for masonry unit holes filled with mortar and is defined by Eq. 3 (Paulay, 1992).

$$f'_{cb} = x f'_c + (1 - x) f'_j \quad (\text{Eq. 3})$$

where  $x$  is the ratio of net unit area to gross area (Paulay, 1992). Good agreement is achieved between the experimental results, 15.56 MPa, and those obtained by Eq. 1, 15.48 MPa. The single wythe prisms failed in a brittle nature brought on by the extremely rapid propagation of splitting cracks.

### 1.4.2 Double Wythe Grouted Prisms - Unconfined

The unconfined clay brick masonry prisms first showed signs of pending failure at approximately 75% of the maximum compression load on the rising curve of the stress-strain

relationship. At this point, visible splitting cracks appeared. From this point on, the density of the vertical splitting cracks increased until spalling of the face shell occurred as the maximum load was reached. Extensive crushing of the masonry was observed as the prisms' load carrying capacity rapidly dropped after reaching the ultimate load. Paulay et al. (1992) suggests that Eq. 4 can be used to determine the compressive strength of grouted brick masonry.

$$f_m = \phi [x f'_p + (1-x) f'_g] \quad (\text{Eq. 4})$$

$f'_g$  is the compressive strength of the grout and  $\phi$  is 1.0 for clay brick masonry. The equation gives a value of 18.0 MPa, while experimental results gives an unconfined masonry prism strength of 25.9 MPa. Further details of the testing procedure and their results are available in Ewing and Kowalsky (2003).

### **1.4.3 Double Wythe Grouted Prisms - Confined**

The confined masonry prisms were able to maintain their structural integrity much better than the unconfined prisms. Minor vertical splitting cracks were not observed until shortly prior to reaching the maximum load. Spalling of the face shell was practically eliminated for the prisms confined every course, while the prisms with confinement plates placed in alternate courses exhibited a tremendous reduction in the size of the material that spalled off from the prism. In this case only the section of prism that extended beyond the confining plates separated from the core. Generally, the crushing of the masonry prisms was limited to one or two courses while the physical appearance of the remaining prism appeared structurally sound.

**Table 2: Double wythe prism results**

PRISM TYPE		$f'_m$ (MPa)	$\epsilon_{rm}$	$\epsilon_{50\% f_m}$	$\epsilon_{20\% f_m}$
Unconfined	1	28.35	0.0016	0.0037	0.0073
	2	22.57	0.0019	0.0064	0.0104
	3	26.79	0.0016	0.0049	0.0086
	<b>mean</b>	<b>25.90</b>	<b>0.0017</b>	<b>0.0050</b>	<b>0.0087</b>
	st. dev.	2.99	0.0002	0.0014	0.0015
Alternate Course Confined	1	30.48	0.0026	0.0135	0.0205
	2	29.46	0.0036	0.0165	0.0588
	3	31.12	0.0027	0.0154	0.0241
	<b>mean</b>	<b>30.35</b>	<b>0.0030</b>	<b>0.0151</b>	<b>0.0344</b>
	st. dev.	0.84	0.0005	0.0015	0.0212
Every Course Confined	1	35.66	0.0063	0.0268	0.0403
	2	35.19	0.0056	0.0396	0.0585
	3	35.97	0.0063	0.0366	0.0490
	<b>mean</b>	<b>35.61</b>	<b>0.0061</b>	<b>0.0344</b>	<b>0.0493</b>
	st. dev.	0.39	0.0004	0.0067	0.0091
Solid Plate, Every Course Confined	1	35.28	0.0065	0.0242	0.0588
	2	36.30	0.0075	0.0393	0.0705
	3	38.50	0.0078	0.0415	0.0777
	<b>mean</b>	<b>36.69</b>	<b>0.0073</b>	<b>0.0350</b>	<b>0.0690</b>
	st. dev.	1.65	0.0007	0.0094	0.0095

After reviewing the data, it was observed that the prism reached its ultimate load at approximately the same time that the confinement plates began to yield. Two of the confinement plates in the prisms confined every course ruptured; one standard plate and one solid plate. This rupture resulted in a sharp drop in load and/or an increase in masonry strain; however, the result was not catastrophic as the prism continued to sustain load and deformation at approximately the same rate as that prior to the plate rupture. This is due to the presence of several confinement plates which were still effective in resisting tension.

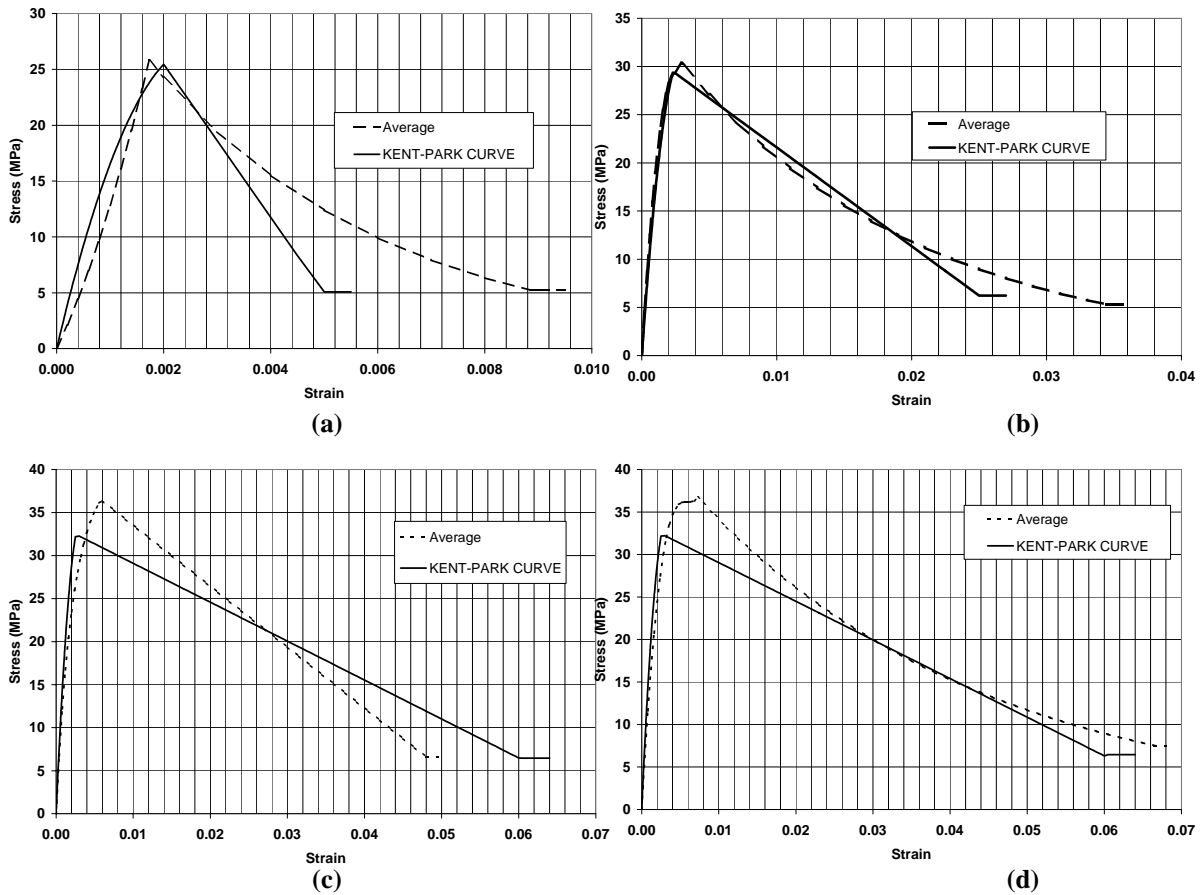


**Figure 2: Stress-Strain Relationships; (a) Unconfined; (b) Alternate Course Confined; (c) Every Course Confined; (d) Solid Plate, Every Course Confined**

#### 1.4.4 Stress-strain relationships

Results of the stress-strain relationships are shown in Table 2. In Table 2,  $\epsilon_{f'_m}$  refers to the strain at  $f'_m$ , while  $\epsilon_{50\%f'_m}$  and  $\epsilon_{20\%f'_m}$  refer to the strain at 50% and 20% of  $f'_m$  on the descending curve, respectively. The average stress-strain relationships for each set of tests; (1) Unconfined, (2) Alternate courses confined, (3) Every course confined, and (4) Every course confined with solid plates, are shown in Fig. 2. Visual observations reveal that confinement plates had a significant effect on the ultimate strength and deformation capacity. The masonry strain at  $0.2f'_m$  is significant because this is where the falling curve of the stress-strain relationship begins to plateau. Priestley et al. (1983) observed the same behavior

during the investigation of concrete masonry prisms and therefore decided to prescribe the masonry strain at  $0.2f'_m$  as the masonry strain capacity for the “modified” Kent-Park Curve.

Confinement plates placed within every mortar joint increased the ultimate unconfined masonry strength by nearly 40%. The confinement plates had a dramatic effect on the ultimate masonry capacity strain.

A visual inspection of the prisms with and without bonding holes reveals some interesting trends. The prisms with solid plates had an ultimate strength of 36.7 MPa while the plates with holes reached a maximum stress of 35.6 MPa. Even though both plates have the same volumetric steel ratio, the prisms containing the solid confinement plates consistently outperformed the prisms that incorporated the confinement plates with the additional holes. It is believed that the source of the enhanced performance of the solid plates versus its counterpart is the lack of bonding holes and larger cross sectional area of the plate flanges. Although the bonding holes increase bond between the plate and the mortar, the holes introduce stress concentrations within the plates that act to locally increase the stresses in the plates and reduce the confining masonry compression strain.

## **1.5 COMPARISON WITH KENT-PARK MODEL**

Limited research has been done on the stress-strain relationships of confined clay brick masonry. Research of the past decade has focused on the failure mechanisms and criterion of brick masonry. These investigations range from uniaxial monotonic testing of clay brick prisms to cyclic biaxial studies of scaled models (Alshebani et al., 2000). Although knowledge of the failure mechanisms and failure criterion is helpful, more information about the stress-strain relationship of clay brick masonry is needed for design in seismic regions.

Priestley et al. (1983) conducted tests on concrete masonry prisms and decided to use a “modified” Kent-Park Curve for their investigation and it is used in this investigation as well. The “modified” Kent-Park Curve is a function of the unconfined compression strength, confinement yield strength, volumetric steel ratio, lateral dimension of confined core, and longitudinal spacing of confinement steel. The curve is broken into three separate portions; a parabolic rising curve, a linear falling branch, and a final horizontal plateau. The curve is detailed as follows:

Rising Curve

$$\varepsilon_c \leq 0.002K \quad (\text{Eq. 5})$$

$$f'_m = 1.067 f_m K_c \left[ \left( \frac{2\varepsilon_c}{0.00267K} \right) - \left( \frac{\varepsilon_c}{0.00267K} \right)^2 \right] \quad (\text{Eq. 6})$$

Where:

$$K = 1 + \rho_s \frac{f_{yh}}{f'_c} \quad (\text{Eq. 7})$$

And  $f_m$  is the unconfined prism strength,  $f_{yh}$  is the confinement steel yield strength, and  $\rho_s$  is the volumetric ratio of the confinement steel.

Descending Curve

$$f'_m = K f_m [1 - Z_m (\varepsilon_c - 0.00267K)] \quad (\text{Eq.8})$$

Where

$$Z_m = \frac{0.5}{\left( \frac{3 + 0.29 f'_c}{145 f'_c - 1000} \right) + \frac{3}{4} \rho_s \sqrt{\frac{h''}{s_h}} - 0.00267K} \quad (\text{Eq. 9})$$

And  $h''$  is the lateral dimension of the confined core and  $s_h$  is the longitudinal spacing of the confinement plates. The modified Kent-Park Curve plateaus at  $0.2 f'_m$ .

Upon inspection of Fig. 2a and 2b, the Kent-Park model is adequate in predicting the stress-strain relationships of clay brick masonry. However, Fig. 2c and 2d show that the model is consistently conservative with respect to the ultimate strength and its corresponding strain. Previous research has shown good agreement with the Kent-Park model in regards to concrete masonry at low volumetric steel ratios (Priestley, 1983). It is speculated that the prisms considered in this research had volumetric steel ratios of confinement steel much higher than that previous considered. Nonetheless, the existing model seems to provide a reasonably conservative estimate of both of these variables.

## **1.6 LIMIT STATES OF CLAY BRICK MASONRY BASED ON EXPERIMENTAL RESULTS**

Performance-based design approaches rely on characterization of structural performance at a variety of limit states. Work by Hart et al. (1988) defined four limit states for confined concrete masonry as shown in Table 3. Strain values used to define the limit states in Table 3 varied depending on the type of confinement utilized as discussed by Hart et al. (1988). Shown in Table 3 are the values for the confinement plates developed by Priestley and Bridgeman (1974) that are utilized in this research. Based on the tests conducted in this research program, slightly different limit state definitions for clay brick masonry are proposed, namely:

Limit State 1: Initiation of vertical splitting cracks, occurring at  $0.75f'_m$  for unconfined masonry. This limit state does not apply to confined masonry as vertical splitting is virtually eliminated when the clay masonry units are confined.

Limit State 2: Excessive density/propagation of splitting cracks occurring at  $0.90f'_m$ . This limit state does not apply to confined masonry.

Limit State 3: Yielding of confinement plates occurring at  $0.95f'_m$ . This limit state does not apply to unconfined masonry.

Limit State 4: Maximum dependable masonry compression strain, occurring at  $0.50f'_m$ . This limit state applies to both confined and unconfined masonry.

Limit State 5: Ultimate masonry compression strain occurring at  $0.20f'_m$ . This limit state applies to both confined and unconfined masonry.

**Table 3: Hart et al. (1988) confined concrete masonry limit states**

Limit States	Prism Compression Strain	
	Type 1 <sup>*</sup>	Type 2 <sup>**</sup>
1 Serviceability	0.0014	0.0014
2 Maximum Strength (100% $f'_m$ )	0.0018	0.0017
3 Design Strength (50% $f'_m$ )	0.0068	0.0054
4 Ultimate Strength (20% $f'_m$ )	0.0153	0.0192

<sup>\*</sup>Type 1: Steel Volume Equivalent to #3 @ 8" o.c. (Hart et al., 1988)

<sup>\*\*</sup>Type 2: 2 Times Type 1 Confinement Steel (Hart et al., 1988)

Limit states 4 and 5 are consistent with that proposed by Hart, however, limit states 1, 2, and 3 are different based on the data obtained in the prism tests conducted. This is particularly important for limit state 3 where instrumentation of the confinement plates allowed for a correlation between yielding of the plates and the masonry reaching its maximum compression strength of  $f'_m$ . Table 4 summarizes the limit states proposed for clay brick masonry. Note that compression strain values for each limit state are defined based on both the modified Kent-Park curve and the average experimental results. This data will be utilized in the subsequent section on development of equivalent rectangular stress block parameters.

**Table 4: Limit states of clay brick masonry**

Limit States	Unconfined		Alternate Course Confined		Every Course Confined	
	Kent-Park	Average	Kent-Park	Average	Kent-Park	Average
1 Initiation of Splitting Cracks	0.75f <sub>m</sub>		-----			
	0.0012	0.0014	-----	-----	-----	-----
2 Excessive Cracks/Spalling	0.9f <sub>m</sub>		-----			
	0.0016	0.0016	-----	-----	-----	-----
3 Yielding of Confinement Plates	-----		0.95f <sub>m</sub>		0.95f <sub>m</sub>	
	-----	-----	0.0021	0.0022	0.0023	0.0047
4 Maximum Dependable Compression Strain	0.5f <sub>m</sub>		0.5f <sub>m</sub>		0.5f <sub>m</sub>	
	0.0039	0.0050	0.0168	0.0151	0.0387	0.0344
5 Ultimate Compression Strain	0.2f <sub>m</sub>		0.2f <sub>m</sub>		0.2f <sub>m</sub>	
	0.0049	0.0088	0.0245	0.0344	0.0595	0.0493

## 1.7 EQUIVALENT STRESS BLOCK PARAMETERS

**Table 5: Equivalent stress block parameters**

### Limit State 4

Prism Type	modified Kent-Park Curve			Experimental Results		
	$\alpha$	$\beta$	$\epsilon_{mu}$	$\alpha$	$\beta$	$\epsilon_{mu}$
Unconfined	0.86	0.86	0.00386	0.93	0.66	0.00498
Alternate Course Confined	0.73K	1.05	0.01675	0.71K	1.06	0.01514
Every Course Confined	0.71K	1.08	0.03866	0.74K	1.08	0.03435

### Limit State 5

Prism Type	modified Kent-Park Curve			Experimental Results		
	$\alpha$	$\beta$	$\epsilon_{mu}$	$\alpha$	$\beta$	$\epsilon_{mu}$
Unconfined	0.75	0.96	0.00486	0.44	1.13	0.00875
Alternate Course Confined	0.56K	1.15	0.02450	0.45K	1.26	0.03444
Every Course Confined	0.51K	1.20	0.05950	0.55K	1.20	0.04926

The equivalent stress block is specified by two parameters,  $\alpha$  and  $\beta$ , such that (1) the average stress,  $\alpha f'_c$ , extends  $\beta c$  from the extreme compression fiber and (2) the equivalent stress block has the same area and centroidal height as the original stress-strain relationship (Paulay and Priestley, 1992). Equivalent rectangular stress blocks are defined for limit states four and five shown in Table 4. The purpose for multiple definitions is to accommodate performance-based design procedures such as displacement-based design which may require

that strengths be evaluated at a different limit states. Although a section analysis utilizing proper steel and masonry stress-strain constitutive relationships could be employed for analysis and design, the simplicity of an equivalent rectangular block is useful for fast estimates of strengths at multiple limit states.

In Table 5, two sets of stress block parameters are shown. The values labeled as ‘modified Kent-Park Curve’ refer to those obtained using Eqs. 5-9 with the strain values obtained from the Kent-Park curve (see Table 4) for the limit state under consideration. The column labeled ‘Experimental Results’ refers to the values obtained using the average of the experimental stress strain-curves (see Table 4). The Masonry Standards Joint Committee (2002) suggests the equivalent stress block parameters,  $\alpha$  and  $\beta$ , are equal to 0.8 when coupled with a masonry compression strain of 0.0035. The MSJC values approaches those obtained for the modified Kent-Park Curve for unconfined masonry, but are vastly different from those found for confined masonry as expected. It is imperative that use of the appropriate stress block parameter be employed when evaluating the strength of a masonry member. In order to use the stress block parameters in Table 5, the confinement factor,  $K$ , is evaluated using Eq. 7. The table is then entered with  $K$  and the parameters obtained for the design limit state under consideration.

## **1.8 CONCLUSIONS AND RECOMMENDATIONS**

The objective of the research described was to assess the influence of confinement on the strength and ductility of clay brick masonry prisms, and to define design limit states and equivalent rectangular stress block parameters based on the results. The following conclusions may be drawn:

Confinement plates dramatically improve the compressive strength of clay brick masonry. The plates in this research program increased the ultimate strength by as much as 40%. Using a higher grade of steel could theoretically enhance the performance even more.

The Kent-Park Model properly models the stress strain relationship of clay brick masonry regardless of the volumetric ratio of the confining steel tested. As implied by the Kent-Park equations (Eqs. 5-9) there is a direct relationship between the volumetric ratio of confining steel and the ultimate strength and strain. As the amount of confining steel increases, so does the ultimate strength and strain.

Solid confining plates (those without bonding holes) proved to be as effective as plates with holes. It is postulated that greater cross-section and the lack of bonding holes (and their resultant stress concentrations) improved the ultimate strength and masonry strain capacity. The ultimate strength is 3% higher and the strain at  $0.2f'_m$  21% greater. Solid confining plates are cheaper to manufacture than the plates with holes. However, more must be known about the bonding stress profile across the lateral length of the confinement plate. Simply from reviewing the stress-strain relationships of the two types of confinement plates, it would appear the bond along the solid plate was adequate.

Confinement plates may reduce the effect that workmanship has on the behavior of clay brick masonry structures. The quality of workmanship has an enormous effect on the strength of all masonry structures. However, because of the comparative size of clay brick to concrete block, the effects could be magnified. But this size disadvantage could be beneficial if the clay brick masonry is confined. Clay brick masonry can allow for higher volumetric steel ratios than concrete block masonry. One of the trends that become evident from the

inspection of Table 2 is that as the volumetric steel ratio increases, the standard deviation in ultimate strength reduces dramatically.

Performance limit states for clay masonry are defined on the basis of stress and strain levels, and associated equivalent rectangular stress block parameters obtained. The resulting data can be utilized directly in performance-based design procedures such as displacement-based design to evaluate the strength of masonry walls quickly at the chosen design limit state.

## **1.9 ACKNOWLEDGEMENTS**

This research was carried out with the financial assistance of the Partnership for Advancing Technology in Housing (PATH) and the National Science Foundation (NSF) under grant number 0080210. Additional acknowledgement goes to the North Carolina State University Department of Civil Engineering, Pinnacle Mason for mason's labor, General Shale Brick for clay brick units, and Jerry Atkinson of NCSU's Constructed Facilities Laboratory.

## **1.10 REFERENCES**

1. Alshebani 2000: Alshebani, Milad M. S. N. Sinha, "Stress-Strain Characteristics of Brick Masonry Under Cyclic Biaxial Compression," *Journal of Structural Engineering*, Vol. 126, No. 9, September 2000, pp 1004-1007.
2. Ewing 2003: Ewing, B. D. and M. J. Kowalsky, "Compressive Behavior of Unconfined and Confined Clay Brick Masonry." *The Masonry Society Journal*,
3. Hart 1988: Hart, G., J. Noland, G. Kingsley, R. Englekirk, and N. A. Sajjad, "The Use of Confinement Steel to Increase the Ductility in Reinforced Concrete Masonry Shear Walls." *The Masonry Society Journal*, Vol. 7, No. 2, pp T19-T42.

4. Hilsdorf 1969: Hilsdorf, H. K., "An Investigation into the Failure Mechanism of Brick Masonry Under Axial Compression in Designing," *Engineering and Constructing with Masonry Products*, F. B. Johnson, Ed., Gulf Publishing, Houston, May 1969, pp. 34-41.
5. Kent 1971: Kent, D. C. and R. Park, "Flexural Members with Confined Concrete," *ASCE Journal*, Vol. 97, No. ST7, July 1971, pp. 186-195.
6. Masonry Standards Joint Committee 2002: Masonry Standards Joint Committee, "Building Code Requirements for Masonry Structures (ACI 530-02/ASCE 5-02/TMS 402-02)," American Concrete Institute; Structural Engineering Institute of the American Society of Civil Engineers; The Masonry Society, 2002.
7. Paulay 1992: Paulay, T. and M.J.N. Priestley, *Seismic Design of Reinforced Concrete and Masonry Buildings*, A Wiley-Interscience Publication, New York, 1992.
8. Priestley 1974: Priestley, M.J.N. and D. O. Bridgeman, "Seismic Resistance of Brick Masonry Walls." *Bulletin of the New Zealand National Society for Earthquake Engineering*, Vol. 7, No. 4, December 1974, pp 167-187.
9. Priestley 1983: Priestley, M.J.N., and D.M. Elder, "Stress-Strain Curves for Unconfined and Confined Concrete Masonry." *ACI Journal*, May-June 1983, Vol. 80, No. 3, pp 192-201.

A P P E N D I X B

**1 ANSYS MODELING**

B R Y A N E W I N G

# ANSYS MODELING

## 1.1 INTRODUCTION

ANSYS finite element modeling was used throughout the entire research project. ANSYS was used to create a model that would show good agreement with experimental tests. Once the model was verified against full scale test specimens, ANSYS was then used to conduct parametric studies. This appendix outlines the basic steps used to model unbonded post-tensioned clay brick masonry walls.

## 1.2 ELEMENT TYPES

Four kinds of elements were adopted in the finite element model:

- Solid186 element. This element is defined by 20 nodes having three degrees of freedom at each node, namely translations in the nodal x, y, and z directions. The element has quadratic displacement capabilities which were desirable for acquiring accurate data along the masonry wall/foundation interface. It was used for 3-D modeling of the masonry wall and the concrete foundation.
- Conta174 element. This element is defined by a single point and is mapped on top of the masonry wall nodes that will come into contact with the foundation. It is used to represent contact and sliding between two 3-D surfaces. The element can record frictional forces, gap opening displacements, and sliding displacements.
- Targe170 element. This element is defined by a single point and is mapped on top of the foundation nodes that will come into contact with the masonry wall.

This element is paired with the Conta174 element. It is used to represent contact and sliding between two 3-D surfaces.

- Link8 element. This 3-D spar element is a uni-axial tension–compression element with three degrees of freedom at each node, namely translations in the nodal x, y, and z directions. No bending of the element is considered. In addition to the locations of the beginning and ending nodes, it is defined by a cross-sectional area and initial strain. It was used to model the post-tensioning bars in the masonry wall.

### 1.3 MATERIAL PROPERTIES

Three different materials were used in the models. Figures 1 – 3 show the stress-strain relationships for the masonry wall, concrete foundation, and the post-tensioning steel bars.

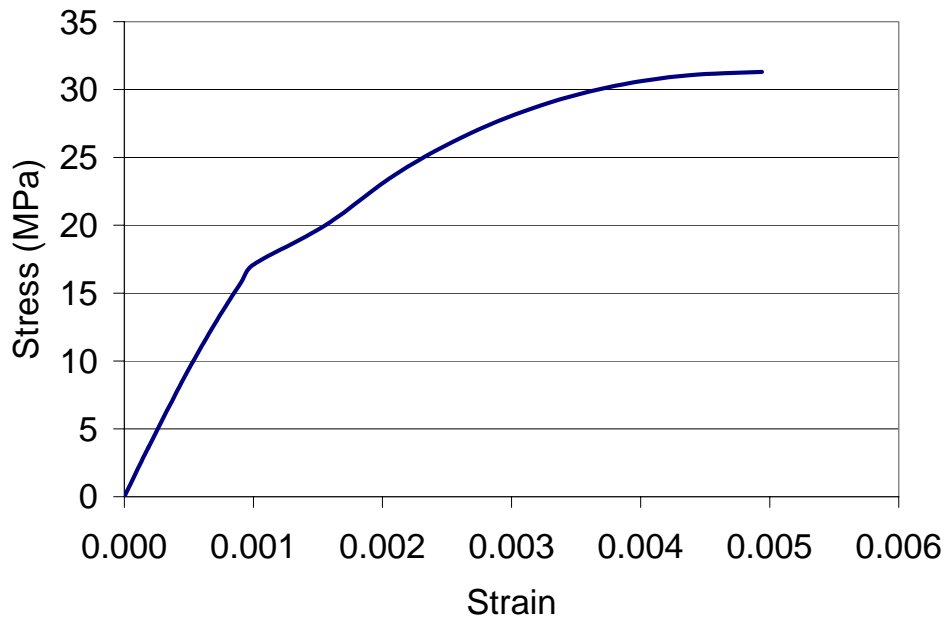


**Figure 1: Masonry Stress-Strain Relationship**

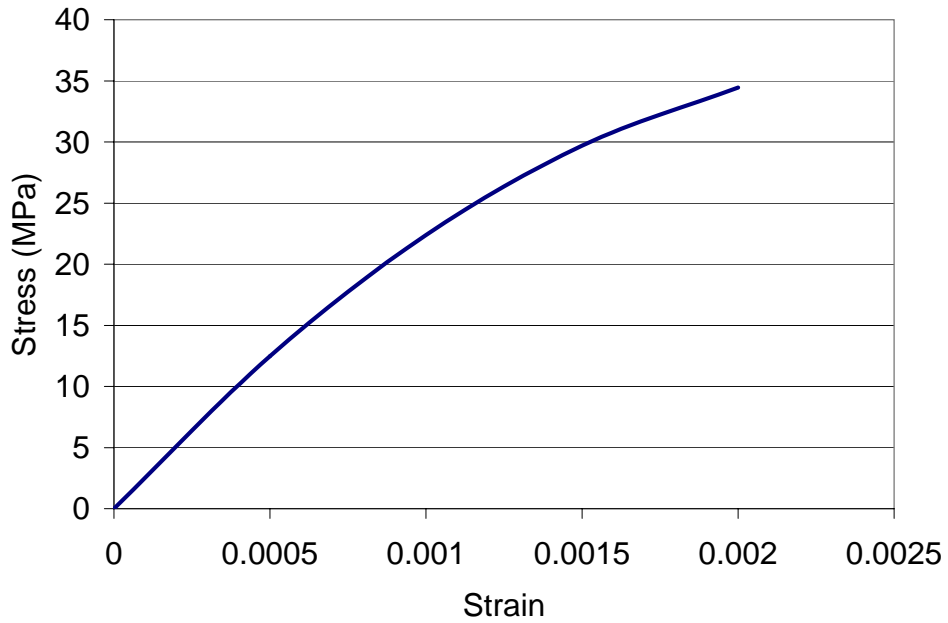


**Figure 2: Concrete Foundation Stress-Strain Relationship**

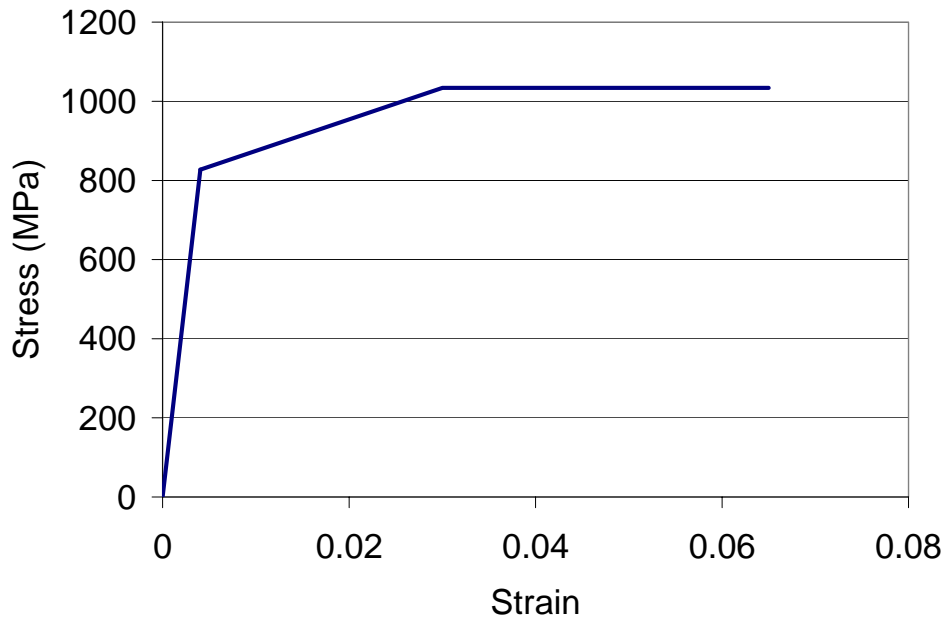


**Figure 3: Post-Tensioning Steel Bar Stress-Strain Relationship**

In addition to the stress-strain relationships, other material property inputs include density,  $1.963 \times 10^{-9} \text{ N/mm}^3$ , and a coefficient of friction,  $\mu_s = 0.8$ .

## 1.4 MODELING

Figure 4 shows a sample finite element model used for parametric studies. The masonry wall was mapped with 50 mm cubes so that an accurate representation of its contact surface can be made. After several iterations of the model it was found that if the nodes of the masonry wall and foundation were coincidental then the results were improved. Therefore, the foundation was mapped with 50 mm cubes as well. The ends of the link8 elements of the post-tensioning steel bars were coupled with their corresponding coincident nodes, thereby modeling the anchorage load transfer into the structural system and the lateral translation of the masonry wall. Finally, the entire bottom surface of the foundation was fixed and a gravitational acceleration was applied.

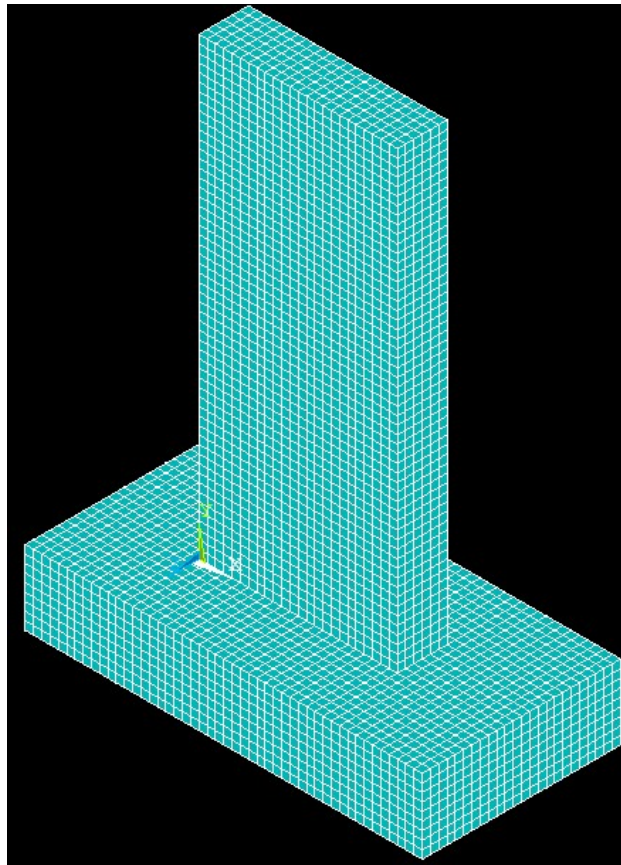


**Figure 4: Finite Element Model of Unbonded Post-Tensioned Masonry Wall**

A P P E N D I X C

**1 TESTING PICTURES**

B R Y A N E W I N G

# TESTING PICTURES

## 1.1 OPENING PANEL 1 – CONTROL



Figure 1: Construction of Masonry Wall with Opening



Figure 2: Formation of Base Crack and Vertical Crack at 0.35 Drift Ratio



**Figure 3: Base Crack at 0.75 Drift Ratio**



**Figure 4: Excessive Crack Width at 1.25 Drift Ratio**



**Figure 5: Vertical Crack at 1.75 Drift Ratio**



**Figure 6: Crushing of Masonry at 2.25 Drift Ratio**

## 1.2 OPENING PANEL 2 – CONFINEMENT PLATES



**Figure 7: Finished Wall Setup**



**Figure 8: Continued Vertical Crack Growth Resulting Entire Side of Wall Rocking at 1.75 Drift Ratio**



**Figure 9: Observed Sliding of Masonry Wall at 1.75 Drift Ratio**

### **1.3 OPENING PANEL 3 – HORIZONTAL REINFORCEMENT**



**Figure 10: Reduced Crack Width at 0.75 Drift Ratio**



**Figure 11: Rocking Mechanism and Limited Crack Width at 1.75 Drift Ratio**

## **1.4 SHAKE TABLE TESTS**



**Figure 12: Shake Table Setup**

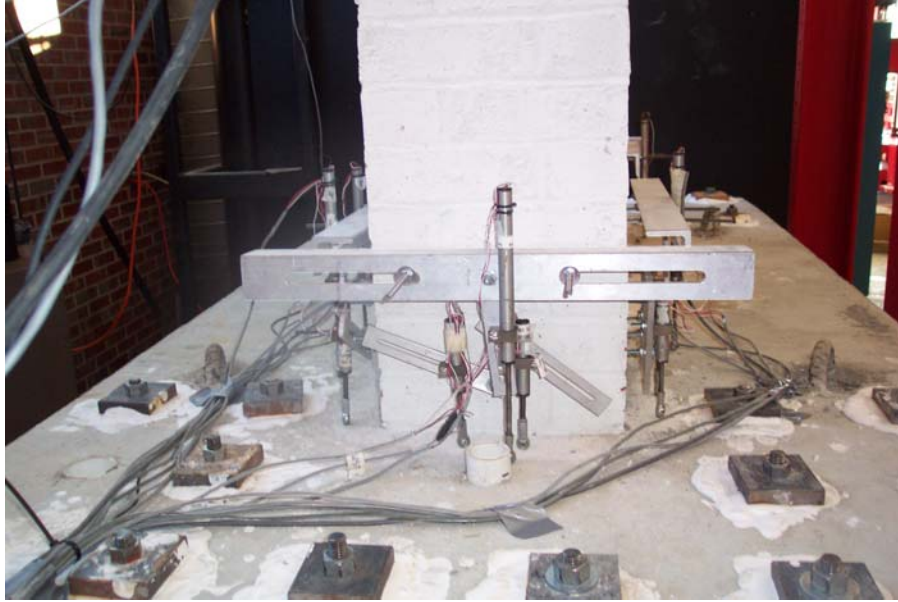


**Figure 13: Instrumentation and Bolt Tie-Downs**



**Figure 14: Masonry Wall "Damage" After 56 Earthquake Runs**